Modelling large scale ocean circulation: The role of mixing location and meridional pressure gradients for the Atlantic overturning dynamics

Dissertation

zur Erlangung des akademischen Grades
doctor rerum naturalium
(dr. rer. nat.)
in der Wissenschaftsdisziplin Physikalische Ozeanographie

eingereicht an der
Mathematisch-Naturwissenschaftlichen Fakultät I
Universität Potsdam

von

Alexa Griesel

Potsdam, im April 2005

Wenn die Welt so einfach wäre, dass wir sie verstehen würden, dann würden wir gar nicht existieren um sie verstehen zu wollen.

(frei nach Emerson M. Pugh)

Abstract

Due to its relevance for global climate, the realistic representation of the Atlantic meridional overturning circulation (AMOC) in ocean models is a key task. In recent years, two paradigms have evolved around what are its driving mechanisms: diapycnal mixing and Southern Ocean winds. This work aims at clarifying what sets the strength of the Atlantic overturning components in an ocean general circulation model and discusses the role of spatially inhomogeneous mixing, numerical diffusion and winds. Furthermore, the relation of the AMOC with a key quantity, the meridional pressure difference is analyzed.

Due to the application of a very low diffusive tracer advection scheme, a realistic Atlantic overturning circulation can be obtained that is purely wind driven. On top of the winddriven circulation, changes of density gradients are caused by increasing the parameterized eddy diffusion in the North Atlantic and Southern Ocean. The linear relation between the maximum of the Atlantic overturning and the meridional pressure difference found in previous studies is confirmed and it is shown to be due to one significant pressure gradient between the average pressure over high latitude deep water formation regions and a relatively uniform pressure between 30°N and 30°S, which can directly be related to a zonal flow through geostrophy. Under constant Southern Ocean windstress forcing, a South Atlantic outflow in the range of 6-16 Sv is obtained for a large variety of experiments. Overall, the circulation is winddriven but its strength not uniquely determined by the Southern Ocean windstress.

The scaling of the Atlantic overturning components is linear with the background vertical diffusivity, not confirming the 2/3 power law for one-hemisphere models without wind forcing. The pycnocline depth is constant in the coarse resolution model with large vertical grid extends. It suggests the ocean model operates like the Stommel box model with a linear relation of the pressure difference and fixed vertical scale for the volume transport. However, this seems only valid for vertical diffusivities smaller $0.4\,cm^2s^{-1}$, when the dominant upwelling within the Atlantic occurs along the boundaries. For larger vertical diffusivities, a significant amount of interior upwelling occurs. It is further shown that any localized vertical mixing in the deep to bottom ocean cannot drive an Atlantic overturning. However, enhanced boundary mixing at thermocline depths is potentially important.

The numerical diffusion is shown to have a large impact on the representation of the Atlantic overturning in the model. While the horizontal numerical diffusion tends to destabilize the Atlantic overturning the verital numerical diffusion denotes an amplifying mechanism.

Kurzzusammenfassung

Wegen ihrer Bedeutung für das globale Klima ist die realistische Darstellung des Atlantischen meridionalen overturnings in Ozeanmodellen eine zentrale Aufgabe. In den letzten Jahren haben sich zwei verschiedene Hypothesen darüber entwickelt, was diese Zirkulation antreibt: diapyknische Vermischung und Winde im südlichen Ozean.
Die vorliegende Arbeit zielt darauf aufzuklären, welche Rolle eine räumlich inhomogene Verteilung der Vermischung, die numerische Diffusion und Winde beim Bestimmen der Stärke des Atlantischen overturnings spielen. Ausserdem wird die Beziehung des Atlantischen overturnings zu meridionalen Druckgradienten untersucht.
Durch Anwenden eines sehr gering diffusiven Tracer-Advektionsschemas kann eine realistische Zirkulation erzeugt werden, die rein von den Winden im südlichen Ozean getrieben wird. Ausgehend von der windgetriebenen Zirkulation werden Änderungen der Dichtegradienten durch Verstärkung der parametrisierten Eddy Diffusion im Nordatlantik und südlichen Ozean hervorgerufen. Dadurch wird das Bild einer vom Wind bestimmten Zirkulation in der letztendlich Druckgradienten nicht ausschlaggebend sein würden, modifiziert. Das lineare Verhältnis zwischen dem Maximum des Atlantischen overturnings und dem meridionalen Druckgradienten wird bestätigt und erklärt. Diese Linearität ist auf einen signifikanten Druckgradienten zwischen den Tiefenwasserbildungsgebieten und einem zwischen 30°N and 30°S homogenen Druck zurückzuführen. Der Volumentransport bei 30°S variiert über eine Bandbreite von 10 Sv für verschiedene Experimente unter konstantem Wind über dem südlichen Ozean. Zusammenfassend ist die Zirkulation zwar windgetrieben aber ihre Stärke nicht allein vom Wind bestimmt.
Die Skalierung des Atlantischen overturnings ist linear mit vertikaler Vermischung, was die Skalierung mit einem Exponenten von 2/3 in einhemisphärischen Modellen ohne Wind-Antrieb nicht bestätigt. Die Tiefe der Pyknokline bleibt mit der groben vertikalen Auflösung konstant. Die Ergebnisse deuten darauf hin, dass das Ozeanmodell sich wie das Stommel-Box Modell verhält mit einer linearen Beziehung zum meridionalen Druckgradienten und einer festen vertikalen Skala für den Volumentransport. Das scheint jedoch nur für Diffusivitäten kleiner als $0.4\,cm^2s^{-1}$ zu gelten, wenn das Aufsteigen im Atlantischen Ozean bevorzugt an den Ozeanrändern statt findet. In Bezug auf den Antrieb des Atlantischen overturnings wird gezeigt, dass vertikale Vermischung in der Nähe des Ozeanbodens keinen Einfluss hat. Verstärkte vertikale Vermischung an den Ozeanrändern in der Tiefe der Thermokline jedoch ist potentiell wichtig.
Die numerische Diffusion hat einen grossen Einfluss auf das Atlantische over-

turning im Modell. Während die horizontale numerische Diffusion das overturning eher zu destabilisieren tendiert, bewirkt die vertikale numerische Diffusion einen Verstärkungsmechanismus.

Contents

Chapter 1

Introduction

The oceanic meridional overturning circulation (MOC) is a key player in Earth's climate - in the North Atlantic its maximum northward heat transport is about 1 PW (10^{15} W), contributing to the mild climate predominant in northwestern Europe. The global overturning system consists of four main branches: surface currents that transport relatively less dense waters toward the high latitudes, deep water formation and sinking of dense waters, deep western boundary currents transporting the dense waters southward and upwelling processes that close the loop, ultimately leading to the conversion of dense to less dense waters again. Besides transporting large amounts of heat, the overturning system exerts a strong control on the stratification and distribution of water masses and is particularly important for the cycling of tracers, such as carbon dioxide, within the ocean. The global overturning system is sketched in a highly simplified and illustrative form in figure 1.1.
Elucidating which mechanisms control the strength of the Atlantic branch of the meridional overturning circulation (AMOC) is of primary interest both for physical understanding as well as for the understanding of what determines its stability properties. Evidence from the past suggests that temperature changes of several degrees during the last ice ages occuring within only a few decades are coupled to the reorganization of the AMOC (Rahmstorf, 2002). In the future, there is a risk that substantial changes in ocean circulation could occur as a result of global warming (Manabe and Stouffer, 1994; Rahmstorf and Ganopolski, 1999; Wood et al., 1999; Schaeffer et al., 2002). Also, the stability properties of the AMOC might depend on the relative contributions of its ultimate energy providers, namely diapycnal mixing and Southern Ocean winds (Schmittner and Weaver, 2001; Prange et al., 2003).

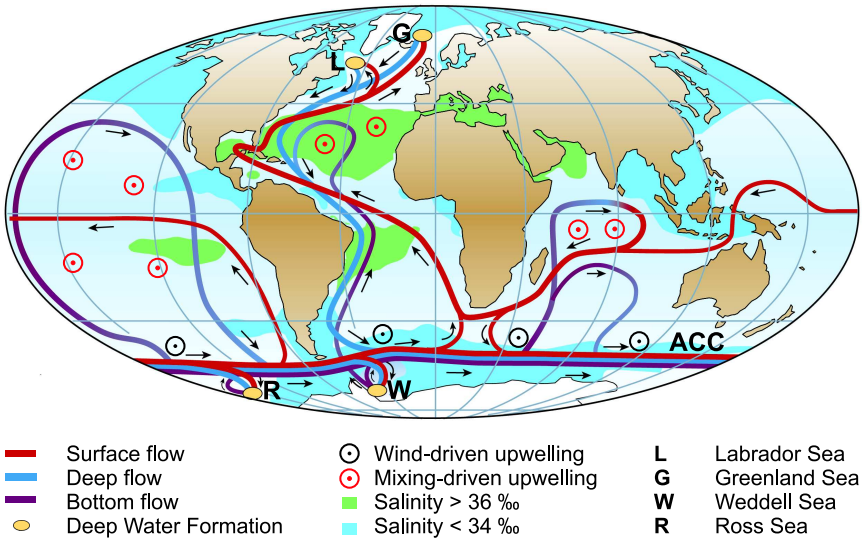

Figure 1.1: *Simplified sketch of the global overturning circulation system. In the Atlantic, warm and saline waters flow northward all the way from the Southern Ocean into the Labrador and Greenland Seas where North Atlantic Deep Waters (NADW) are formed. By contrast, there is no deep water formation in the North Pacific, and its surface waters are fresher. Mixing-driven upwelling potentially takes place widespread in low latitudes and wind-driven upwelling occurs along the Antarctic Circumpolar Current (ACC). From Kuhlbrodt et al. (2005).*

Already Sandström (1908)'s experiments have led to the conclusion that *surface* heat and freshwater fluxes alone cannot drive a deep overturning circulation. He placed heating and cooling sources at opposite sides in a water tank and observed that a deep overturning circulation can only be sustained if heating occurs at depth, otherwise the tank fills up with cold water. Since the ocean is heated from above and no substantial geothermal heat source exists at depth, some mechanism must exist that puts mechanical energy into the system allowing the dense waters to rise to the surface again. It has led to the understanding that, unlike the atmosphere which is heated from below, the ocean is not a heat engine but rather a mechanical engine (Huang, 1999) whose energy sources of winds and tides are ultimately mechanic.
Hence, since deep water formation is only the prerequisite of an overturning circulation, discussions in the last years have evolved around the issue which mechanisms ultimately *drive* the MOC in the sense that they provide the

necessary potential energy input into the ocean that is capable of sustaining a steady-state deep overturning circulation. These driving processes ultimately are connected to the way in which deep waters upwell and are converted to lower density surface waters again. Figure 1.2 sketches the two paradigms described below in a simplified conceptual way.

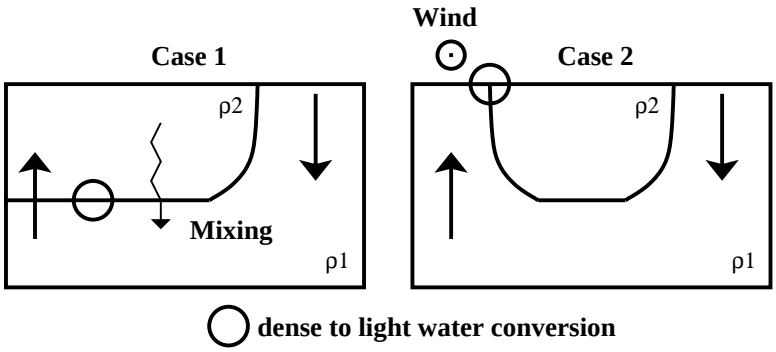

Figure 1.2: *Sketch of the two cases: "only diapycnal mixing" (case 1) and "only wind driven upwelling" (case 2). The sketches represent highly simplified meridional sections with NADW at the right (northern) end. The curved solid line indicates the thermocline that separates higher density (ρ_1) from lower density (ρ_2) waters. The circles represent regions of conversion of water masses. In the wind-driven case 2, the Southern Ocean winds are represented by a circle with a dot inside. Straight arrows indicate volume transport, while the zig-zag arrow stands for diapycnal mixing (from Kuhlbrodt et al. (2005))*

The prevailing picture is that of a circulation *driven* by diapycnal mixing in the ocean interior and, perhaps, *controlled* by the volume rate of formation of North Atlantic Deep Water (NADW) (Munk and Wunsch, 1998; Huang, 1999; Wunsch and Ferrari, 2004). Within this framework, deep water upwelling occurs at low latitudes in order to balance the downward turbulent transport of heat and compensating downwelling associated with deep ocean convection taking place in the North Atlantic. The strength of the AMOC would then be determined by the amount of energy involved in the vertical mixing of heat with this energy being ultimately provided by winds and tides.
An alternative description has been supported by (Toggweiler and Samuels, 1993a, 1995, 1998) in which the sinking of NADW is identified as the closing branch of a circulation driven by wind-driven upwelling in the Southern Ocean. Waters at the surface of the Southern Ocean move northward as a result of strong Ekman drift caused by circumpolar winds and are returned

at depths below that of the Drake Passage sill. This "Drake Passage effect"is explained at the latitude of Drake Passage above the depth of its sill and, accordingly, no net meridional geostrophic flow at shallower depths exists. Within this framework, the strength of the AMOC would be determined solely by the strength of the upwelling caused by the dominant westerlies in the Southern Ocean. However, observations and model studies have indicated that not all of these upwelling waters flow northward again to reach the North Atlantic; rather, a significant amount recirculates back to the Southern Ocean, depending crucially on the amount of mesoscale eddy activity in the Southern Ocean.
To adequately model the meridional overturning circulations and its driving and rate controlling mechanisms in ocean general circulation models (OGCMs) is of great importance. As indicated above, the small scale turbulent and eddy mixing processes play an essential role for ocean and climate dynamics and yet, they both are commonly not resolved in coarse resolution models and their parameterization is one of the most uncertain components in OGCMs. Mixing is pronounced along isopycnal surfaces where it occurs with the least expenditure of energy while diapycnal mixing is orders of magnitudes smaller, but essential for the overturning dynamics as indicated above. Eddy motions occur on spatial scales of 10 km and can lead to significant horizontal redistributions of mass within isopycnal classes. Since most models are non-eddy resolving, they also need to be parameterized. In general, mixing does not occur uniformly over the ocean and it arises from many different mechanisms. Yet, since there are a lack of theories how to parameterize mixing in terms of the large scale model quantities, it is usually represented in ocean models by single horizontally homogeneous parameters.
A number of simple conceptual models for the strength of the overturning circulation also exist that aim at providing a system that can be solved and understood analytically and yet still is supposed to capture the main physics of the real system. One of the first of such conceptual models is the one devised by Stommel (1961), consisting of a high- and a low-latitude box whose density difference determines the strength of the AMOC. Together with modified or extended versions, this model has been widely applied. However, with the main balance in the ocean being geostrophy, only a *zonal* flow can directly be explained with a meridional density or pressure difference.

The following questions reflect the primary motivations of this work:

What determines the strength of the AMOC in OGCMs ? What is the role

of small scale turbulent and eddy mixing in different regions of the ocean model and for driving and shaping the circulation ?
Can simple models of the AMOC, like the Stommel box model, be reconciled with the outcome of more complex global GCMs and ultimately the behaviour of the real ocean ?
Are there simple quantities, such as the meridional pressure difference, that determine the strength of the circulation ?

The main concepts of this work are introduced as follows.

1.1 Diapycnal mixing as a driver for the Atlantic overturning circulation

Due to the lack of data and out of simplicity diapycnal mixing was initially assumed to be constant throughout the ocean interior, leading to a uniformly distributed, slow upwelling over large regions of the oceans. Such a uniform upwelling was postulated by the theory of Stommel and Arons (1960). Assuming that the dominant terms in the transport equation of a tracer T are vertical advection and diffusion leads to the following vertical advection-diffusion balance:

$$w\partial_z T = \kappa_v \, \partial_{zz} T, \tag{1.1}$$

with a *constant* vertical diffusion coefficient κ. Munk (1966) estimated a uniform value of $\kappa = 1\, cm^2 s^{-1}$ for the diapycnal diffusivity by fitting this balance point-wise to tracer data from the central Pacific Ocean. $\kappa = 1\, cm^2 s^{-1}$ has since widely been regarded as the diapycnal mixing coefficient needed to return the deep waters back to the surface.

However, in recent years direct and indirect measurements of mixing coefficients have revealed that diapycnal mixing is highly variable in space and time. Interior mixing rates away from topographic features and boundaries indicate values of the order of only $\kappa = 0.1\, cm^2 s^{-1}$ (Moum and Osborn, 1986; Ledwell et al., 1993; Oakey et al., 1994) and even lower close to the equator (Gregg et al., 2003). Strong mixing with diffusion coefficients' orders of magnitudes higher than $\kappa = 1\, cm^2 s^{-1}$, on the other hand, can be found near highly variable bottom topography (Polzin et al., 1997; Ledwell et al., 2000) or along continental slopes (Moum et al., 2002).

Taking these findings into account, Munk and Wunsch (1998) re-estimated the global average diapycnal diffusivity by applying the vertical advection-diffusion balance to globally-zonally averaged densities. They interpreted the resulting diffusivity as a surrogate for a small number of con-

centrated mixing regions from which the mixed water masses are exported to the ocean interior. Their analysis was based on the assumption that all 30 Sv of deep water that is formed at high latitudes upwells at low latitudes between depths of 1000 and 4000 m. This approach resulted in the same globally averaged value of $\kappa = 1\, cm^2 s^{-1}$. Munk and Wunsch (1998) hypothesized that the power required to mix waters with a uniform coefficient of $\kappa = 1\, cm^2 s^{-1}$ is the same as if concentrated mixing occurred with much higher coefficients in only 1% of the ocean, thus reaffirming $\kappa = 1\, cm^2 s^{-1}$ as the average diapycnal mixing coefficient required to return the deep waters back to the surface.

As previously mentioned, in order to establish what drives the oceanic overturning circulation, and in particular the AMOC, it is ultimately the ocean's rate of creation of potential energy one has to consider. Munk and Wunsch (1998) and Wunsch and Ferrari (2004) assessed the amount of energy production ϵ(z) required to maintain the abyssal stratification against an upwelling velocity w(z):

$$\epsilon(z) = \kappa(z)\ g\ \partial_z\ \rho(z), \tag{1.2}$$

where κ is the depth-dependent diffusivity as computed from the density distribution with the assumed upwelling of 30 Sv in the low latitude oceans and ρ is the potential density. Integrated over the global abyssal ocean volume a total of 0.4 TW of energy input is obtained.

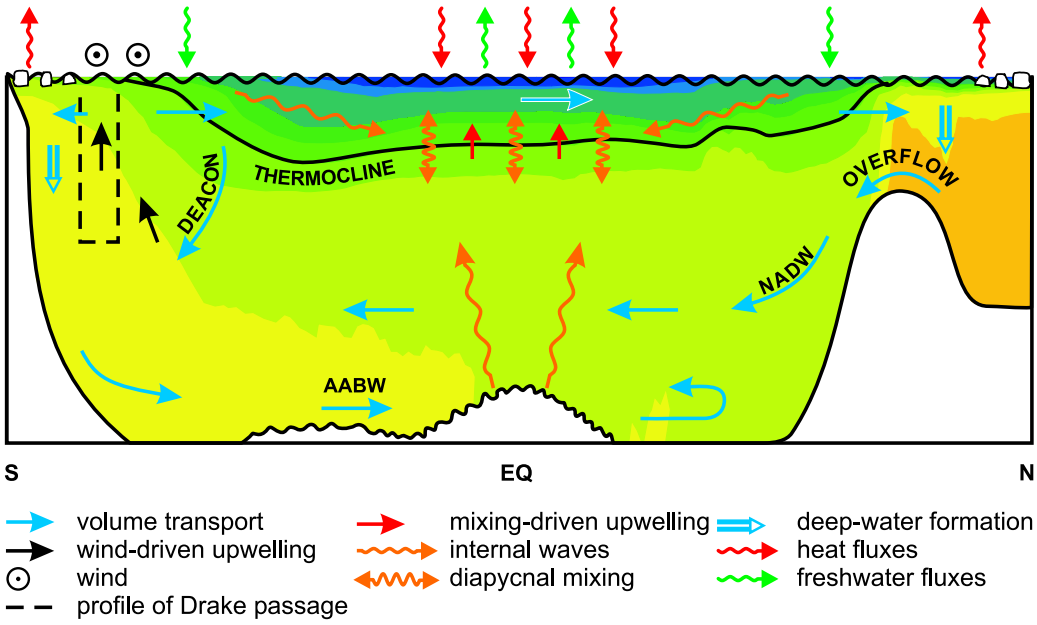

Figure 1.3: *Idealized meridional section representing a zonally averaged picture of the Atlantic ocean. Blue and black arrows sketch the MOC. The color shading depicts a zonally averaged density profile derived from observational data. The pycnocline, the region where the vertical density gradient is large, separates the less dense and warmer upper water from the denser and cooler deep waters. The two main upwelling mechanisms, wind-driven and mixing-driven, are displayed. Wind-driven upwelling is a consequence of a northward flow of the surface waters in the Southern Ocean, the Ekman transport, that is driven by strong westerly winds. Mixing along the density gradient, called diapycnal mixing, causes mixing-driven upwelling; this is partly due to internal waves triggered at the ocean's boundaries . Deep water formation (DWF) occurs in the high northern and southern latitudes, creating North Atlantic Deep Water (NADW) and Antarctic Bottom Water (AABW), respectively. The locations of DWF are tightly linked with the distribution of surface fluxes of heat and freshwater. The freshly formed NADW has to flow over the shallow sill between Greenland, Iceland, and Scotland. Close to the zone of wind-driven upwelling in the Southern Ocean is the Deacon Cell recirculation, visible in the zonally integrated meridional velocity in ocean models. Note that in the real ocean, the ratio of the meridional extent to the typical depth is 5000 to 1 (from Kuhlbrodt et al. (2005)).*

The question remains as to whether this energy production is available

in reality. This depends crucially on how and where the turbulent kinetic energy provided by the winds and tides is made available for mixing. Of the aforementioned mechanisms, both internal wave generation by the wind at the surface and its radiation into the ocean interior and creation of internal waves through interaction of the eddy field with bottom topography (sketched in Fig. 1.3) are thought to lead to the bulk of interior mixing, whereas abyssal tidal flow directly associated local diapycnal mixing is probably responsible for most of the localized elevated mixing at the bottom of the ocean.
Insight regarding the implications of the spatial distribution of vertical mixing for the AMOC can be gained from modeling studies. Most ocean models show that the deep overturning circulation and heat transport are very sensitive to the employed diapycnal diffusivity (Bryan, 1987; Zhang et al., 1999; Mignot et al., 2004).

Given the lack of theories on how to parameterize small scale mixing in terms of the large scale quantities, mixing coefficients in ocean models are often used as tuning parameters to achieve the most realistic simulation regarding large-scale observable quantities (surface currents, tracer concentrations and transports, etc.). However, it has to be kept in mind that the employed mixing partly corrects for model errors that might have little to do with the physics of mixing or their parameterization. In addition, mixing is not allowed to evolve with the ocean in a changing climate. Most commonly, uniform mixing coefficients or an arctangent vertical profile with interior mixing values of 0.3 $cm^2 s^{-1}$ increasing to 1.3 $cm^2 s^{-1}$ at the ocean bottom (Bryan and Lewis, 1979) are employed.

Attempts to express mixing coefficients in terms of model parameters include stratification dependent vertical diffusivity (Cummins et al., 1990) or a relation to the Richardson number (Large et al., 1994). Some studies have examined the effect of mixing location on meridional overturning dynamics in ocean models. Marotzke (1997) imposed mixing only at the boundaries and following from that, Scott and Marotzke (2002) concentrated mixing entirely at high or low latitudes, in or below the thermocline or at the boundaries. They concluded that boundary mixing is more efficient in driving the MOC, as interior upwelling hinders the processes leading to east-west density differences that determine the volume transport. They found that mixing at depth is not required to generate a deep flow and has little effect on the strength of the circulation through the thermocline. Both studies employed a one hemisphere model without wind-forcing and without bottom topography. Hasumi and Suginohara (1999) investigated the effects of topographically enhanced mixing by increasing the diffusivity where sub-grid scale roughness exceeded a certain threshold in a global ocean model with realistic topography and

wind forcing. Their simulations show that upwelling and circulation of the deep water masses is affected by localized deep mixing but that the maximum of the AMOC is insensitive to these changes.

Modeling studies which employ fixed mixing coefficients disregard the amount of mechanical energy required for the mixing. Huang (1999) considered fixed energy profiles from which diffusivities are calculated in an idealized ocean basin. However, his parameterization is not conservative, i.e. a heat source is introduced where stratification vanishes, which makes it difficult to interpret the results. Recently, Simmons et al. (2003) incorporated a global barotropic tidal model that calculates energy fluxes from model density distributions and tidal flows into an OGCM. They added a constant weak background diffusivity of 0.1 cm^2s^{-1} to the predicted diffusivities in order to account for other non-local sources of mixing. This bottom enhanced mixing improved the representation of deep water mass properties. The strength of the AMOC was reduced by 50% compared to a simulation with uniform mixing with a coefficient equal to the average of the non-uniform one. They point out that an energy profile which increases with depth leads to downwelling. Their decrease in AMOC maximum can be attributed to the lower value of $\kappa = 0.1\, cm^2s^{-1}$ at thermocline depths compared to the 0.9 cm^2s^{-1} for the uniform mixing case.

The abovementioned studies indicate the importance of switching from fixed constant diffusivities to nonuniform coefficients based on energy considerations. What still seems to be unresolved is whether localized enhanced mixing at the boundaries can work such that it explains basin-averaged diffusivities and leads to the same driving of an overturning circulation.

In this work, what has been indicated in the study by Scott and Marotzke (2002) for a one-hemispheric model without wind forcing, is confirmed. A parameterization of vertical mixing dependent on the roughness of bottom topography and stratification is employed. The arising mixing coefficients are locally elevated at depth and their role for driving the Atlantic overturning circulation is assessed. It is shown that what counts for the strength of the AMOC is not any localized mixing at depth but rather the background value of the diapycnal mixing at thermocline depths. Since however from observations, no significant background mixing away from topographic features at thermocline depths has yet been identified the role of enhanced boundary mixing at these depths is further explored. The results using the global model also suggest that what counts for driving the AMOC is the diapycnal mixing within the Atlantic ocean and that the AMOC is rather independent of the mixing rates in the Indopacific.
Although in the past decades spurious diapycnal mixing has been minimized

through the incorporation of isopycnal mixing schemes (Redi, 1982; Gent and McWilliams, 1990), possibly most current ocean models still overestimate the contribution of diapycnal mixing as a driver of the AMOC. Models mostly employ coefficients in the interior ocean much larger than the observed 0.1 $cm^2 s^{-1}$, resulting in deficient heat transport because the temperature contrast between cold southward and warm northward flows is too weak. The coefficient is sometimes increased to get a stronger present day AMOC. Yet, too weak an overturning circulation is not necessarily a result of too weak diapycnal mixing but can be the result of erroneous surface fluxes, insufficient representation of deep water formation processes, etc. In addition, ocean models make use of computational schemes with implicit numerical diffusion. This additional diffusion is rarely considered. Yet, it can be of the same order as the explicitly applied diffusivity (Gerdes et al., 1991) and limits the ability to test the model's behavior in the limit of very low diapycnal mixing (Toggweiler and Samuels, 1998).
In the work here, the application of a very low diffusive tracer advection scheme, developed by Prather (1986) and devised by Hofmann and Morales-Maqueda (2004) for the ocean model, allows to assess this behaviour and to associate changes in the overturning circulations solely to the explicitly put diffusion parameters. In particular, the representation of the Atlantic overturning with this scheme as compared to the more diffusive FCT tracer advection scheme introduced by Zalesak (1979) is analyzed. It is shown that the spurious horizontal diffusion with this scheme tends to destabilize the Atlantic overturning whereas the spurious numerical diffusion denotes a significant amplifying mechanism.

1.2 Wind driven upwelling and the role of mesoscale eddies

The alternative hypothesis to upwelling of deep water masses driven by diapycnal mixing is wind-driven deep upwelling in the Southern Ocean as outlined in the first section of this introduction. Several lines of evidence question that deep upwelling occurs in a broad, diffuse manner. There is no indication either of a substantial fraction of it occuring in the tropics, since low-latitude waters which upwell in the Indian and Pacific Oceans are not of deep origion. However, there is evidence for subtantial upwelling of deep water masses in the Southern Ocean. These findings basically stem from the distribution of pre-bomb radiocarbon (Toggweiler and Samuels, 1993b), rates of biogenic silica production (Gnanadesikan and Toggweiler, 1999) and transect studies

of further tracers (Wunsch et al., 1983; Robbins and Toole, 1997). The few available eddy resolving model simulations indicate substantial upwelling of deep water masses in the Southern Ocean south of the ACC in the latitude band of Drake Passage (Döös and Coward, 1997).
The tight link of Southern Ocean westerlies and the North Atlantic sinking as proposed by Toggweiler and Samuels (1993a) has been questioned by a number of studies. Rahmstorf and England (1997) obtained a relatively small sensitivity of the AMOC with respect to changes in Southern Ocean winds and argued the larger sensitivity found in previous studies was due to the neglect of the negative temperature feedback on the Atlantic overturning. Also, observations (Schmitz, 1995, 1996) indicate that the northward flow at about 40°S is in fact much smaller than the Ekman transport, implying that a substantial part of return flow back to the Southern Ocean takes place. In accordance with this, inverse model results (Sloyan and Rintoul, 2001a) and eddy resolving ocean models (Killworth and Nanneh, 1994) indicate significant poleward transport in layers above the shallowest sill of Drake passage. In ocean models, this return cell is apparent as the Deacon cell (see figure 1.3). An important property of this cell appears to be that it is associated with very little density change (Döös and Webb, 1994), meaning the return flow occurs along isopycnals. In the presence of eddies, the return flow can even occur above sill depth at Drake passage latitudes as explained by Rintoul et al. (2001) and as advanced by Speer et al. (2000) based on observations of potential vorticity gradients. Hence, eddies in the Southern Ocean have been identified as playing a crucial role for the Atlantic overturning dynamics in terms of affecting the Deacon cell.
However, the "Toggweiler"mechanism has received further theoretical support in a recent work by Nof (2003). Nof (2003) considered the net momentum balance of a water column from the surface down to the depth of the sill of Drake Passage. In order to cancel out the effects of pressure, Nof (2003) calculated the integral of such a balance along a closed contour passing through the tips of the Americas, Africa and Australia. As it turns out, this integral provides a direct relation between the wind stress along the contour and the meridional transport across it showing that the net inflow into the Atlantic, Indian and Pacific oceans above the sill of Drake Passage is uniquely determined by the surface wind. According to Nof's estimate, around $10\,Sv$ cross this contour into the Atlantic, marking the starting point of the northbound branch of the Atlantic MOC. An important point stressed by Nof (2003) is that the flow in this branch is partitioned between a northbound Sverdrup transport in the ocean interior and a southbound western boundary current flow. Hence, ocean pressure gradients need to somehow adapt so that the Sverdrup flow minus the western boundary flow equals the

Ekman transport, a result that highlights the importance of the interaction between the wind-driven and thermohaline-driven components of the circulation. However, regardless of the nature of such an interaction, changes in the pressure gradients will not affect the net northward transport. If one then assumes, as Nof (2003) does, a partitioning of the wind-driven transport between the Indopacific and the Atlantic proportional to the widths of the respective basins along the integration contour, then the conclusion that the Atlantic inflow and outflow cannot be affected by alterations in the zonal and meridional pressure gradients seems inescapable.

In this work, this conclusion is put to the test by running a series of experiments with the global ocean model in which changes in pressure gradients are forced by varying the strength and geographical distribution of the diffusion coefficients of the parameterized baroclinic eddy transport. More specifically, it is shown how changes in the density gradients in the Southern Ocean and North Atlantic affect the water inflow into the Southern Ocean on the one hand and the deep water formation in the North Atlantic on the other hand. To do so, modifications in the density gradients are caused by changing the magnitude of the Gent and McWilliams (1990) eddy thickness diffusivity in different regions of the ocean. However, note that the focus is not on how the representation of baroclinic eddies affects the simulated ocean circulation, but, in a more conceptual way, on how changing the density gradients in different regions of the ocean may change the volume transports. Kamenkovich and Sarachik (2004) have recently reported on experiments with a similar design, and this work largely confirms, as well as extends, their findings. As in Kamenkovich and Sarachik (2004), these experiments show that changing eddy diffusivities, and hence density gradients, in the North Atlantic significantly affects the upwelling within the Atlantic but has little impact on the South Atlantic outflow, whereas changing eddy diffusivities in the Southern Ocean has the biggest impact on the South Atlantic outflow. However, in contrast to Kamenkovich and Sarachik (2004), the resulting changes in volume transport are investigated in a parametric regime that is very close to the limit of no diapycnal mixing. In this model, strictly horizontal diffusion is negligible since the model operates with zero explicit horizontal diffusivity and implicit diffusion caused by the numerical advection scheme (Prather, 1986) is very low. Vertical diffusivities (0.05 cm^2 $s{-}1$) are much lower than commonly used. It is shown that even without horizontal diffusion and its associated Veronis effect (Lazar et al., 1999), there is a significant amount of upwelling and meridional recirculation in the North Atlantic that is affected by the strength of the eddy diffusivities, and that it is therefore important to clearly distinguish between the maximum of the Atlantic MOC and the South Atlantic outflow (the difference between the two being equal to the

recirculation within the Atlantic), even in an ocean close to the limit of no diapycnal mixing and hence with little upwelling driven by downward heat diffusion.

1.3 Simple models of the meridional circulation and scaling laws

In his early two-box model of the meridional overturning circulation, Stommel (1961) used a simple linear relation of the meridional density difference between the high and low latitudes with the meridional circulation. This model has given important insights into the meridional circulation, explaining the existence of multiple stable equilibria and highlighting the importance of surface heat- and freshwater fluxes in determining the density difference that sets up the flow. Following theories for the structure of the thermocline, Bryan and Cox (1967) derived a scaling for the meridional circulation based on geostrophy and on advective-diffusive heat balance leading to a non-linear scaling with the density difference. His derivation implies that the vertical scale for the meridional flow, the depth of the pycnocline, is not fixed as in the Stommel (1961) framework: Given the density difference between the equator and the pole, $\Delta\rho$, an equation for the zonal velocity u follows from geostrophy and thermal wind balance:

$$f\partial_z u = \frac{g}{\rho_0}\partial_y \rho \tag{1.3}$$

Inserting typical scales for the horizontal velocity U, pycnocline depth D and meridional extent L_y of the flow and with $\Delta\rho$ beeing the imposed meridional density difference, one obtains:

$$U = \frac{g}{f\rho_0}\frac{\Delta\rho}{L_y}D \tag{1.4}$$

At the base of the thermocline, the advection-diffusion balance equation (1.1) is assumed to hold for the density. The idea behind the pycnocline scaling without wind is that changes in vertical diffusivity only change the depth of the pycnocline but not the density difference (Robinson and Stommel, 1959). Inserting typical scales into equation (1.1) provides

$$D = \frac{\kappa_v}{W} \tag{1.5}$$

The relation between meridional and vertical flow is governed by vorticity dynamics:

$$\beta v = f\partial_z w, \quad \frac{V}{\beta} = f\frac{W}{D} \tag{1.6}$$

It is assumed that the zonal flow scales like the meridional flow, such that $UL_yD = VL_xD$. Combining equations (1.4), (1.5) and (1.6) gives an expression for the meridional overturning:

$$\Psi = VL_xD = \left(\frac{gfL_x^2}{\rho_0\beta^2}\right)^{1/3} \kappa^{2/3}\Delta\rho^{1/3} \tag{1.7}$$

The meridional volume transport is proportional to $\Delta\rho^{1/3}$ and it scales like $\kappa_v^{2/3}$. Hence, this derivation is different from the scaling in the Stommel box model with a constant pycnocline depth. It is important to note that this kind of scaling is the result of multiple assumptions.
One main assumption is that the pycnocline depth D is determined from advective diffusive balance and is also the scale for the volume transport. But, in the presence of wind forcing, Ekman pumping creates the 'bowl shaped' structure of the pycnocline (figure 1.4). Recently, Marshall et al. (2002) and Radko and Marshall (2004) suggested that lateral eddy fluxes rather than the small scale mixing at the base of the thermocline are key to maintaining the structure of the pycnocline and balance the downward transport of heat through Ekman pumping.

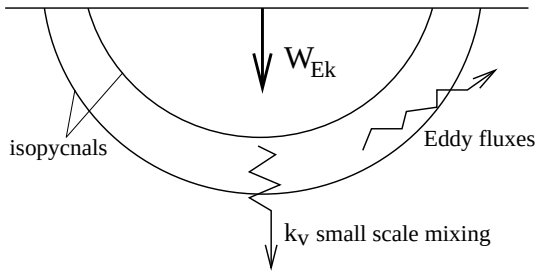

Figure 1.4: *Idealized pycnocline with Ekman pumping W_{Ek}, small scale vertical mixing and eddy fluxes as potentially important for determining its stucture and depth.*

Apart from that, Rahmstorf (1996) noted that a NADW flow rate being independent of D would be consistent with NADW not upwelling within the Atlantic. He obtains a linear relation of the Atlantic overturning with an interhemispheric meridional density difference in a global OGCM. Also, his hysteresis curves from the OGCM follow closely that of an interhemispheric box model related to the Stommel box model, using a linear scaling with the

density difference.
The scaling of equation (1.7) has been extensively tested mostly in single hemisphere models without wind forcing (de Verdiere, 1988; Marotzke, 1997; Zhang et al., 1999) and reviewed (Park and Bryan, 2000). For the scaling with diffusivity, power laws with varying exponents not necessarily equal to 2/3 have been found. Park and Bryan (2000) attributed discrepancies to a significant amount of spurious recirculation in the North Atlantic when the overturning is diagnosed in z-coordinates. Park (1999) included the non-linear mass transport law into Stommel's box model and concluded that this model has different stability properties.
There is a lack of studies with global ocean models including wind forcing where Southern Ocean wind-driven upwelling and diffusivity-driven upwelling in the Indopacific play potential roles that reassess the above scalings. Prange et al. (2003) used a global model and found an agreement with the 2/3 power law when taking into account the dependence of the density difference on vertical diffusivity. However, his calculations are associated with large error bars and his work focused more on the dependence of the hysteresis behavior on the amount of vertical mixing. It is shown in the framework of a global model that it is crucial to distinguish between different components of the Atlantic overturning such as the upwelling within the Atlantic and the South Atlantic outflow. The scaling with vertical diffusivity using a global coupled model is evaluated. The components are shown to scale differently with the vertical diffusivity. It turns out to be important to distinguish between the effect of vertical mixing on high and low latitudes and that a residual upwelling along the boundaries in the low latitude Atlantic exists even in the limit of no vertical and horizontal diffusion.
Another assumption of the scaling equation (1.7) as well as for the Stommel-type box models is that, since the meridional density gradient explains only a zonal flow with geostrophy, it scales like the meridional flow. One common picture to underline this assumption is that as the zonal flow is bounded by continental barriers it will lead to a secondary meridional flow: The North-South density difference leads to an eastward flow, which piles up water that downwells on the eastern wall. This resulting east-west gradient in the surface elevation then leads to a northward flow (Wright et al., 1995). This is a qualitative argument and has never been derived from the equations. Marotzke (1997) analytically derived an expression for the east-west pressure difference and therefore the meridional flow in relation to the North-South surface density difference for a one-hemisphere model without wind forcing and with the assumption that convection takes place in the eastern boundary. A linear relation between some measure of the interhemispheric meridional pressure gradient and the maximum Atlantic overturning has been found diagnosti-

cally in global OGCMs. Hughes and Weaver (1994) used a measure of the depth integrated baroclinic pressure, Thorpe et al. (2001) took the density integrated between the surface and 3000 m.
Gnanadesikan (1999) assumed the North-South pressure difference produces a frictional flow in the Western boundary and through that directly related the meridional pressure difference to the meridional flow. He extended the scaling from equation (1.7) and included two more processes into the conceptual model that would influence the pycnocline depth: Southern ocean winds through the Drake passage effect and Southern Ocean eddies. In his framework, Northern sinking is balanced by a diffusively driven upwelling in low latitudes and a wind-driven upwelling in the Southern Ocean minus an eddy return flow. He tested his theory qualitatively with OGCM runs employing different vertical mixing and eddy coefficients and Southern ocean windstresses. His model has been under intense investigation as a possible paradigm for the meridional overturning circulation (Saenko and Weaver, 2003; Klinger et al., 2003; Kamenkovich and Sarachik, 2004). However, Levermann and Griesel (2004) discussed that the model does not lead to a linear scaling with the pressure difference $\Delta\rho D$ which seems contradictory to the diagnostic outcome of OGCMs.
With this work, the relation of meridional pressure differences with the Atlantic overturning components is reassessed. The linear relation is explained by associating one significant meridional pressure difference through geostrophy directly to a zonal flow that sets up the maximum of the Atlantic overturning. The baroclinic pressure component is distinguished from the surface pressure component. The correlations at different depths and for hemispheric- or interhemispheric gradients are analyzed. The contradiction between the linear scaling of the density and pressure difference of the Stommel-type box models and the non-linear one of the Bryan and Cox (1967)-type models is identified. The model behavior is argued to be closer to the Stommel model with linear scaling and an Atlantic pycnocline depth being rather independent of vertical diffusivity.

1.4 Outline

This work is organized as follows:
The following chapter introduces the ocean model, which is based on the MOM-3 model from the Geophysical Fluid Dynamics Laboratory (GFDL), incorporating a non-linear free surface formulation and a very low diffusive tracer advection scheme not available in the original MOM-3 code. Particular focus is set on the splitting of the momentum integration into baroclinic

and barotropic modes which is associated with the decomposition of the pressure into the surface- and baroclinic pressure component. Also, a new time-stepping scheme is introduced.
Chapter 3 describes the circulations and tracer distributions arising from a standard model configuration with very low vertical mixing and discusses briefly the role of horizontal resolution and numerical diffusion for the representation of the Atlantic overturning in the model. Also, the outcome of experiments where the surface windstress is decreased in certain regions of the model is described.
In chapter 4, the role of eddies in the Southern Ocean and North Atlantic is assessed for determining the meridional pressure gradients that ultimately set up the components of the Atlantic overturning. The concepts of Nof (2003) and Gnanadesikan (1999) are discussed, extending the scaling analysis with meridional gradients to a variety of experiments not only varying in the eddy coefficient.
The first part of chapter 5 discusses the scaling of the coupled version of the ocean model with the vertical diffusivity in the framework of decomposing the Atlantic overturning into different components. The second part deals with the implication non-uniformly distributed vertical mixing has for driving an Atlantic overturning circulation and reassesses the scaling with vertical diffusivity by eliminating high latitude vertical mixing effects. Furthermore, the role played by numerical diffusion for driving an overturning circulation is discussed.
Chapter 6 provides the conclusions and outlines further research needs.

Chapter 2

Model description and the introduction of a new time stepping scheme

In this chapter, the ocean model used is described with particular emphasis on subgridscale parameterizations and the splitting of the solution of the velocity field in barotropic and baroclinic mode. This method leads to a separation in baroclinic and barotropic pressure components, which are discussed in chapter 4. A problem is pointed out in the time integration of the tracer and momentum equations in the nonlinear free surface formulation, that has not been identified as being crucial before. A new time stepping scheme is introduced, that conserves volume and tracers and the consequences of this new scheme are discussed.
The sea-ice component and simple atmosphere module are described briefly in sections 2.7 and 2.8.

2.1 The governing equations for the ocean model

The ocean model is the MOM-3 model developed at the Geophysical Fluid Dynamics Labaratory (Pacanowski and Griffies (1999)). One important feature as compared to previous MOM versions is that it incorporates a nonlinear free surface formulation, meaning the ocean volume is allowed to change through explixit freshwater fluxes coming from the atmosphere or sea ice. A free surface formulation is in contrast to the still widely used "rigid lid" formulation where the ocean volume and surface are fixed and freshwater fluxes need to be converted to a salinity flux. The governing equations are based

on the Navier-Stokes equations, subject to the Boussinesq and hydrostatic approximations:

- Momentum and volume conservation, formulated in spherical coordinates with longitude λ and latitude Φ:

$$\partial_t u = -\nabla \cdot (u\mathbf{u}) + v\left(f + \frac{u\tan\phi}{r}\right) - \frac{1}{r\rho_0\cos\phi}\partial_\lambda p + \partial_z\left(\kappa_m\left(\partial_z u\right)\right) + F^u \tag{2.1}$$

$$\partial_t v = -\nabla \cdot (v\mathbf{u}) - u\left(f + \frac{u\tan\phi}{r}\right) - \frac{1}{r\rho_0}\partial_\phi p + \partial_z\left(\kappa_m\left(\partial_z v\right)\right) + F^v \tag{2.2}$$

$$\partial_z w = -\nabla_h \cdot \mathbf{u_h} \tag{2.3}$$

$$\partial_z p = -\rho g \tag{2.4}$$

- Potential temperature and density conservation, and equation of state

$$\partial_t \theta = -\nabla \cdot \left(\theta\mathbf{u} + \mathbf{F}^\theta\right) \tag{2.5}$$

$$\partial_t s = -\nabla \cdot \left(s\mathbf{u} + \mathbf{F}^s\right) \tag{2.6}$$

$$\rho = \rho\left(\theta, s, p\right) \tag{2.7}$$

The prognostic variables are the two horizontal velocity components u, v, the potential temperature θ, salinity S and the free surface height η (see section 2.3.1). The vertical velocity w, density ρ and pressure p are diagnostically determined from the equations. The density is a non-linear function of temperature, salinity and pressure and is determined from the equation of state. All variables refer to the large scale quantitites that are resolved by the model. For the subgridscale processes, represented by the terms $\mathbf{F}^n$ and $\partial_z\left(\kappa_m\left(\partial_z u|v\right)\right)$, the typical eddy viscosity/diffusivity hypothesis is applied. They will be discussed in sections 2.5.1 and 2.6. The radial component of a fluid parcel is displaced by the mean radius of the Earth r ("thin-shell-assumption"). Correspondingly, the Coriolis component involving vertical velocity in the horizontal momentum equations is neglected.
The Boussinesq approximation consists of replacing density by its oceanic mean value $\rho_0 = 1.035\, g/cm^3$ except in the buoyancy term of the vertical momentum equation (2.4) and in the equation of state (2.7). It implies that the fluid is treated as incompressible ($\nabla \cdot \mathbf{u} = 0$). Equation (2.4) is the hydrostatic equation, relating the vertical pressure gradient to the

vertical distribution of density. With the hydrostatic aproximation, the vertical momentum equation basically reduces to equation (2.4) and the vertical velocity w is determined by continuity ((2.3)). The consequence of the Boussinesq approximation in OGCMs is that mass conservation is replaced by volume conservation, which for instance does not allow for steric effects to be represented. Steric sea level changes are caused when changes in the density of the water column imply an expansion or contraction of the column. They can be in the order of 1 m for global warming scenarios. This effect can however be diagnosed a posteriori from the model density distribution as a global correction factor. A method for modifying existing Boussinesq code to make it fully non-Boussinesq is described in (Greatbatch, 1994). Losch et al. (2003) have shown that otherwise the associated errors of the hydrostatic and Boussinesq approximations are at the noise level for coarse OGCMs.

In order to solve equations (2.1) - (2.4) and (2.5) - (2.7), the ocean is divided into a three dimensional latitude-longitude-depth grid and the equations are discretized on a staggered Arakawa-B grid (Arakawa, 1966), meaning scalars are replaced by half a grid cell from vectors. They are then solved in time and space by finite difference techniques. The next sections describe how the time integration is accomplished via a splitting of the momentum equations in baroclinic and barotropic modes.

2.2 Time integration

The integration in time of equations (2.1) - (2.4) is complicated by the fact that the solution includes waves with a range of timescales. To numerically guarantee a stable solution, the CFL criterion must be satisfied, meaning that the speed of the fastest waves in the model must be less than or equal to the grid spacing divided by the time step.

Since the fastest wave speed is that of surface gravity waves $\sqrt{gH} \simeq 200 - 250 m/s$, the timestep for a typical grid spacing at high latitudes in the order of 100 km would lead to time steps in the order of minutes. An integration of the whole momentum field with this time step would lead to a far too time consuming integration. Bryan (1969) introduced an efficient and fundamental technique for the solution of equations (2.1)-(2.4) which involves the separation of the velocities into the depth-average-velocity and the deviation from this depth average, also refered to as the barotropic and baroclinic modes.

2.3 Barotropic and Baroclinic Mode

The solution of the linearized momentum equations can be separated in orthogonal eigenmodes with different vertical structures of which the zeroth is denoted as the barotropic mode and the higher orders as the baroclinic modes (Gill, 1982). The barotropic mode is only weakly depth dependent and corresponds to gradients in surface elevation (therefore also called external mode) whereas the baroclinic mode is associated with undulations of the internal density surfaces (therefore also called internal mode). It is the integration of the barotopic mode that is the most time consuming since it is associated with the fast surface gravity waves. Strictly speaking, the depth averaged velocities in a free surface ocean model do not exactly correspond to the barotropic mode, since the barotropic mode is weakly depth dependent The baroclinic mode however is well approximated by the deviation of the depth average. Keeping this discrepancy in mind, in the following, "barotropic" or "external" is nevertheless used for the vertically averaged and "baroclinic" or "internal" for the depth dependent modes. The velocities from equations (2.1) and (2.2) are separated into their depth average and the deviation from depth average $\mathbf{u} = \bar{\mathbf{u}} + \hat{\mathbf{u}}$. Along the same lines, the horizontal pressure gradient terms from equations (2.1) and (2.2) need to be separated into baroclinic and barotropic pressure gradients.

$$\nabla_h p = \nabla_h p_a + g\,\rho\,(z=\eta)\,\nabla_h \eta + g\int_z^\eta \nabla_h \rho\, dz \tag{2.8}$$

The first term on the right hand side denotes the gradient of the surface air pressure, the second term the pressure gradient associated with the gradient in surface elevation η and the third term represents the vertically integrated baroclinicity in the water column above depth z. With the valid assumption that the area between $z = 0$ and $z = \eta$ is well mixed ($\rho(\eta) = \rho(z = 0)$) the pressure gradient can be separated in a term associated solely to the gradient in surface elevation η and a term associated with the baroclinicity of the water column:

$$\nabla_h p = \nabla_h(p_a + p_s + p_b) = \nabla_h p_a + g\nabla_h(\rho\,(z=0)\;\eta) + g\int_z^0 \nabla_h \rho\, dz \tag{2.9}$$

p_s is the surface pressure gradient and p_b denotes the baroclinic pressure gradient, arising from the baroclinic effects between depth z and the surface of the resting ocean $z = 0$. Hence, for $z < 0$ the depth dependent baroclinic pressure is separated from the depth independent atmospheric and surface pressures.

2.3.1 The barotropic system

To obtain the barotropic mode velocities, equations (2.1) and (2.2) need to be vertically integrated. With the Leibniz rule this yields for the horizontal vertically integrated velocity (U, V):

$$\partial_t U - fV = \partial_t \eta u(\eta) - \frac{H+\eta}{a\rho_0 cos\Phi}\,\partial_\lambda\left(p_a + p_s\right) + X \tag{2.10}$$

$$\partial_t V - fU = \partial_t \eta v(\eta) - \frac{H+\eta}{a\rho_0}\,\partial_\Phi\left(p_a + p_s\right) + Y \tag{2.11}$$

The separation of the pressures has been inserted and $H+\eta$ is the total ocean depth. X and Y are the "forcing terms" that incorporate the interactions with the baroclinic field:

$$X = \int_{-H}^{\eta} dz \left(-\nabla\cdot(u\mathbf{u}) + \frac{uvtan\Phi}{a} + \partial_z\left(\kappa_m \partial_z u\right) - \frac{\partial_\lambda p_b}{a\rho_0 cos\Phi} + F^u\right) \tag{2.12}$$

$$Y = \int_{-H}^{\eta} dz \left(-\nabla\cdot(v\mathbf{u}) + \frac{v^2 tan\Phi}{a} + \partial_z\left(\kappa_m \partial_z v\right) - \frac{\partial_\Phi p_b}{a\rho_0 cos\Phi} + F^v\right) \tag{2.13}$$

Note the baroclinic pressure gradient in the "forcing terms" and the depth independent surface and air pressure gradients in equations (2.10)-(2.11). To complete the barotropic system, the equation for the free surface height η is needed. Integration of the continuity equation (2.3) and applying the surface and bottom boundary conditions

$$w = -u_h \nabla_h H \qquad \text{at the ocean bottom} \tag{2.14}$$

$$w + q_w = \partial_t \eta + \mathbf{u}_h \cdot \nabla_h \eta \qquad \text{at the ocean surface} \tag{2.15}$$

yields

$$\partial_t \eta = -\nabla_h \cdot U + q_w \tag{2.16}$$

This is a fundamental balance with the free surface. The time tendency for the free surface height is determined by the horizontal convergence of the vertically integrated transport plus the fresh water flux through the sea surface. Equations (2.10), (2.11) and (2.16) form the barotropic system that is solved in time separately from the baroclinic system.

2.3.2 The baroclinic system

The baroclinic system solves for the depth dependent velocities $\hat{\mathbf{u}}$, that are the velocities after the vertical mean has been removed. This implies integrating equations (2.1)-(2.2) with the pressure gradient replaced by the baroclinc pressure gradient as in equation (2.9). After the integration, the vertical mean needs to be subtracted to obtain the pure internal mode velocity whose depth average is zero.
The total velocity is then essentially given by the sum of the barotropic and baroclinic part:

$$\mathbf{u} = \frac{\mathbf{U}}{H+\eta} + \hat{\mathbf{u}} \tag{2.17}$$

2.4 Asynchronous timestepping of tracers and momentum and a conservation problem arising with a nonlinear free surface

The ocean represents a system that has a very large frequency range - on the one hand, as discussed in the previous sections, the smallest timescale is governed by the speed of surface gravity waves. On the other hand, the timescale for the deep water masses to adjust to a changed surface forcing is in the order of a few thousand years. This large timescale is governed by the advective timescales and the diffusion of heat and salt from the surface downwards as incorporated in the tracer equations. An integration to an equilibrium thus requires an integration in the order of several thousand model years. As discussed in the previous sections, the integration of the momentum equations will be done with different timesteps for the baroclinic and barotropic mode: The cost intense integration of the three dimensional baroclinic velocity field can be done with a much larger timestep than needed for the barotropic integration. However, since the timestep for the tracer integration is governed by the much larger advective timescale, the three dimensional tracer field can be integrated with a timestep that is several times larger than even the baroclinic timestep.
A very time honored technique to accelerate the integration of both momentum and tracers is therefore the stretching of the tracer time step relative to the baroclinic momentum time step which accelerates the approach to equilibrium. The technique was introduced by Bryan (1984). It means, that tracers and momentum usually are integrated *asynchronously* as illustrated in figure 2.1. The tracer concentrations at

time $t+\Delta t_{tr}$ are exchanged with the velocity field at a different time $t+\Delta t_{bcl}$.

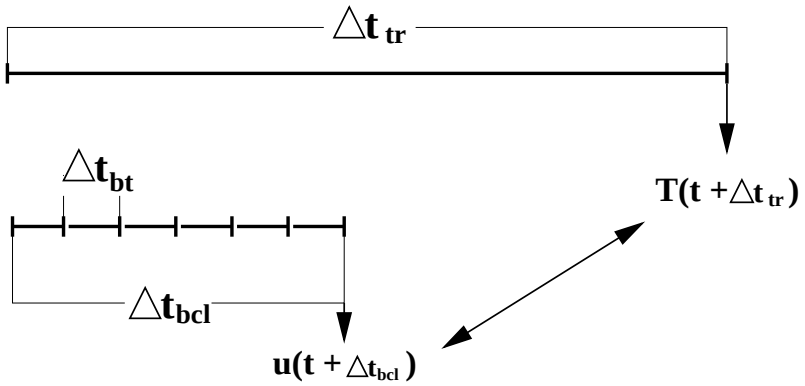

Figure 2.1: *Asynchronous time stepping with baroclinic timestep Δt_{bcl} and tracer timestep Δt_{tr} as in the original MOM-3 code. The barotropic system, which includes the integration of both free surface and vertically integrated transport, is integrated with timestep Δt_{bt}, but synchronously with the baroclinic system.*

The philosophy behind this is to create a new physical system with the same equilibrium solution but with modified timescales that decrease the frequency band of the system by distorting its physics. This is manifested in the phase velocities and amplitudes in the approach to equilibrium being different from the synchronous solution by a factor determined by the ratio of the tracer and baroclinic time step. If the equilibrium solution is unique and no transient states are of interest, this technique is completely valid. Without this acceleration method, the integration to equilibrium is not feasible and it is thus widely used in ocean general circulation models.

However - the time stepping as sketched in figure 2.1, leads to a valid simulation only when the ocean volume is prescibed as is assured with rigid lid or *linear* free surface formulations. Using a full nonlinear explicit free surface scheme, the effects of the undulating surface height are incorporated not only into the ocean dynamics but also into the tracer equations, which now explicitly take into account the presence of fresh water forcing. In MOM-3, the surface freshwater fluxes are held constant over one tracer timestep and hence, with the time stepping as in figure 2.1, while the tracers see a freshwater flux q_w of $\Delta t_{tr} \times q_w$, the ocean volume changes only by $\frac{t_{bcl}}{t_{tr}}$ times that.

2.4.1 A new time stepping scheme

The new time stepping scheme involves integrating the free surface and tracers synchronously (figure 2.2). It allows the integration to be volume and tracer conservative while still accomodating stretched tracer timesteps. The method introduces another 'distortion' into the system. As sketched in figure 2.2, there are now two kinds of asynchronisities: The first one is between the tracers and the baroclinic velocities and imposes distorted physics on the baroclinic system as discussed and introduced by Bryan (1984). The second asynchronisity is now between the free surface and the barotropic transport and introduces distortion in a similar way but into the barotropic system.

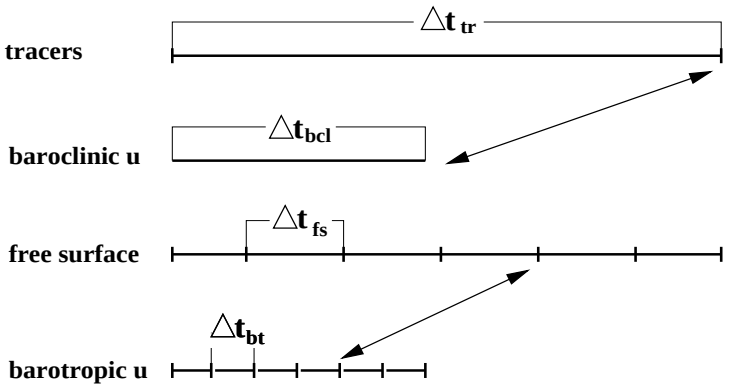

Figure 2.2: *New time stepping scheme, allowing for volume and tracer conservation. The arrows represent the asynchronisity. The barotropic system is now integrated asynchronously with* $N \times \Delta t_{fs} = \Delta t_{tr}$ *and* $N \times \Delta t_{bt} = \Delta t_{bcl}$.

In the following, we will describe the new timestepping in more detail and its implications for the barotropic system.
The introduction of unequal timesteps in the free surface and vertically integrated velocity integration is equivalent to introducing a factor α into the system:

$$\partial_t \, \eta' = -\nabla \, . \, \mathbf{U}'_{\mathbf{h}} + q_w \tag{2.18}$$

$$\alpha \, \partial_t \, \mathbf{U}'_{\mathbf{h}} = \partial_t \eta' \, \mathbf{u}'_h \, (\eta) + f \, \hat{z} \times \mathbf{U}'_{\mathbf{h}} - \frac{(H + \eta')}{\rho_0} \, \nabla_h p'_s + \mathbf{G}' \tag{2.19}$$

$$\alpha = \frac{\Delta t_{tr}}{\Delta t_{bcl}} = \frac{\Delta t_{fs}}{\Delta t_{bt}} > 1 \tag{2.20}$$

The system is written in vector form and $\mathbf{G}'$ represents the vector form of the forcing terms X, Y (equations (2.12) and (2.13)) for the distorted system. The distorted system has different velocities and free surface elevation, denoted with a prime, however for $\partial_t \longrightarrow 0$ the solutions transform into the non-distorted ones. We have chosen the timestep for the free surface to be our baseline timestep. Since the free surface integration is synchronized with the tracers, our 'clock' to measure the solution will be determined by the surface forcing that is held constant over one tracer timestep.
To achieve insight into how the solutions are affected, we consider the simplyfied linearized one-dimensional distorted barotropic system:

$$\partial_t \eta' = -H\ \partial_x U' \tag{2.21}$$
$$\alpha\ \partial_t U' = -g\ \partial_x \eta' \tag{2.22}$$

for which the solution is well known. The solutions are free waves with the following amplitudes and phase speed:

$$A'_U = \left(\frac{g}{H\ \alpha}\right)^{1/2} A'_\eta \tag{2.23}$$
$$c' = \left(\frac{g\ H}{\alpha}\right)^{1/2} \tag{2.24}$$

Hence, the distorted system is characterized by slower phasespeeds and a smaller amplitude ratio for the free waves. The CFL constraint necessary for linear stability now applies to the reduced phasespeed $c' = c/\sqrt{\alpha}$ and becomes:

$$(\Delta t_{fs} \Delta t_{bt})^{1/2} < \frac{2\Delta x}{(gH)^{1/2}} \tag{2.25}$$

With this constraint, the timesteps from figure 2.2 are given as follows:

$$\Delta t_{fs} \times N = \Delta t_{tr} \tag{2.26}$$
$$\Delta t_{bt} \times N = \Delta t_{bcl} \tag{2.27}$$
$$(\Delta t_{fs}\, \Delta t_{bt})^{1/2} =: \Delta t_{dist} \tag{2.28}$$

Through this, the number of timesteps N for the distorted barotropic system is given and the timesteps on the right hand sides are determined by the CFL constraints for the tracer-advection velocity, the internal wave velocity and the phase velocity of the distorted system respectively. The 'timestep' Δt_{dist}

is never used as a real timestep but it denotes the quantity for which the CFL constraint for the distorted system needs to be satisfied.
We have seen that introducing asynchronous integrations means to modify the phase speeds and amplitudes of the resulting wave solutions. Note that the same factor α will be introduced into the baroclinic system, since the integration between tracers and the baroclinic velocity is also asynchronous. This has been discussed by Bryan (1984) and will also affect the internal wave solutions. The difference resulting from a synchronous and an aysnchronous integration of the model can be interpreted as how large the departure from equilibrium is. However, in a model with seasonal forcing, the equilibrium is a quasi steady state that varies slowly and periodically with time. Since the partial derivative with respect to time will be small compared to the other terms in any case, the distorted system is expected to give a good approximation to the true system. We will analyze these differences in the next section.

2.4.2 Comparison of simulations with equal and nonequal timesteps

We conducted two runs with the model: The first one employs different time steps for the tracer and baroclinic velocity integration and the free surface and barotropic integration. In the second run the tracer and baroclinic timestep and hence also the baseline timesteps for the free surface and barotropic integration are the same and there is no asynchronisity. The amount of distortion for the first run is given by the factor $\alpha = 43200sec/3600sec = 12$.

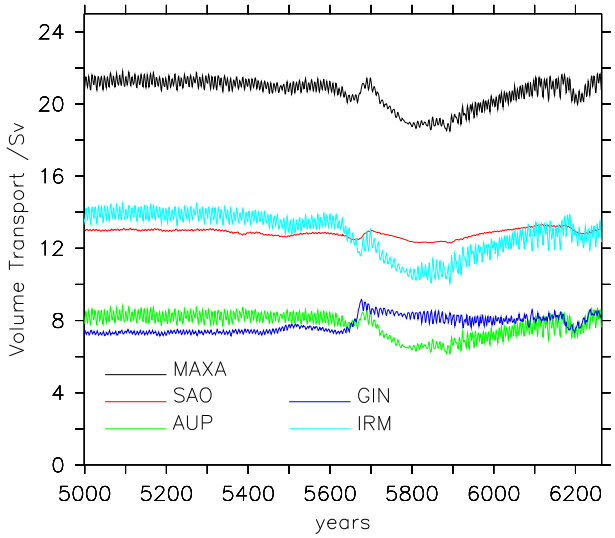

Figure 2.3: *Atlantic overturning components: Maximum Atlantic overturning (MAXA), South Atlantic outflow at 30°S (SAO), upwelling within the Atlantic (AUP) and sinking in the Greenland-Iceland-Norwegian (GIN) and Irminger (IRM) seas.*

Figure 2.3 shows a time series of the components of the Atlantic overturning where the integration has switched from asynchoronous to synchronous integration at year 5600. The solution reacts immediately and seems to go back to its original values after 800 years. Since a synchronous integration is very time consuming, the experiment has not fully reached equilibrium yet.

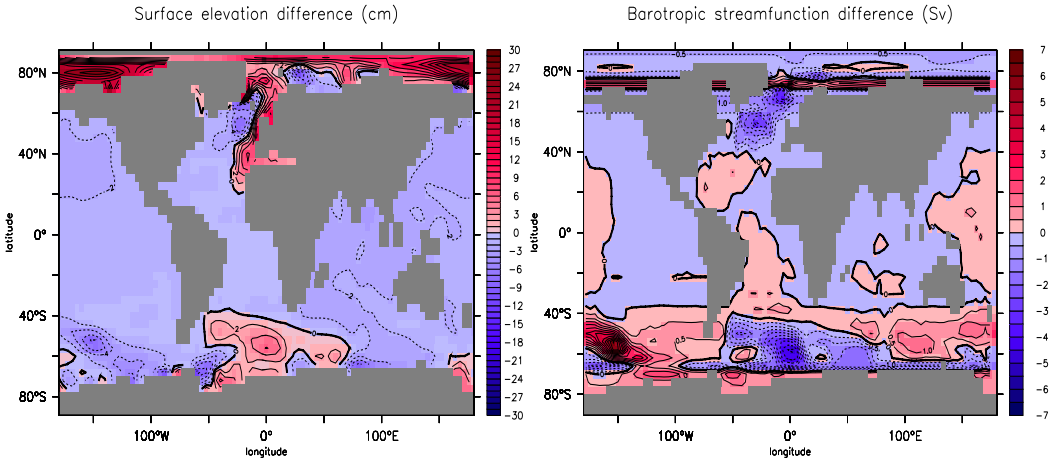

Figure 2.4: *Equal - Nonequal integration. Left: Free surface elevation difference (cm). Right: vertically integrated transport difference (Sv).*

Figure 2.4 compares the free surface elevation and vertically integrated transport at year 6700 in the two integrations. Significant differences occur in high latitudes where sea ice is present. Using a smaller tracer time step means that also the forcing, i.e. the surface freshwater fluxes and the windstress forcing are updated with a smaller timestep. The strong differences in surface elevation can be explained with changes in sea ice growth and decay when the timescale for the surface forcing is decreased: Typical timescales for sea-ice response to surface forcing are in the order of hours. In winter, surface cooling leads to the creation of sea-ice. The growth of sea-ice will however moderate the cooling due to the thermal insulation provided by the ice. As a result, cooling rates applied during intervals of one day are likely to be too high compared to the actual cooling rates that would occur if the ice cover were allowed to evolve on timescales of hours. As a result, with long times steps, ice production and salt rejection in winter are likely to be overestimates. The synchronous integration requires smaller time steps and so the representation of ice growth and surface heat and freshwater fluxes associated with it are better described.

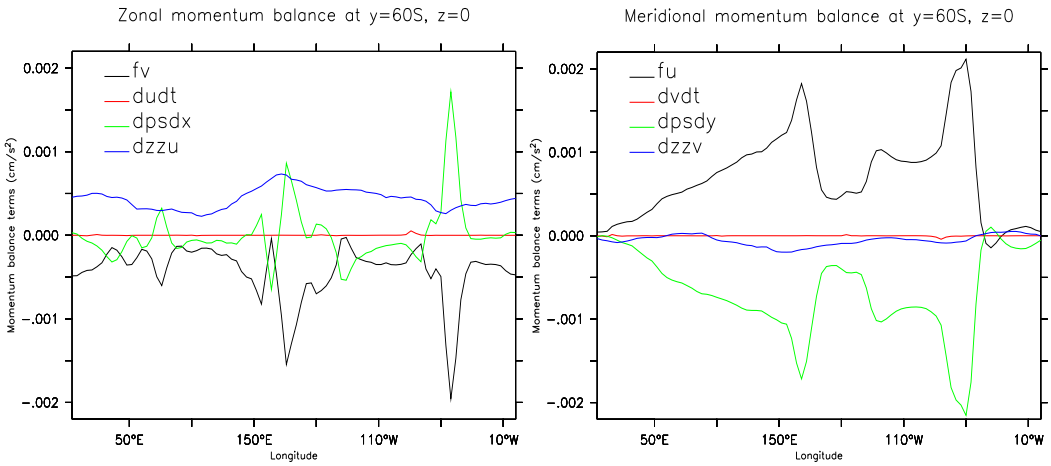

Figure 2.5: *Terms of the zonal (left) and meridional (right) momentum balance at 60°S at the ocean surface.*

With the above sea-ice effect it is not possible to assess the amount of distortion with figure 2.5 but a measure of the amount of introduced distortion is the magnitude of the time derivative. It is shown in comparison with the other momentum balance terms in figure 2.5 for the surface at 60°S at year 6250. The time derivative is practically zero for the runs. It is therefore reasonable to assume that the integration with unequal timesteps has very little effect on the solution in a quasi-steady seasonal equilibrium. The differences as apparent in figures 2.3 and 2.4 arise from the different update of the surface fluxes.

2.4.3 Notes on general time-stepping and filtering

Because the model is formulated in spherical coordinates, convergence of meridians near the Earth's poles reduces the effective grid size in longitude. At high latitudes, the solution may start to become unstable because of too large time steps. Instead of decreasing the time step, all prognostic variables are filtered with a Shapiro filter.
The general time discretization employs a centered leapfrog scheme. Associated with this or any other scheme which involves two time-steps are two solutions: a physical and a numerical one. The numerical one is the so-called computational mode and must be damped. For this purpose, the Robert Asselin time filter is applied to all tracers and velocity components. The barotropic integration employs a hybrid leapfrog and Euler forward-backward scheme. The checkerboard mode associated with the free-surface

is damped by employing an upstream scheme to compute the free-surface height.

2.5 Tracer advection and diffusion

The next two subsections discuss the advection and diffusion terms from the tracer equations. We will first see how the subgridscale processes F^θ and F^s from equations (2.5) and (2.6) are expressed with parameterizations, then the discretization of the tracer advection term is discussed.

2.5.1 The parameterization of subgridscale mixing in the tracer equation

There is the need in large scale ocean models to parameterize the effect of mesoscale eddies and turbulent mixing. Decomposing the quantities into a mean (denoted with an overbar, representing an average over space and time scales large compared to the eddy scales) and a departure from the mean (denoted with a prime), the tracer equations can be written:

$$\partial_t \overline{T} + \mathbf{u}_h \cdot \nabla_h \overline{T} + \overline{w}\, \partial_z \overline{T} = -\nabla_h \cdot (\overline{\mathbf{u}_h' T'}) - \partial_z \left(\overline{w' T'}\right) \tag{2.29}$$

T is a tracer that can be temperature, salinity or a passive tracer, $\mathbf{u}_h$ is the horizontal and w the vertical velocity. The right hand side of equation (2.29), which represents the effects of both mesoscale eddies and small scale mixing, needs to be parameterized in terms of the large scale quantities. A usual approach has commonly been to suppose a horizontal and vertical downgradient transfer (Fickian diffusion):

$$\overline{\mathbf{u}_h' T'} = -\kappa_h \nabla_h \overline{T} \tag{2.30}$$

$$\overline{w' T'} = -\kappa_v \partial_z \overline{T} \tag{2.31}$$

However, mixing of tracers in the ocean occurs mainly along surfaces of constant density and the above introduces large amounts of horizontal cross-isopycnal mixing in regions with steeply sloping isopycnals. To introduce a more accurate parameterization of the adiabatic mixing by mesoscale eddies into coarse resolution z-coordinate models, Redi (1982) introduced a mixing tensor for ocean circulation models that would mix tracers along isopycnal surfaces rather than horizontal surfaces. Yet, pure isopycnal diffusion (in the absence of surface fluxes) has no effect on the density distribution and is an incomplete representation of the effect of mesoscale eddies. An alternative

approach is given by the Transformed Eulerian Mean (TEM) formulation: It was first recognized in the atmosphere that properties are not advected by the Eulerian mean circulation $\overline{\mathbf{u}} = (\mathbf{u}_h, w)$ but by the residual circulation being the sum of the Eulerian mean and an eddy induced transport velocity $\mathbf{u}^* = (\mathbf{u}_h^*, w^*)$ which is comparable in magnitude and often in opposite direction to the mean flow. Equation (2.29) can be rearranged into its TEM formulation:

$$\partial_t \overline{T} + (\overline{\mathbf{u}_h} + \mathbf{u}_h^*) \cdot \nabla_h \overline{T} + (\overline{w} + w^*)\, \partial_z \overline{T} = \overline{R} \tag{2.32}$$

$$\mathbf{u}_h^* = \partial_z \mathbf{\Psi}, \quad w^* = -\nabla_h \cdot \mathbf{\Psi} \tag{2.33}$$

$$\Psi = \frac{\overline{\mathbf{u}_h' b'}}{\partial_z \overline{b}} \tag{2.34}$$

Ψ is the eddy vector-streamfunction (or quasi Stokes streamfunction), $b = -g\rho/\rho_0$ is buoyancy and ρ is the potential density. $\overline{R}$ represents the pure along- and cross isopycnal mixing processes. The eddy velocities have been constructed such that $\nabla \cdot \mathbf{u}_h^* + \partial_z w^* = 0$ which ensures tracer conservation between potential density sheets. Note that no attempt has been made to parameterize vertical eddy fluxes $\overline{w'b'}$ so that w^* is basically chosen such that the total velocity is divergence free.

The eddy buoyancy fluxes can now be parameterized following Gent and McWilliams (1990) and Gent et al. (1995) as horizontal transfer down the mean buoyancy gradient:

$$\overline{\mathbf{u}_h' b'} = -\kappa_{gm} \nabla_h \overline{b} \tag{2.35}$$

Then the eddy induced transport velocities are given by:

$$\mathbf{u}_h^* = \partial_z \left(\kappa_{gm} \mathbf{S}\right) \tag{2.36}$$

$$w^* = -\nabla_h \cdot \left(\kappa_{gm} \mathbf{S}\right) \tag{2.37}$$

$\mathbf{S} = -\nabla_h \rho / \partial_z \rho$ is the isopycnal slope. The parameterization can be seen as representing (approximately) the 'diffusion of thickness of an isopycnal', so the Gent-McWilliams (GM) velocity is directed towards decreasing isopycnal layer thickness. It thus mimics the effect of mesoscale eddies in the ocean that tend to 'flatten' isopycnals and reduce available potential energy.

By taking into account that the eddy-induced transport velocities are generally equivalent to antisymmetric components in the tracer mixing tensor whereas the symmetric components represent the irreversible downgradient

diffusion, the effects of subgridscale processes (including small scale mixing and eddy effects) can all be incorporated in one tensor $\underline{\mathbf{J}}$ (Griffies (1997)) so that the tracer equation becomes:

$$\partial_t T + \mathbf{u} \cdot \nabla T = \nabla \cdot (\underline{\mathbf{J}} \nabla T) \tag{2.38}$$

with

$$\underline{\mathbf{J}} = \begin{bmatrix} A_I & 0 & (A_I - \kappa_{gm}) S_x \\ 0 & A_I & (A_I - \kappa_{gm}) S_y \\ (A_I + \kappa_{gm}) S_x & (A_I + \kappa_{gm}) S_y & A_I S^2 + \kappa_v \end{bmatrix} \tag{2.39}$$

$(S_x = \partial_x \rho / \partial_z \rho,\ S_y = \partial_y \rho / \partial_z \rho)$
Here, the right hand side of equation (2.38) describes the F^θ and F^s from the governing equations (2.5) and (2.6). The mixing-tensor (2.39) now combines all subgridscale processes and we can summarize: A_I is the isopycnal diffusion coefficient and represents the pure diffusion of tracers isopycnally and tracer-downgradient, κ_{gm} is the eddy coefficient from the "Gent-McWilliams" parameterization and represents the isopycnal advection of tracers down the "thickness gradient", κ_v is the vertical mixing coefficient.It is important to note, that in the tracer equation, the formulation above with the "skew flux approach" for the eddy induced fluxes is equivalent to the formulation of the fluxes with the eddy induced advection velocity:

$$\begin{aligned} (\partial_t T)_{gm} &= \nabla \cdot \mathbf{F}_{skew} = \nabla \cdot \mathbf{F}_{adv} && (2.40) \\ \mathbf{F}_{adv} &= \mathbf{u}^* T = (-\partial_z \left[\kappa_{gm} \mathbf{S}\right] T,\ \nabla_h \cdot \left[\kappa_{gm} \mathbf{S}\right] T) && (2.41) \\ \mathbf{F}_{skew} &= (\kappa_{gm} \mathbf{S}\, \partial_z T,\ -\kappa_{gm} \mathbf{S} \cdot \nabla_h T) && (2.42) \end{aligned}$$

The skew flux is directed parallel to the tracer isolines, in particular, the horizontal component of the skew flux is directed down the tracer gradient and the vertical component is upgradient. Note that the net effect on the tracer concentration from the eddy parameterization will be zero if there are no isopycnal slope gradients, i.e. $\nabla \cdot \mathbf{F}_{skew} = 0$. (However, it can be nonzero if spatially varying coefficients are used). When the divergence of the skew flux is nonzero, the effect on tracer concentrations is such that a rotation of isolines occurs that tends to flatten isopycnals.

For the implementation of the isopycnal mixing in the ocean model, some stability constraints have to be considered. When the isopycnal slopes become steep, numerical stability can become an issue. The critical slope is

determined by the time step, grid size and the diffusivity. To ensure stability, the A_I, κ_{gm} are tapered in regions where slopes reach the critical slope. The isopycnal coefficient is tapered by a linear approximation of the hyperbolic tangent (Danabasoglu and McWilliams, 1995) and the κ_{gm} by a less strong tapering in a quadratic manner (Gerdes et al., 1991). This splitting of the tapering is not available in the origional MOM-3 code but was implemented to prevent excessive convection in the Southern Ocean when κ_{gm} goes too strongly to zero in the mixed layers. It is physically sensible to mimic the eddies associated with the instability of a mixed patch: the eddy induced circulation carries buoyancy towards the centre of 'convection' (to balance the buoyancy loss from the surface), the water then 'slides down' into the interior and is drawn away below. This process is essential for restabilizing the water column. The A_I on the other hand are tapered more strongly to prevent excessive vertical mixing in the mixed layers.
To ensure physical consistency with the hydrostatic approximation, a convection algorithm is applied that removes vertical density instabilities in the water column. Usually, convection parameterizations work such that the water column is mixed when it becomes unstable as a whole, leading to mixing over too large scales in a coarse model. The scheme employed here is a simplified version of the Paluszkiewicz and Romea (1997) scheme which was not in the original MOM-3 code. The idea behind this parameterization is that convection occurs in very narrow water columns, or plumes (Marshall and Schott, 1999) with spatial scales $\leq 1\,km$, thus well below the resolution of the model. The grid cells are assumed to be divided vertically into slices: if the veritcal density stratification turns out to be unstable, the uppermost slice is taken down to the level of neutral buoyancy, the slices above this level are shifted upward and the upper box is remixed. In this way, a mimimum amount of mixing is achieved in order to stabilise the vertical stratification of the water column.

2.5.2 Tracer advection

While the previous section was concerned with deriving expressions for the diffusion term of the tracer equations (2.5)-(2.6), this section is devoted to the discretization of the tracer advection part, namely the advection by the resolved portion of the velocity field :

$$\partial_t T = -\mathbf{u} \cdot \nabla T \tag{2.43}$$

Here, T stands for temperature, salinity or any passive tracer. The discretization of the tracer advection term can be particularly important as,

depending on the numerical scheme used, there are two important computational errors that are introduced: numerical diffusion and dispersion. Dispersion occurs when different wave components of the advected field propagate with different wave speeds. This leads to oscillations, causing over- and undershoots and unphysical solutions. Numerical diffusion on the other hand causes the advected field to be smeared out and erodes the gradients of the tracer distribution. These numerical errors are closely related to the order of approximation of the tracer advection equation by a difference scheme. Even-order schemes tend to be dispersive whereas odd-order schemes tend to be diffusive. To illustrate how numerical diffusion comes about, we consider a prominent example of a scheme introducing substantial amounts of numerical diffusion in coarse resolution ocean models: the first order upstream scheme. For simplicity, we consider the advection equation in one dimension, discretized with the upstream scheme, assuming a positive velocity u:

$$\frac{T_i^{n+1} - T_i^n}{\Delta t} = -u \frac{T_i^n - T_{i-1}^n}{\Delta x} \tag{2.44}$$

To estimate what the discretization (2.44) means for the solution, we compare it to the true solution by expanding the tracer concentration at grid point $(i-1)$ into a Taylor series:

$$T(x - \Delta x) = T(x) - \Delta x\, \partial_x T(x) + \frac{\Delta x^2}{2} \partial_x^2 T(x) - \frac{\Delta x^3}{3!} \partial_x^3 T(x) + ... \tag{2.45}$$

Doing a Taylor expansion in time as well and inserting both expansions into equation (2.44), by ignoring terms higher than second order and with setting $\partial_t^2 = u^2 \partial_x^2$ we obtain:

$$\partial_t T = -u\, \partial_x T + \kappa_{num}\, \partial_x^2 T \tag{2.46}$$

Solving the tracer advection equation with the upstream scheme is hence equivalent to solving equation (2.46), where an additional term that looks like a diffusion term with the numerical diffusivity $\kappa_{num} = (u\Delta x - u^2 \Delta t)/2$ is introduced. For typical values of $\Delta x = 100\, km$, $\Delta z = 100, m$ and $u = 20\, cm/s$, $w = 10^{-3}\, cm/s$ the introduced horizontal numerical diffusion is of the order of $10^4 m^2/s$ and the vertical one in the order of $5 cm^2/s$, which both are in the order or larger than the physical diffusivities. The advantage of the upstream scheme is that it does not introduce any numerical dispersion.

Another widely used scheme is the "central in time, central in space"(CTCS) scheme, which is second order accurate in time and space. As compared to

the upstream scheme, it is associated with negligible numerical diffusion. It however introduces large amounts of dispersion, most noticable near large tracer gradients. To eliminate these errors, the grid Peclet number $Pe = u\Delta x/\kappa$ needs to be smaller than 2 (κ here is the explicitly employed diffusivity). To satisfy the Peclet number criterion often means applying very large explicit diffusivities leading to a diffusively dominated tracer balance in regions where it is not justified.
The upstream scheme and the central difference scheme hence both minimize one kind of numerical error, at the expense of the other.

2.5.2.1 The Flux Corrected Transport scheme (FCT)

The philosophy of the FCT algorithm is based on the idea of employing a low order non-dispersive but diffusive scheme, to which a minimum amount of 'anti diffusive flux', as computed from the difference to a higher order non-diffusive scheme, is added, thus aiming at maximizing the benefits of each individual scheme and minimizing their respective numerical errors (Boris and Book (1973), Zalesak (1979)). It was implemented in MOM by Gerdes et al. (1991), using the flux difference of the CTCS scheme and an upstream scheme. As a first step, this difference is regarded as the largest "anti-diffusice flux"that can be used to correct the initial low order flux. The second step involves choosing anti-diffusive fluxes as large as possible by at the same time avoiding over- and undershoots. This is done by applying appropriate correction factors or limiters. We use here the flux limitation method as recommended by Zalesak (1979). Details of the whole algorithm can be found in Gerdes et al. (1991). The FCT algorithm results in smaller numerical diffusivites than from the pure upstream scheme, but, as we will schow in this work, still results in too large numerical diffusion.

2.5.2.2 The Second Order Moments scheme (SOM)

The SOM method (Prather (1986)) is a modified upstream scheme, based on the idea that the advected tracer field is preserved by taking into account moments of the subgrid tracer distribution of order 2 (in the FCT and CTCS schemes, only the grid mean values of the tracers are calculated, i.e. the zero moments). This results in very low numerical diffusivities. The subgrid tracer distribution in cell i for the x direction can be developed into a polynomial distribution of the form

$$T_i^n(x) = m_{0,i}^n + m_{x,i}^n K_x(x) + m_{xx,i}^n K_{xx}(x) \tag{2.47}$$

Where the K_{lm} form an orthogonal basis of the vector space of quadratic polynomials defined over the interval $0 \leq x \leq \Delta x$ (details of the selection of the orthogonal functions can be found in Prather (1986)). Note that we only consider one dimension. In one timestep, the fluid will be transported by $\delta = u\Delta t$ and the grid box is divided into left and right cells of widths δ and $\Delta x - \delta$ respectively. For each of the two subdivisions, the moments are calculated. After they have been transported, the moments for the left and right sides need to be recombined to obtain the new moments over the whole grid cell. It has been shown that the accuracy of the scheme compares with fourth order differencing schemes but is only as time consuming as a second order scheme. However, the storage of the moments up to order 2 requires a fair amount of memory. Note that for the advection in 3 dimensions, 10 terms are needed ("0,x,xx,y,yy,z,zz,xy,yz,xz"). For a more detailed description and for the implementation in MOM-3, see Hofmann and Morales-Maqueda (2004). The SOM scheme is the default tracer advection scheme for all experiments discussed in this work and its very low numerical diffusion is of extreme benefit for the representation of tracers and circulations in the model and the assessment of the role of explicitly prescribed diffusion.

2.6 Advection and diffusion of Momentum

Just as the isopycnal and vertical diffusion in the tracer equation, the 'mixing' of momentum is parameterized via Laplacian mixing. In addition to the vertical components from equations (2.1) and (2.2) the horizontal components are given by:

$$F^u = \nabla_h \left(A_m \nabla_h u \right) + \hat{z} \cdot \nabla_h v \wedge \nabla_h A_m \tag{2.48}$$

$$F^v = \nabla_h \left(A_m \nabla_h v \right) + \hat{z} \cdot \nabla_h u \wedge \nabla_h A_m \tag{2.49}$$

with cross-terms to assure angular momentum conservation and A_m is the horizontal viscosity.
The advection of momentum uses second order accurate centered differencing in space and time (CTCS). A few numerical contraints need to be fullfilled. As for the CTCS scheme and the Peclet number constraint for the tracers, the centered difference scheme for momentum results in the Reynolds number criterion, meaning $Re = u\Delta x / A_m$ needs to be smaller than 2. This would give a lower limit for the viscosity. On the other hand, to ensure stability, an upper limit on the viscosity is set by a constraint similar to the CFL criterion. To relax this condition, the horizontal viscosity is tapered by the cosine of the latitude. Finally, the Munk boundary layer needs to be resolved by at least

one grid point. The width of the boundary layer is given by $\delta \approx (A_m/\beta)^{1/3}$, where β is the meridional derivative of the Coriolis parameter. The width is determined from scale analysis for the balance between advection of planetary vorticity βv and the dissipation of relative vorticity through lateral friction Munk (1950)). For a model resolution of 100 km, A_m needs to be in the order of $10^9\, cm^2/s$.

2.7 Sea-ice component

The sea-ice model is the Ice and Snow Interfaces (ISIS) model developed by Fichefet and Maqueda (1997). It is a two-dimensional (latitude-longitude) thermodynamic-dynamic model. Like the ocean model, it uses a horizontal staggered Arakawa B-grid. The thermodynamics run synchronously with the atmosphere and the dynamics with the ocean. A few modiciations have been made in comparison to the original model, notably the thermodynamics are formulated in a two-layer system (one layer of snow and one layer of ice). Temperature profiles inside each layer are assumed to be parabolic rather than linear. The model takes into account both vertical and lateral growth and decay of sea-ice. Its prognostic variables are the surface temperature, the sea-ice and snow temperature, their thickness, their concentration, and the sea-ice velocities. The thermodynamics are an improved version of Semtner (1976). The model accounts for the presence of sea-ice, snow and leads. It takes into account the heat capacity of ice and snow. Unresolved ice floes of different thickness contribute differently to conductivity, resulting in a larger heat conductivity than for a uniform distribution. To account for this, an effective snow and ice heat conductivity, corresponding to a uniform distribution between zero and twice the ice thickness, is employed. The model takes into account the storage of latent heat ("brine damping") in internal brine pockets in the ice which are formed due to the penetration of shortwave radiation into the sea-ice, which melts it internally. This heat is released by refreezing of the brine pockets, retarding the surface temperature dropping below the freezing point in autumn. Snow-ice formation is taken into account: when the load of snow on ice is large enough to depress the snow-sea-ice interface below the water level, leading to the infiltration and freezing of sea-water into the submerged snow. Whenever the temperature below the surface leads to below-freezing temperatures, it is reset to the freezing point and the corresponding latent heat released taken into account as a source term for the ocean temperature, simulating heat release via frazil-ice formation. The reader is referred to Fichefet and Maqueda (1997) for a thorough description of all parameterizations and their effect on the model performance. The sea-

ice dynamics allows the sea-ice to flow under the effect of winds and currents and to self-interact, deforming. The dynamics employs an elasto-visco-plastic rheology formulation (Hunke and Dukowicz, 1997) conserving mechanical energy. This scheme represents a modification of the standard Hibler (1979) visco-plastic rheology, in which sea-ice is allowed to flow plastically for normal strain rates and to deform in a linear viscous manner for very small strain rates. Inertial terms (the advection of momentum) is neglected. Advection is thus applied to the ice and snow concentration, their volume per unit area, their enthalpy per unit area, and the latent heat per unit area contained in brine pockets. As in the ocean model, the advection scheme employed is that of Prather (1986) and at high northern latitudes a Shapiro filter is applied to all prognostic quantities to remove the instabilities due to the convergence of meridians.

2.8 Atmosphere

The ocean model is driven by heat and moisture fluxes computed from "bulk"formulae using observed climatological data from the atmosphere. The fluxes are calculated separately for sea-ice and leads. The atmosphere-ocean heat flux is given by the sum of the radiative (downward longwave radiation and net solar radiation at the surface) and turbulent fluxes (sensible and latent heat fluxes). Absorbed shortwave radiation is calculated as in Zillmann (1972) over open water and as in Shine (1984) over sea ice. Net surface logwave radiation is parameterized following Berliand and Berliand (1952). Turbulent heat and momentum fluxes formulations are those of Large and Pond (1981) and Large and Pond (1982) over the ocean and of Parkinson and Washington (1979) over sea ice. The surface air temperatures, specific humidities and winds needed for these calculations are derived from long-term monthly mean climatologies calculated from NCEP reanalysis fields. (Kalnay et al., 1996). The humidity climatologies are not directly used in the flux calculations. Rather the effective atmospheric fields consist of the climatological values q_a^{clim} plus anomaly terms δq_a and a term that accounts for atmospheric transport of water vapour with $\gamma_q = 1 - 2$ days.

$$\partial_t (\delta q) = \left(\frac{\partial F_s}{\partial q} \right)_{q=q^{clim}} \delta q + \frac{1}{\gamma_q} (q_{clim} - q) \tag{2.50}$$

where F_s is the net surface freshwater flux (positive upward). The ocean freshwater flux is given by precipitation, evaporation, river runoff and by sea ice creation or melting. Precipitation is taken directly from the climatology, while river runoff is calculated via restoring to Levitus et al. (1994) sea

surface salinities along the coastlines if the model simulated salinity is smaller than the observed. As a result, the only dependence of F_s on q is due to turbulent evaporation.

This atmospheric module is suited for simulations that stay relatively close to the present day ocean, consistent with the NCEP climatology. The presumably most important feedback missing is the temperature feedback. For the calculation of the fluxes, the prescribed atmospheric temperatures from the NCEP climatology are used, with no feedback of the ocean heat transport on the atmospheric temperatures.

Chapter 3

Model circulations and tracers - sensitivity to tracer advection, resolution and windstress

This chapter introduces the outcome of model simulations with respect to the representation of tracers and circulations and particular emphasis on the Atlantic overturning circulation. It should be noted that the basis for these experiments was the ultimate goal to set up a model suitable for climate studies, notably regarding the representation of the meridional overturning in the Atlantic. Hence, a wealth of sensitivity experiments exists, all of which cannot receive detailed attention and analyses. We will however outline the most interesting aspects of these simulations that can be related to the outcome of the experiments in the subsequent chapters.
The first section 3.1 describes the outcome of a model baseline setup that employs very low vertical and Gent-McWilliams eddy mixing coefficients and will be shown to realize a purely wind-driven state of the Atlantic overturning. We then study the role of horizontal resolution and tracer advection scheme in section 3.2 and discuss their role in achieving a present day Atlantic overturning circulation without the need to use a restoring to sea surface salinities. Finally, section 3.3 discusses briefly the role of the windstress in different regions of the ocean model for determining the strength of the Atlantic overturning components.

3.1 A standard configuration

Our standard model configuration is one in which a very low vertical diffusivity and Gent-McWilliams eddy diffusion is applied in order to be able

to successively add more mixing in chapters 4 and 5. Note that the standard configuation is not meant to be one that has been configured to achieve in the best possible way realistic circulations and tracer distributions. The vertical mixing coefficient is at the low end of what is usually employed in ocean models but it is consistent with what has been found in measurements at thermocline depths (section 1.1).
The baseline configuration employs a horizontal resolution of $4°\times4°$and 24 vertical variably spaced levels ranging from 25 m thickness at the surface to ca. 500 m at depth (table 3.1). The topography is based on the $1/12°$ETOPO5 dataset (National Geophysical Data Center, 1988).
The horizontal viscosity is $3.5 \times 10^5\, m^2 s^{-1}$ at the equator, tapered with the cosine of the latitude to guarantee stability in high latitudes. It ensures, the Munk boundary layer is resolved with one grid point. A constant vertical viscosity of $10 \times 10^{-4} m^2 s^{-1}$ is applied. Mixing of tracers is done with an isopycnal diffusion coefficient of $A_I = 2000\, m^2 s^{-1}$ and a Gent-McWilliams skew diffusion coefficient $\kappa_{gm} = 100\, m^2 s^{-1}$. The vertical diffusivity is set to $\kappa_v = 0.1\, cm^2 s^{-1}$ (compare tensor 2.39, note that for convenience we use different units for the vertical diffusivity compared to the isopycnal ones throughout this whole work, since they differ by several orders of magnitudes). For the advection of tracers, the SOM tracer advection scheme (section 2.5.2.2) is used. No horizontal diffusion of tracers is applied. The timesteps for the momentum and tracer integration are the ones from section 2.4.2: $\Delta t_{tr} = 4320\, sec = 1/2\, day$; $\Delta t_{bcl} = 3600\, sec$; $\Delta t_{dist} = 330\, sec$.

level	depth (m)	Δz (m)	level	depth (m)	Δz (m)
1	12.50	25	13	876.81	212.98
2	37.50	25	14	1108.48	250.83
3	62.50	25	15	1378.48	289.16
4	87.50	25	16	1686.81	327.01
5	112.50	26.50	17	2032.52	336.46
6	140.54	32.50	18	2413.75	397.46
7	177.50	44.34	19	2827.76	428.62
8	229.21	61.74	20	3271.00	455.72
9	301.00	84.27	21	3739.21	478.25
10	397.76	111.37	22	4227.50	478.25
11	523.75	142.38	23	4730.51	507.49
12	682.52	176.53	24	5242.50	513.49

Table 3.1: *Depths to the tracer and velocity grid points and vertical grid extends.*

Runoff from the rivers in the real ocean is very fresh and extends only within a few meters vertically. We have seen that taking data from a runoff database with monthly mean estimates from major rivers is problematic in coarse resolution models with surface grid boxes extending over several tens of meters in depth, leading to extremely fresh single grid cells. Therefore the approach was taken to represent river runoff via a restoring to observed Levitus et al. (1994) sea surface salinities (SSS) only along the coastlines to mimic the effect of river runoff within the coarse resolution grid cell. The diagnosed runoff depends crucially on the amount of vertical mixing employed close to the surface. Higher vertical mixing will mix the freshwater from the surface downward and leads to much larger river runoff restoring fluxes than with a small vertical mixing. The approach taken here is to choose the diagnosed runoff that would best fit the data and still lead to reasonable SSS. A run with zero vertical diffusion at the surface seemed the best choice as the vertical diffusion near river mouths where stratification is high is likely to be much weaker than the interior mixing. The vertical mixing coefficient in the model, κ_v, strictly speaking, mimics only the interior mixing. The

diagnosed river runoff accounts for 1.4 Sv for the global annual mean, 0.1 Sv for the Arctic ocean and 0.15 Sv for the Atlantic.

3.1.1 Tracers

The model has been run for 8000 years, starting from Levitus initial conditions for salinity and temperature and zero velocities. Figure 3.1 shows sea surface temperatures and salinities as compared to the Levitus (1982) climatology. Since heat- and freshwater fluxes in the model are determined from climatologies, it is expected that the surface concentrations are close to observations. Any difference can be attributed to erroneous representations of model phyiscs and numerics within the error margins of the observed climatology. This is the advantage of using climatologies for computing the fluxes as compared to restoring boundary conditions. A restoring can correct for the erroneous model physics and representation of transports and hence disguise studies. Concerning SST, the most striking difference is they are too cold around Antarctica, with the zero-line extending too far northwards (sea-ice, no flux limitation for SOM method). The main discrepancy in SSS occurs in the North Atlantic at around 50°N, where they are too fresh. Since atmospheric freshwater fluxes as well as the amount of freshwater from sea ice melting are realistic, the discrepancy results from an anomalously broad East Greenland current that imports freshwater from the Arctic ocean into the North Atlantic. This is a consequence of the coarse resolution. In reality, most of the freshwater does not leave the Greenland-Iceland-Norwegian (GIN) sea, but recirculates back in the Jan Mayen current and partly in a thin boundary current around Greenland and into the Labrador sea. However, within the GIN sea, the frontal strucure is relatively well resolved and we will discuss the importance of this aspect in the next section.

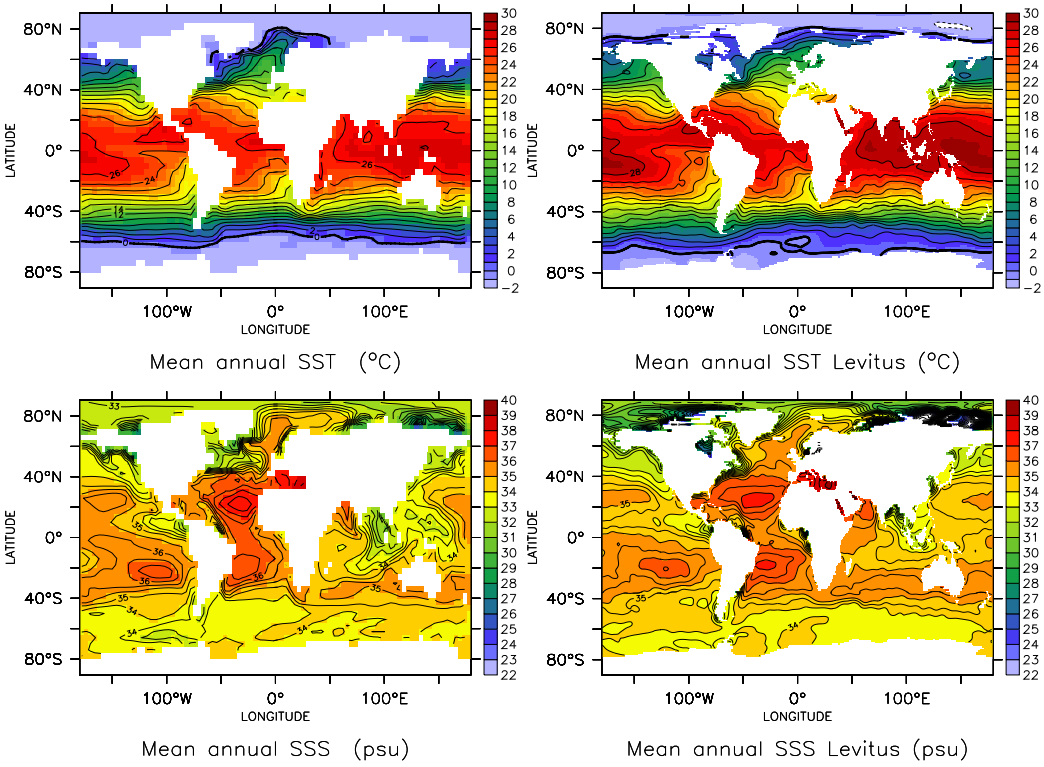

Figure 3.1: *Sea surface temperatures and sea surface salinities for the model (left) and Levitus (right).*

Insight into the deep tracer distributions can be gained from the salinity and temperature sections in figures 3.2 for the Atlantic ocean and 3.3 for the Pacific ocean. The southward flowing NADW, with a salinity of around 34.9 psu and the northward flowing AAIW are apparent in the salinity sections. Note also the upwelling of NADW in the Southern Ocean up to the surface. The deep Pacific ocean appears too stratified in temperature as compared to observations. The salinity and temperature structures of the upper ocean until a depth of 1500 m however are relatively well represented. Hence, the low interior vertical mixing of 0.1 cm^2/s is consistent with observations of mixing and seems also consistent with the modelled upper ocean tracer distribution. Increasing the vertical mixing worsens the upper ocean distributions (not shown), but it improves the temperature sections with respect to the deep and bottom temperatures.

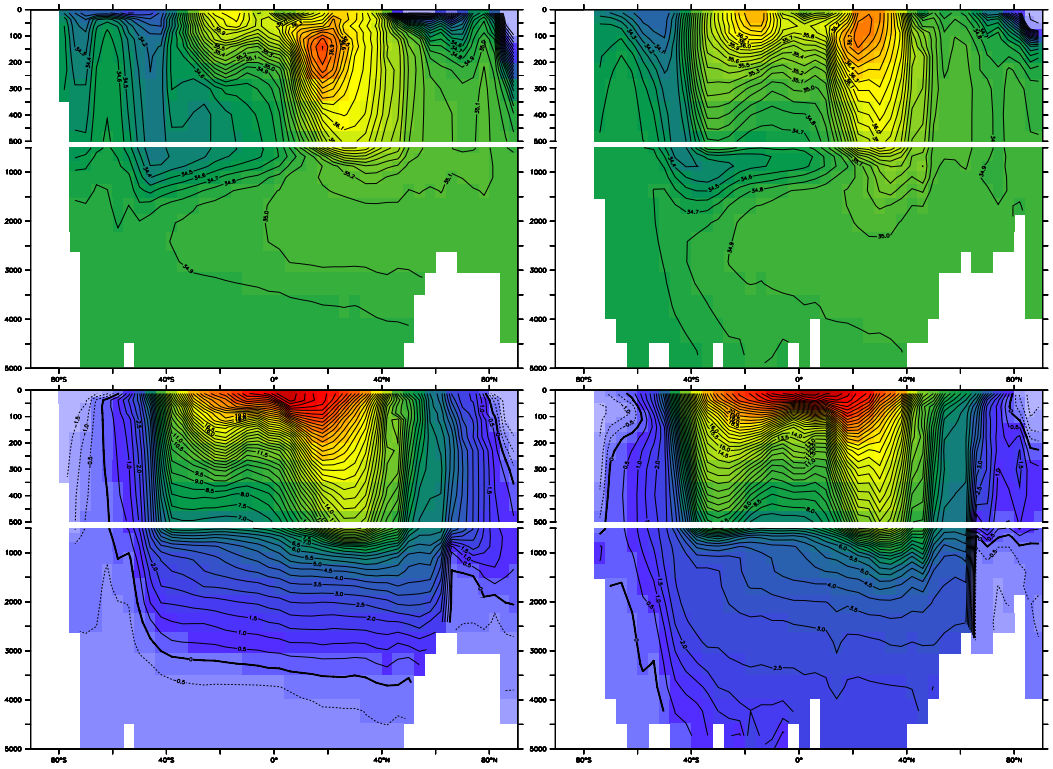

Figure 3.2: *Annual mean salinity (psu, upper panel) and temperature (°C, lower panel) sections, zonally averaged over the Atlantic, including the Atlantic segment of the Southern Ocean. Left: Model. Right: Levitus interpolated on model grid. Upper 500 m are enlarged*

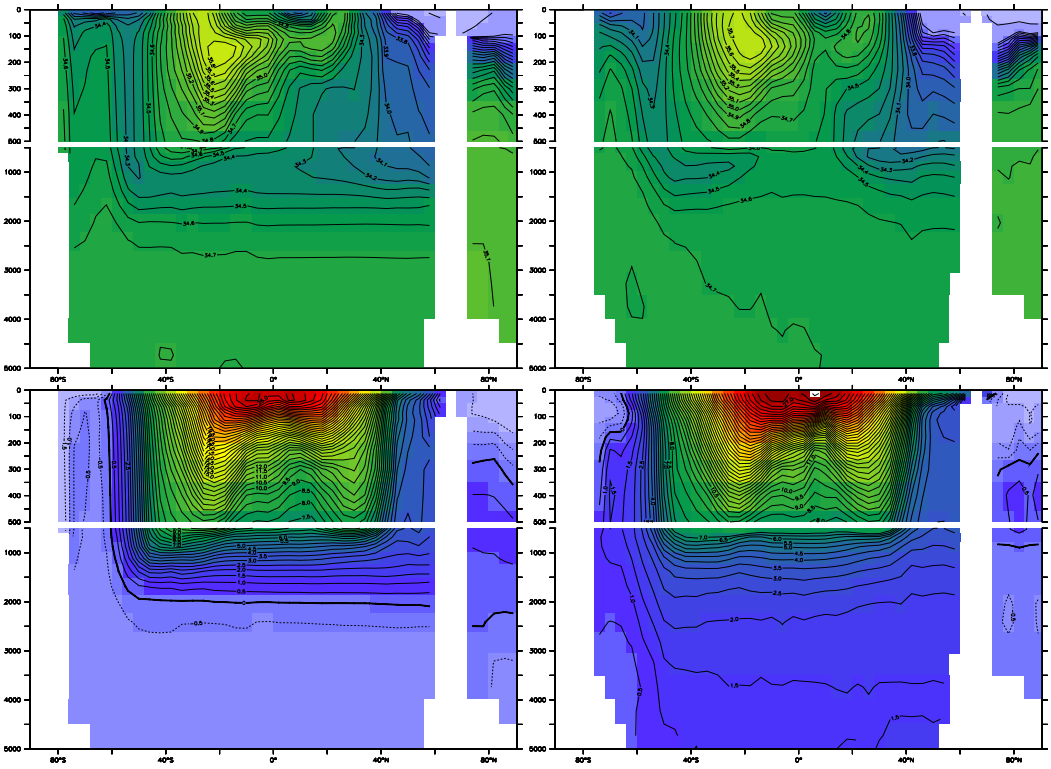

Figure 3.3: *Annual mean salinity (psu, upper panel) and temperature (°C, lower panel) sections, zonally averaged over the Pacific, including the Pacific segment of the Southern Ocean. Left: Model. Right: Levitus interpolated on model grid. Upper 500 m are enlarged.*

Overall, in spite of a very low Gent-McWilliams (GM) eddy and vertical mixing coefficient, surprisingly good tracer distributions are obtained.

3.1.2 Circulation

Figure 3.4 shows the Atlantic, Indopacific, global and barotropic streamfunctions. The Atlantic overturning has a maximum of ca. 20 Sv, which is rather strong as compared to the observational estimates of Ganachaud and Wunsch (2000) of 15±2 Sv and compared to a recent estimate from Talley et al. (2003) of 18± 5 Sv). Ca. 12 Sv of NADW outflow in the Southern Ocean at 30°S, leaving a localized upwelling cell of 8 Sv within the Atlantic Ocean. There is a total net soutwards transport over the Greenland-Iceland-Norwegian sills of about 6 Sv, which is comparable to the sum of observational esimates

of ca. 2.4-2.9 Sv across Denmark Strait and the estimate for the Iceland-Scotland ridge of 2.4-2.7 Sv together (Dickson and Brown, 1994). About 1 Sv of AABW flows into the Atlantic. From the global and Indopacific streamfunctions it is apparent that there is no deep upwelling in the Indopacific and all NADW upwells winddriven in the Southern Ocean. The barotropic transport is relatively well represented as compared to observations. The strength of the subtropical gyres in the North Atlantic and North Pacific are 27 and 34 Sv respectively. The Antarctic Circumpolar Current has a strength of 100 Sv. Note, that with an increase of the GM coefficient from $100\,m^2s^{-1}$ to $250\,m^2s^{-1}$ the ACC transport drops down to 80 Sv and the maximum Atlantic overturning to 14 Sv.

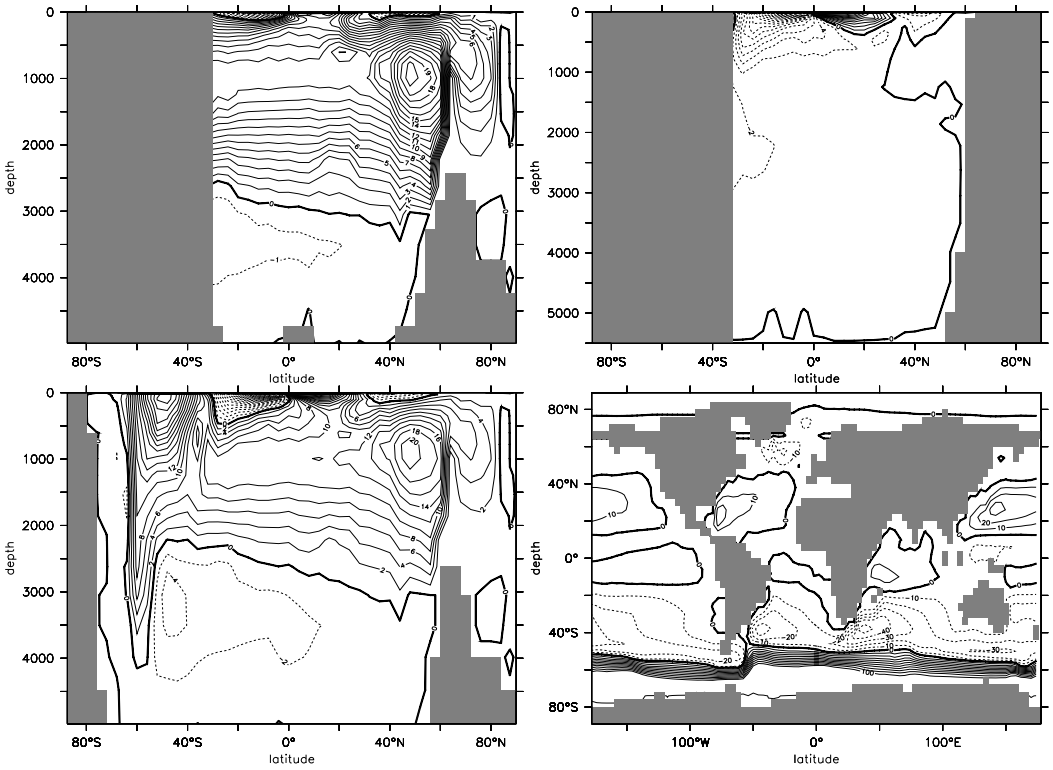

Figure 3.4: *Streamfunctions. Atlantic (upper left), Indopacific (upper right), global ocean (lower left) and barotropic streamfunction (lower right). Contour intervals are 1 Sv, 2 Sv, 2 Sv and 10 Sv respectively.*

Figure 3.5 shows the mixed layer depths as computed from the sigma-theta criterion, determined as the depth from which on the density varies

more than $0.0125\,kgm^{-3}$ as compared to the surface density for a given water column. Deep intense convection takes place in the Greenland-Iceland-Norwegian (GIN) sea and a relatively weak convection down to around 1600 m takes place in a few grid cells in the region of the Irminger (IRM) sea, which has been confirmed in observations (Bacon et al., 2003). In contrast to observations there is no convection in the model Labrador sea, due to the wide transport of freshwater around greenland. Note there is very little convection in the Southern Ocean despite the relatively low Gent-McWilliam eddy coefficient. This is directly a consequence of applying the low-diffusive SOM tracer advection scheme (see section 3.2). The although limited amount is however still sufficient to lead to the spreading of cold deep water masses within the Atlantic and Indopacific oceans as shown in figures 3.2 and 3.3. Note that the summer and winter sea ice distributions and thicknesses are reasonably well represented for both hemispheres (not shown).

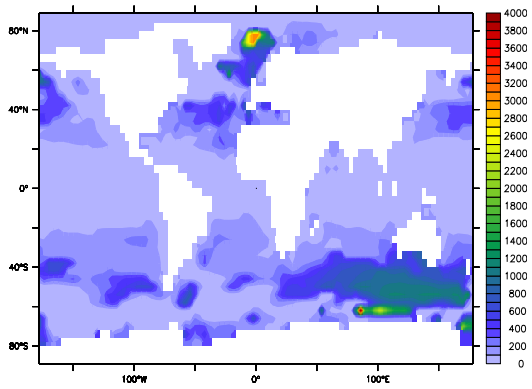

Figure 3.5: *Mixed layer depths (m) as determined from sigma-theta criterion from the surface down.*

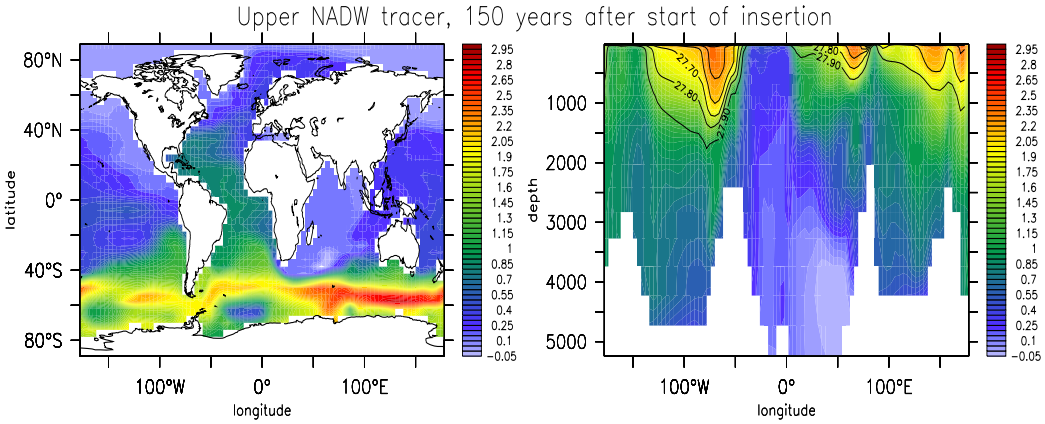

Figure 3.6: *Concentration of upper NADW tracer in percent of the maximum value at the source, 150 years after start of insertion in the southwards flowing WBC at a latitude of 10°S and at a depth of 1500 m. Left: at the ocean surface. Right: depth profile at 60°S, also shown is a contour overlay of potential density.*

A tracer is inserted in the core of the southwards flowing western boundary current in the Atlantic ocean at a depth of 1500 m and a latitude of 10°S to trace the upper NADW. Figure 3.6 shows the concentration of the tracer after 150 years of insertion. The tracer flows southwards in the western boundary current and then turns eastwards to join the ACC. On its way around Antarctica it then upwells along isopycnals and reaches the surface at the latitudes of the maximum of the ACC (left panel of figure 3.6). It is also apparent in the figure how the tracer has started to travel back towards the deep water formation regions in the Northern North Atlantic. The right panel of figure 3.6, showing a depth section at 60°S, illustrates how the tracer upwells along isopycnals (contours in the figure). It reveals the wave-like structure of the isopycnals, correlated with the topography. Upwelling occurs above topographic stuctures such as the Drake passage and the Kerguelen Plateaux. It should be noted that the SOM tracer advection scheme has been applied without a flux limiter, that guarantees full monotonicity. Therefore, slightly negative concentrations of the passive tracer can occur.

3.2 The role of horizontal resolution and tracer advection scheme

The ultimate goal of setting up the ocean model was to be able to achieve a realistic present day Atlantic overturning circulation (and tracer distribution) with the prescribed freshwater fluxes as available from data without the need of using a restoring to sea surface salinities. Freshwater fluxes as diagnosed from the restoring to present day sea surface salinities often correct for deficiencies in the ocean model transports rather than reflecting realistic freshwater fluxes (Killworth et al., 2000).

We study in this section the same version of the model with the same mixing parameters and vertical resolution, except first with a slightly lower horizontal resolution of $5° \times 5°$and then with the same horizontal resolution but with the FCT tracer advection scheme instead of the much less diffusive SOM tracer advection scheme. In both modified versions, an Atlantic overturning can only be achieved with a restoring to sea surface salinities.
With the lower resolution there are fewer grid cells in the GIN-sea region. The shut down of the Atlantic circulation can possibly be explained partly through the fact that the gyre circulation in the GIN-sea and the East-Greenland and Norwegian current system are not resolved properly. Specifically, the fresh East-Greenland current extends too far into the GIN-sea interior and leads to a prevention of convection there. Even with restoring, the overflow over the Greenland-Iceland-Scotland sills is lost. However, the horizontal viscosity with this coarser resolution is increased to $7.2 \times 10^5 m^2 s^{-1}$ and the shutdown of the AMOC could also be a result of the more sluggish currents. Also, the baseline tracer timestep is increased to 1 day.
In the configuration with the FCT tracer advection scheme, the AMOC is shut down as well without restoring to SSS due to the introduction of either horizontal or vertical numerical diffusion. An increase in the explicit vertical diffusion parameter in high latitudes in the model can potentially lead to a decrease in overturning (see chapter 5). However, in an experiment where tracer advection was split into vertical SOM- and horizontal FCT-advection an AMOC could not be achieved either. It is hence concluded that it is the *horizontal* numerical diffusion that prevents the establishment of an Atlantic overturning.

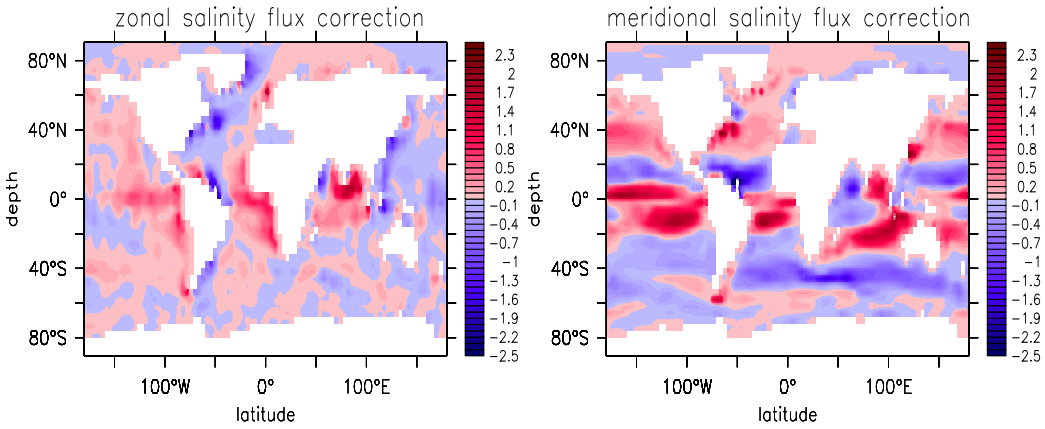

Figure 3.7: *FCT - flux correction at the ocean surface for salinity as computed from the difference between an upstream and CTCS tracer advection scheme ($cms^{-1}psu$) for the experiment with Atlantic overturning and a 30-day restoring to sea surface salinities.*

Figure 3.7 shows the horizontal components of the flux corrections that are applied with the FCT scheme, i.e. the minimum amount of diffusive fluxes needed to guarantee stability. These fluxes are high in the equatorial current system and in the region of the gulfstream and GIN-sea. They act to smear out the tracer gradients associated with these currents and tend to inhibit convection in the GIN- and IRM sea. The meridional flux correction is also high in the Southern Ocean within the ACC where they on the other hand lead to an increase in convection and formation of AABW. The introduced numerical vertical diffusion depends on the vertical velocities and rather tends to enhance the overturning (chapter 5, section 5.3.4).

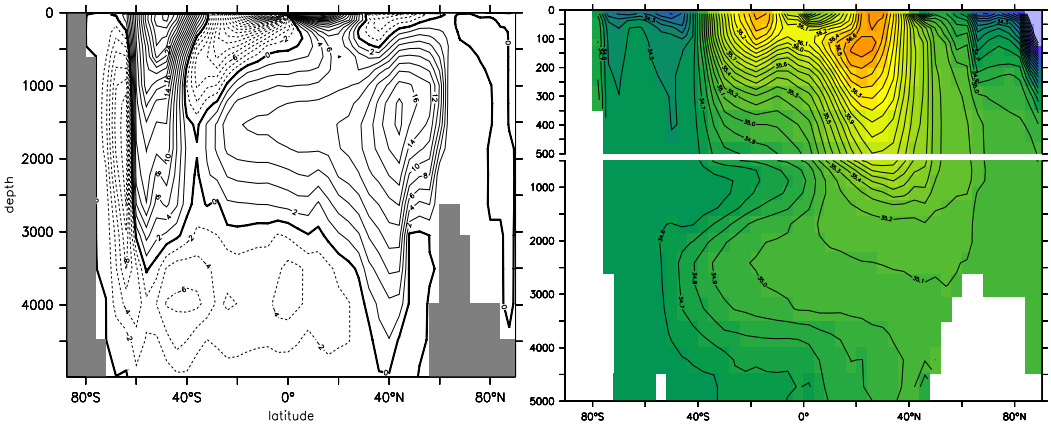

Figure 3.8: *Experiment employing the FCT tracer advection scheme and a restoring to sea surface salinities. Left: Global streamfunction, contour interval is 2 Sv (to be compared to lower left panel of figure 3.4 with the global streamfunction of the same experiment but without restoring and with the SOM tracer advection scheme). Right: Annual mean salinity (psu) zonally averaged over the Atlantic (to be compared to upper left panel of figure 3.2 for the SOM tracer advection scheme).*

Although with the SOM and FCT experiments the same explicit mixing parameters are used, the global streamfunctions indicate qualitatively different circulations (figures 3.8 and lower left panel of figure 3.4). It is apparent from the global streamfunction (left panel in figure 3.8) that, in spite of the explicit low vertical diffusion coefficient, most or all upwelling of NADW (mixed with Circumpolar deep water from the Southern Ocean) now takes place in the Indopacific Ocean. The salinity distributions substantially worsened, especially in the Southern Ocean, where the spurious horizontal diffusion leads to excessive convection and destroys the salinity distribution (right panel of figure 3.8).

3.3 The role of the windstress in different regions

Several studies have demonstrated the sensitivity of the ocean circulation to the wind-stress field applied (Oke et al., 2004), not only in the Southern Ocean (Toggweiler and Samuels, 1995) but also particularly in low and northern high latitudes (Timmermann and Goosse, 2004). We now briefly discuss 5 different runs, where the wind-stress field is reduced to 1 percent of the

original value in different regions and the vertical diffusivity was increased to $0.3\,cm^2/s$:

STD-VD03	standard configuration with $\kappa_v = 0.3\,cm^2 s^{-1}$
WSO-VD03	winds $\times$ 0.01 south of 40°S
WTROP-VD03	winds $\times$ 0.01 between 40°S and 40°N
WGIN-VD03	winds $\times$ 0.01 north of 60°N
NOWIND-VD03	winds $\times$ 0.01 everywhere
REST-NOWIND-VD03	winds $\times$ 0.01 everywhere and restoring to SSS

Table 3.2 summarizes the outcome of these experiments with respect to the components of the Atlantic overturning. The vertical diffusion was increased to be able to still drive an Atlantic overturning when wind driven upwelling is prohibited.
In the limit of no windstress (NOWIND-VD03), there is no Atlantic overturning and the table shows, that the shutdown of the AMOC can be attributed to the elimination of the effect of the windstress on sea surface salinities in the tropical regions. With restoring to sea surface salinities, the AMOC is reestablished (REST-NOWIND-VD03) without winds. Then, the maximum Atlantic overturning is reduced from 19.2 for STD-VD03 to 14 for REST-NOWIND-VD03, which can mainly be attributed to a decrease in GIN-sea sinking.
A very interesting aspect is, that the experiment without Southern Ocean winds (WSO-VD03) has the same maximum Atlantic overturning and almost the same South Atlantic outflow as the one with winds (STD-VD03), although the upwelling characteristics are completely different (figure 3.9).

EXP	MAXA	SAO	AUP	GIN	IRM
STD-VD01	21.0	12.9	8.0	7.2	13.8
STD-VD03	19.2	12.5	6.7	5.5	13.7
WSO-VD03	19.6	11.1	8.5	5.6	14.0
WTROP-VD03	0	0	0	0	0
WGIN-VD03	19.5	12.7	6.7	4.4	15.1
NOWIND-VD03	0	0	0	0	0
REST-NOWIND-VD03	14	8	5.9	1.8	12.1

Table 3.2: *Atlantic overturning components for the experiments with reduced wind stress in different regions and increased vertical diffusivity. Maximum Atlantic overturning (MAXA), South Atlantic outflow (SAO), Atlantic upwelling (AUP), sinking in GIN sea (GIN) and sinking in Irminger sea (IRM). For comparison, the outcome of the run from section 3.1 is included as well (STD-VD01).*

For the STD-VD03 experiment, ca. 12 Sv upwell mainly within the Southern Ocean whereas in the WSO-VD03 experiment, there cannot be any wind-driven upwelling in the Southern Ocean and ca. 11 Sv upwell in the Indopacific. A vertical diffusivity of $0.3\,cm^2s^{-1}$ is sufficient to support almost the same outflow as is accomodated by Southern ocean winds for STD-VD03. There is no Deacon cell and the Antarctic Circumpolar Current is very weak. Note that with a vertical diffusivity of $0.1\,cm^2s^{-1}$ only a shallow and weak overturning exists (not shown).

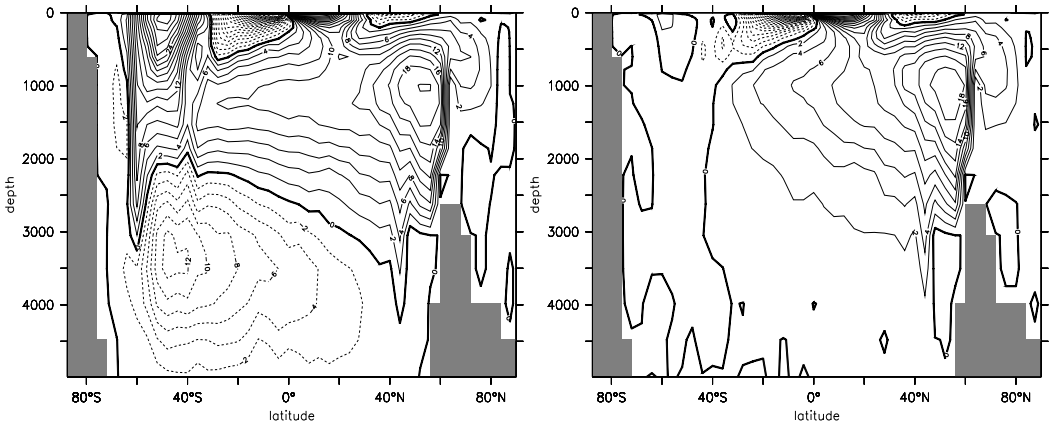

Figure 3.9: *Global streamfunctions. Left: STD-VD03. Right: WSO-VD03. Contour intercal is 2 Sv.*

3.4 Discussion

A version of the ocean model with a very low vertical and GM eddy coefficient is assessed where North Atlantic Deep Waters are upwelled purely winddriven in the Southern Ocean. The numerical diffusion is found to be crucial for the representation of the Atlantic MOC in the model. The horizontal diffusion of the FCT tracer advection scheme has been idendified to lead to a shutdown of the Atlantic overturning, that can be reestablished with a restoring to sea surface salinities. In the Southern ocean, it tends to enhance convection whereas in the North Atlantic it tends to destroy the polar front and the frontal structures in the GIN-seas leading to a shutdown of convection. Both processes work against the establishment of an Atlantic overturning circulation, at least in the limit of a very low vertical diffusion coefficient. The relevance of this aspect will be further discussed in section 5.3.4 where the explicit driving of the Atlantic overturning in the form of vertical mixing is assessed.
The reaction of the Atlantic overturning components is studied when the windstress is drastically reduced in different regions of the ocean. The remarkable result is that an *interhemispheric* Atlantic overturning exists even without Southern ocean winds and the South Atlantic outflow has in fact the same magnitude as with Southern Ocean winds for a vertical diffusivity of $0.3\,cm^2s^{-1}$. This is in contrast to the hypotheses put forward by Nof (2003) as discussed in chapter 5, who argues that the South Atlantic outflow is to first order determined by the Southern Ocean windstress. According to

him, without Southern Ocean winds, any deep water formation in the North Atlantic is required to upwell within the Atlantic basin.

Chapter 4

The relation of meridional pressure gradients and NADW volume transport - the role of eddies in different regions

We show in this chapter how changes in the density gradients in the Southern Ocean and North Atlantic effect the water inflow into the Southern Ocean on the one hand and the deep water formation in the North Atlantic on the other hand. To do so, we cause modifications in the density gradients by changing the magnitude of the Gent and McWilliams (1990) eddy thickness diffusivity in different regions of the ocean. Our focus here is not on how the representation of baroclinic eddies effects the simulated ocean circulation, but, in a more conceptual way, on how changing the density gradients in different regions of the ocean may change the volume transports.
In section 4.3 of the chapter we investigate the relation between meridional pressure gradients at different locations and the meridional volume transport in the model. We show that a linear relation can simply be explained in terms of a significant meridional pressure gradient that is related to a zonal flow through geostrophy. We also discuss the relations with the different pressure components. Since we are interested in the influence of pressure gradients in a wind-driven Atlantic overturning configuration, this is all done in the limit of very low vertical mixing. Section 4.4 discusses the conceptual picture put foward by Nof (2003) (described in section 1.2) in the light of changing density gradients under constant wind forcing. In the following section 4.5 the previous analyses are extended to a variety of experiments including increased vertical mixing and different surface forcings. We comment on the approach taken by Gnanadesikan (1999), who related Southern Ocean eddies

and wind stress, diapycnal upwelling driven by diapycnal mixing and deep water formation in the North Atlantic to changes in the pycnocline depth. Discussing the relation of meridional gradients to the Atlantic overturning is essential refering to the classic paper by Stommel (1961) who related the meridional density difference directly to the overturning. The results of this chapter are summarized in Griesel and Maqueda (2005) and related to the analyses in Levermann and Griesel (2004) and Levermann et al. (2004).

4.1 Baseline model setup

The baseline configuration of the model is as described in chapter 2 and section 3.1, except that we now apply an even lower vertical mixing coefficient of $0.05\,cm^2s^{-1}$ as compared to the $0.1\,cm^2s^{-1}$. Together with the low diffusive SOM tracer advection scheme this gives us the opportunity to test the model's behaviour in the limit of very low vertical mixing. The background Gent-McWilliams (GM) eddy coefficient is set to $100\,m^2s^{-1}$ on top of which the GM coefficients are increased succesively in the Southern Ocean and North Atlantic (section 4.2).

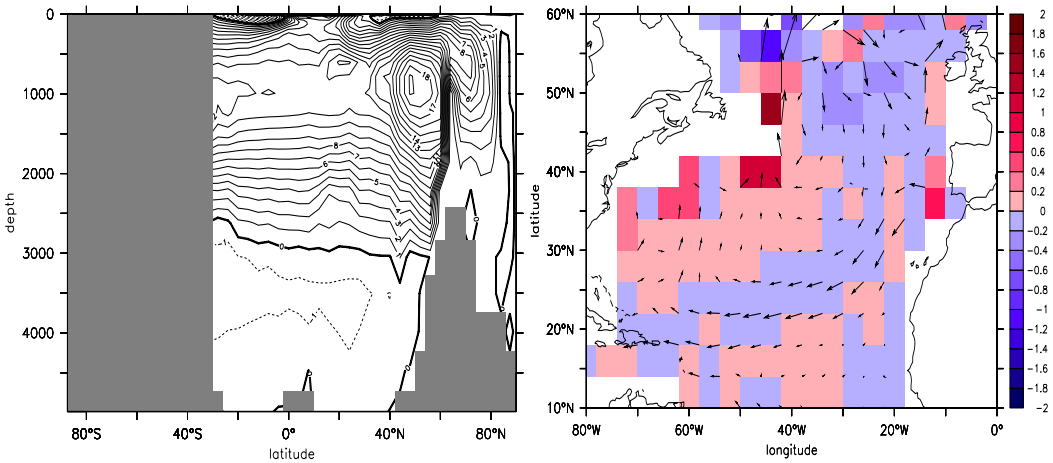

Figure 4.1: *Standard configuration with* $\kappa_v = 0.05cm^2s^{-1}$. *Left: Atlantic overturning streamfunction. Right: upwelling (red) and horizontal currents at 1000 m.*

Figure 4.2 shows the Atlantic overturning streamfunction for the baseline configuration in the left panel and the Atlantic upwelling in Sv at a depth of ca. 1000 m (precisely the 992 m w-grid cell depth) in the right panel. Again, it should be emphasized that even with a vertical mixing coefficient

of only $0.05\,cm^2s^{-1}$ the maximum of the Atlantic overturning is around 19 Sv (being ca. 1 Sv smaller than with a vertical mixing of $0.1\,cm^2s^{-1}$) and with a South Atlantic outflow of 11 Sv (being the same as with $0.1\,cm^2s^{-1}$). Upwelling of North Atlantic Deep Water (NADW) takes place mainly in the Southern Ocean with the exception of a small upwelling cell of 8 Sv within the Atlantic, taking place relatively localized between latitudes of around 35 - 50°N. This upwelling is shown in the right panel of figure 4.2 together with the horizontal currents. The depth of 1000 m corresponds to the depth of the maximum Atlantic streamfunction. The upwelling (red) occurs predominantly along the western boundary at latitudes where the flow at depths above 1000 m detaches from the coast and turns eastward, and for depths below 1000 m turns westward into the western boundary current. The zonal integral of the horizontal currents in figure 4.2 is almost zero and we will denote this level in the following as the 'level of no mean motion'.

We stress, that this localized upwelling occurs in spite of the very low horizontal and vertical mixing. Veronis (1975) attributed this upwelling to spurious horizontal diffusion at steeply sloping isotherms at the Western Boundary Current, associated with strong diapycnal fluxes from the ocean interior (Veronis effect). The inclusion of isopycnal diffusion as compared to purely horizontal one and the Gent-McWilliams parameterization was seen to indeed partly remove this kind of upwelling (Böning et al. (1995),Lazar et al. (1999)). However, due to the low horizontal (and vertical) diffusion, the Veronis effect does not seem to be at play here.

Huck et al. (1998) argued, that the upwelling along the boundaries is not only the consequence of horizontal diffusion but also depends on the formulation of momentum dissipation. They show that Laplacian friction with a no-slip boundary condition generates very large vertical (diapycnal) transports at lateral boundaries whereas a formulation with Rayleigh friction and no-normal-flow boundary conditions reduced the upwelling.

Yang (2003) argued that spurious upwelling along the boundaries could be the result of a poorly resolved western boundary layer. In our configuration, the western boundary layer is only 'resolved' by one grid point and the horizontal scale for dissipating the vorticity imposed by the wind stress curl is fixed. As discussed by Yang (2003) this could potentially lead to spurious horizontal flow convergences and divergences.

We will see in the next section that with higher Gent-McWilliams eddy coefficients in the North Atlantic, the boundary upwelling is reduced.

4.2 Eddies in the North Atlantic and Southern Ocean and their influence on the Atlantic outflow and maximum overturning

We now apply different magnitudes of the Gent-McWilliams eddy coefficient on top of the baseline configuration in the Southern Ocean south of 40°S (SO) and in the North Atlantic north of 60°N (NA). The latter corresponds to the GIN-sea region where deep water formation takes place. Also discussed are experiments where the coefficient is increased in the North Atlantic between the equator and 60°N (TROPNA). The following coefficients are used: 250, 500, 1000 and 2000 $m^2 s^{-1}$ for SO and NA and TROPNA experiments on top of the background 'thickness' diffusion of 100 $m^2 s^{-1}$. The following notations are used: MAXA for maximum Atlantic overturning, SAO for South Atlantic outflow of NADW at 30°S, AUP = MAXA - SAO for the upwelling within the Atlantic Ocean, GIN for the overflow from the Greenland-Iceland-Norwegian Seas and IRM for the sinking south of the sill close to Irminger Sea.

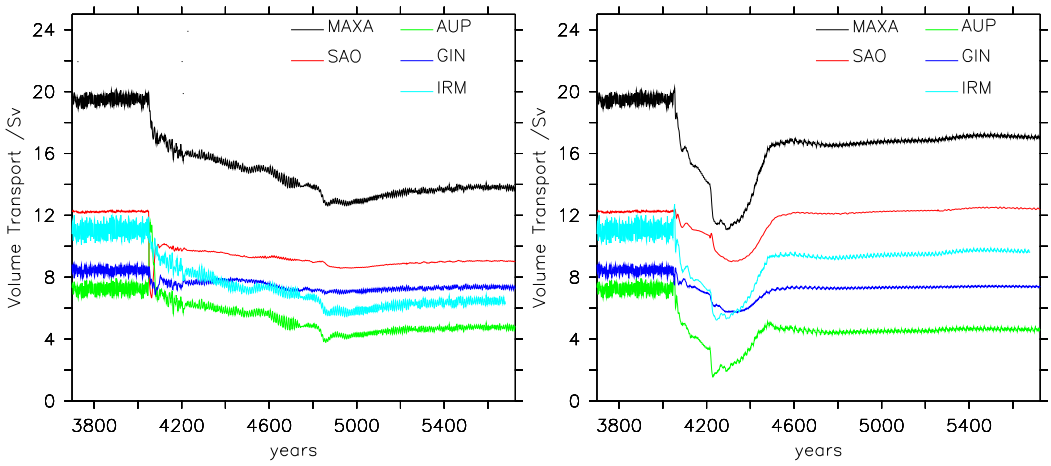

Figure 4.2: *Time series of 'switch-on' experiments. Left: SO1000. Right: NA1000. The switch occured in year 4050.*

Figure 4.2 displays time series of the different volume transport components of the Atlantic overturning, where the eddy activity is 'switched on' in year 4050 from the baseline configuration to SO1000 and NA1000. In both experiments, the maximum Atlantic overturning is decreased, however more drastically in the SO1000 case. In the SO1000 experiment, eddies act immediately to reduce the inflow into the Atlantic, however, since the maximum overturning and deep water formation are not reduced as much, there is an

initial drastic increase in the upwelling within the Atlantic in the first 100 years. It then takes another 800 years to reach a new equilibrium in which the deep water formation has adapted to the decreased South Atlantic inflow and outflow. In the NA1000 experiment, there is an initial decrease in all variables, the equilibrium state however is characterized by a decrease in the maximum Atlantic overturning of only 3 Sv that can mainly be attributed to a decrease in IRM sinking. The South Atlantic outflow goes back to its original amount.

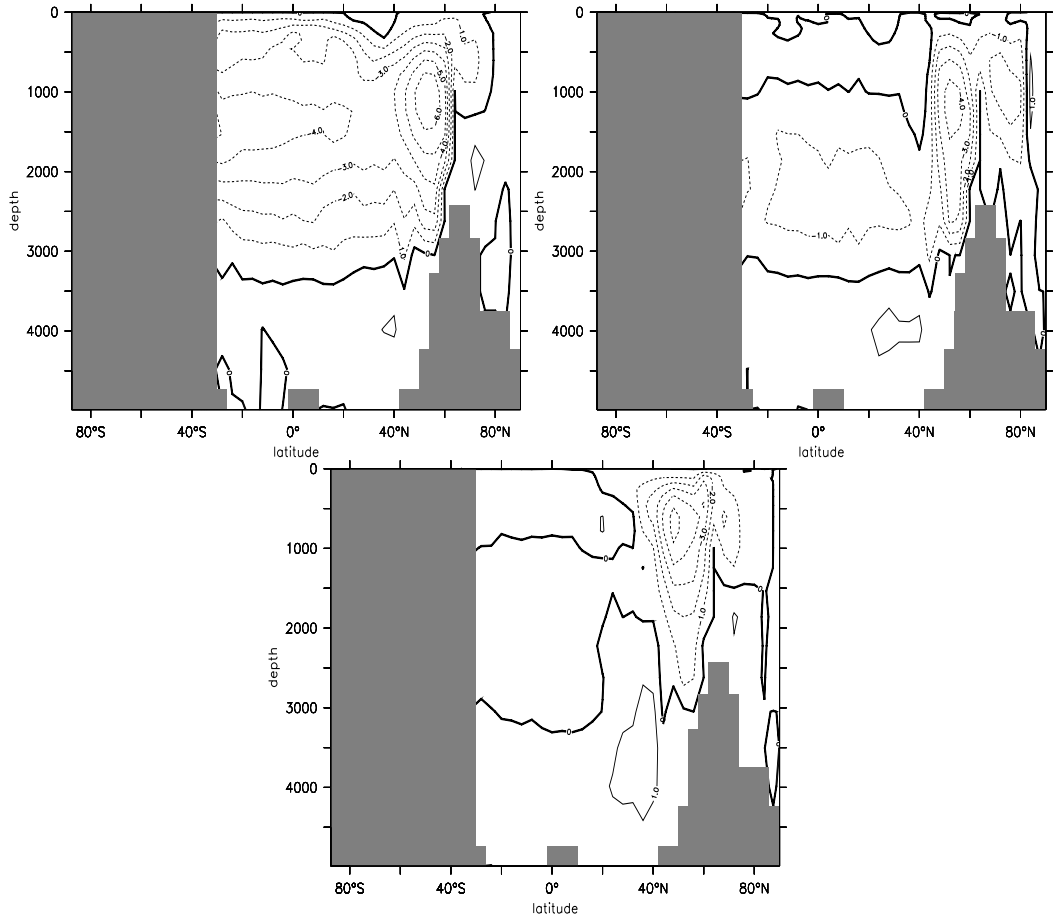

Figure 4.3: *Atlantic overturning streamfunction difference. Upper left: SO1000-STD. Upper right: NA1000-STD. Lower panel: TROPNA1000-STD.*

Figure 4.2 shows the Atlantic streamfunction differences with respect to the standard configuration for the SO1000, NA1000 and TROPNA1000 experiments. When enhanced eddy mixing is applied south of 40°S, both the

South Atlantic outflow and the upwelling within the Atlantic are decreased. For both experiments with increased coefficients in the North Atlantic only, changes occur only north of 40°N where the deep water formation occurs.

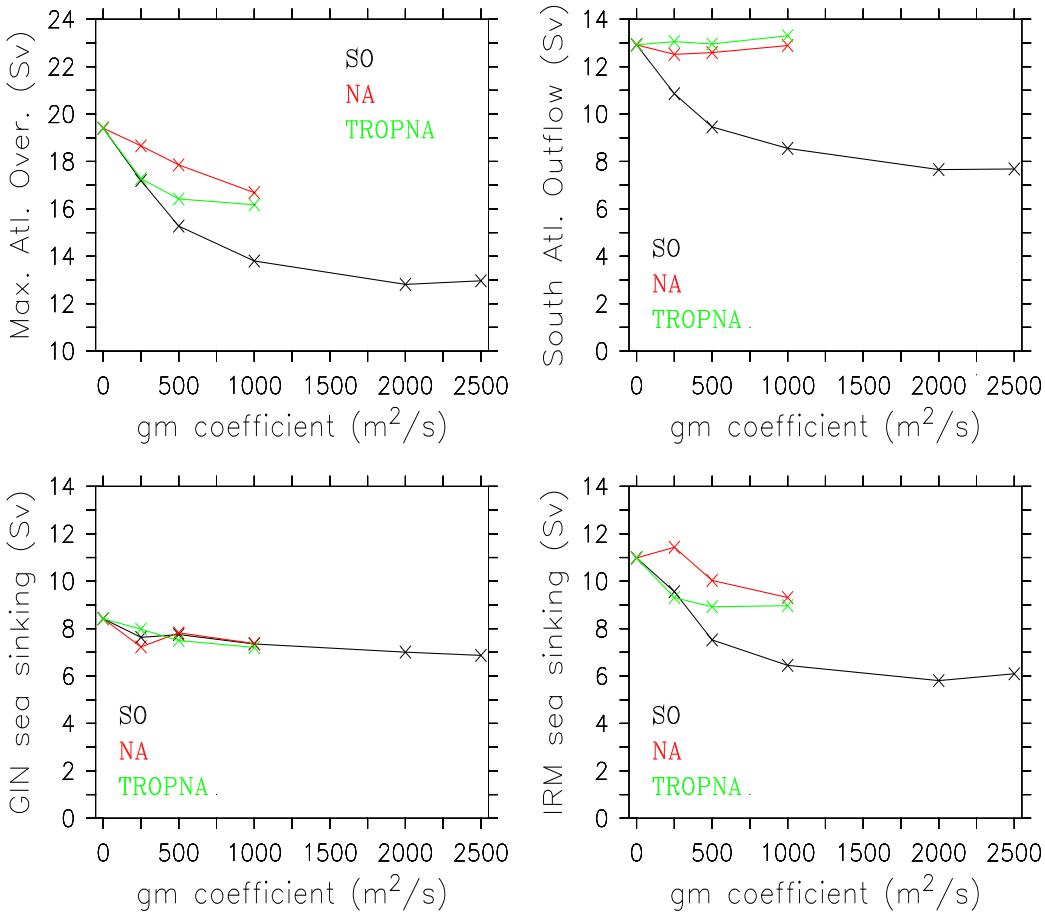

Figure 4.4: *Equilibrium volume transports as a function of enhanced eddy diffusivity for SO (black) and NA (red) runs. Top left (A): maximum Atlantic overturning. Top right (B): South Atlantic outflow. Lower left (C): GIN sea sinking. Lower right (D): sinking south of the sill. Also included are runs with the GM coefficient changed in the North Atlantic only in the northern hemisphere tropics and mid-latitudes between 0 °N - 60 °N (green). Note that the same vertical scale was used for all plots.*

We investigate now the relative changes when different magnitudes of GM coefficients are applied. Figure 4.4 shows the equilibrium solutions for the

SO, NA and TROPNA runs with different coefficients ranging from 250 - 2500 $m^2 s^{-1}$. The striking result is that for the runs where the GM coefficient is changed in the North Atlantic only, the South Atlantic outflow is not changed (figure 4.4B). It is only the upwelling within the Atlantic that decreases with increasing GM coefficient. For all experiments, the GIN-Sea sinking only slightly decreases and in the same way and the decrease in the maximum overturning can mainly be attributed to a decrease in the sinking south of the sills (figures 4.4C and 4.4D). Note, that a plateaux is reached for the SO runs such that for coefficients larger or equal to 2000 $m^2 s^{-1}$ the maximum overturning and South Atlantic outflow are not reduced any further. Note also (not shown) that for coefficients of 2000 $m^2 s^{-1}$ or larger in the North Atlantic, the overturning is completely killed.

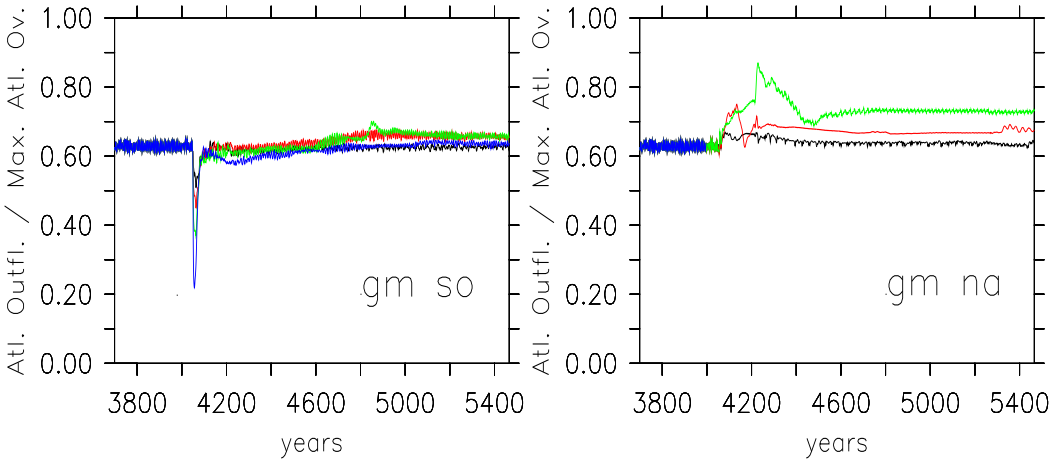

Figure 4.5: *Ratio of South Atlantic outflow over maximum Atlantic overturning for runs where GM is applied in SO (left) and NA (right) only. black: GM250. red: GM500. green: GM1000. blue: GM2000 (no Atlantic overturning for NA).*

To get an estimate of how large the contribution of the SAO is to the maximum overturning, figure 4.5 shows the ratio of the South Atlantic outflow to the maximum overturning, which can be interpreted as a kind of interhemispheric transport efficiency. A ratio of 1 implies that all of the waters that sink in the IRM- and GIN-seas are exported to the Southern Ocean and a ratio of $R = 0$ means that all waters upwell within the Atlantic ocean. Interestingly, for all SO experiments the ratio is constant at ca. 0.6 (left panel of figure 4.5). This means that since the South Atlantic outflow decreases with increasing GM coefficient, the upwelling within the Atlantic 'adapts' such that the SAO is always at 60% of the maximum. In the NA ex-

periments, the ratio varies and increases with increasing coefficient since the upwelling within the Atlantic decreases and the South Atlantic outflow stays the same. It needs to be stressed here again, that in our case a reduction of the upwelling within the Atlantic has nothing to do with any reduction of diapycnal mixing. The upwelling within the Atlantic interior driven by the diapycnal diffusion of $\kappa_v = 0.05\, cm^2 s^{-1}$ can be estimated by (assuming diapycnal diffusion is balanced by diapycnal upwelling W_{ad}) :

$$W_{ad} = \kappa_v \int\int \frac{\partial_{zz}\rho}{\partial_z \rho} dxdy$$

at the depth of the MAXA and as an integral from y = 30°S to the latitude of the MAXA in the Atlantic. For all runs, W_{ad} is relatively constant and below 0.5 Sv. Hence, any change in the Atlantic upwelling cannot be attributed to changes in the diffusivity driven upwelling and it also cannot be attributed to a change in the Veronis effect.

The results described in this section are similar to the outcome of the experiments from Kamenkovich and Sarachik (2004), who obtained a larger reaction of the Atlantic overturning to the eddy activity in the Southern Ocean than in the North Atlantic. However they attribute changes to the switch from horizontal to isopycnal and eddy diffusion and hence a decrease in Veronis effect for the North Atlantic case. They also don't distinguish between eddies acting on the GIN-sea region and eddies acting on the region south of that.

We have shown here that increasing eddies in the northern North Atlantic ocean only (NA experiments) away from the upwelling region, also decreases the overturning. This can be understood as follows: Eddy activity in the GIN-sea tends to flatten the isopycnals that geostrophically balance the East Greenland and Norwegian currents. Consequently, the fresh East Greenland current extends further into the ocean interior of the GIN-sea, decreasing the density of the sinking waters. Hence, although the volume of GIN-Sea deep water formation only slightly decreases (figure 4.4 C), the density of the waters overflowing the sills decreases substantially as shown in figure 4.6. The decreased density of the overflowing waters then effect the density gradient of the polar front and influence the IRM-Sea sinking and upwelling within the Atlantic. For an eddy coefficient as high as $2000\, m^2 s^{-1}$ this density decrease leads to a cessation of the entire Atlantic overturning.

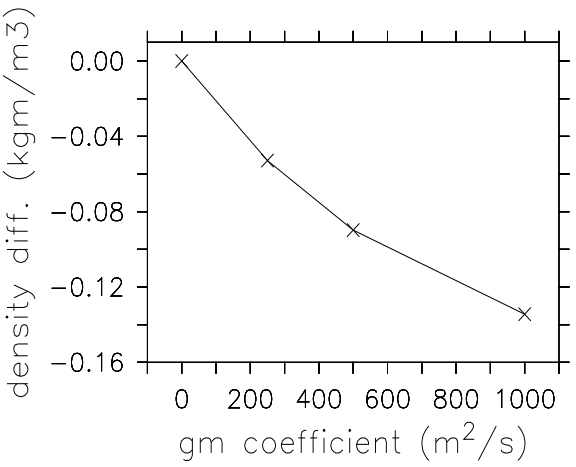

Figure 4.6: *Averaged density of the waters overflowing the sills from the GIN-seas with respect to the density of the baseline model configuration and as a function of the GM coefficient in the GIN sea.*

The eddy activity from the TROPNA experiments on the other hand acts directly on the isopycnals of the polar front.
By applying increased eddy activity in the North Atlantic only we have a means by which we can change the maximum overturning and not the South Atlantic outflow; and by applying it in the Southern Ocean only we can change the Southern ocean inflow and the maximum will change proportionally. This is all done in the limit of no vertical mixing. The density gradient changes in the different regions are attributed to pressure gradient changes and we will explore in the next section how the volume transports are related to meridional pressure differences.

4.3 The relation of the volume transports to the meridional pressure gradients

By increasing the GM coefficient in different regions of the model we decrease the density gradients and accordinlgy pressure gradients and the aim is to deduce wether meridional gradients can be related to the maximum overturning and South Atlantic outflow volume transports. We first investigate the SOGM experiments, where density gradients in the Southern ocean are decreased, and show relations for the total pressure, the baroclinic pressure and the surface pressure difference. Figure 4.7 shows the meridional pressure difference against the maximum overturning for the transient switch-on

experiments, hence the plot contains not only the equilibrium solution but also the points for the transient state. To distinguish between points of the equilibrium and of the transient part of the experiments, the equilibrium solution-points are in purple. The regression analysis gives more weight to these points and should therefore be taken with care. The aim of the linear regression is not to determine in an accurate way the exact regression coefficient or slope but to determine wether qualitatively a linear relation is found. The pressure difference is taken between averages over high and low latitudes within the northern hemisphere, with the average over the high latitudes including the deep water formation regions and both pressures zonally averaged over the Atlantic. The depth of 1500 m lies at a level within the southward flowing core of NADW. There is a very good linear correlation for the SOGM runs. Even the non-equilibrium solutions follow the linear correlation with the same line. Note that the same result is achieved with an interhemispheric pressure difference with averages over latitude strips 35-30°S as southern limits (not shown). The equivalent correlation with the same latitude strips, but taken at a level above the level of no mean motion (500 m) is shown in the right panel of figure 4.7). It is not as good any more as for below the level of no mean motion.

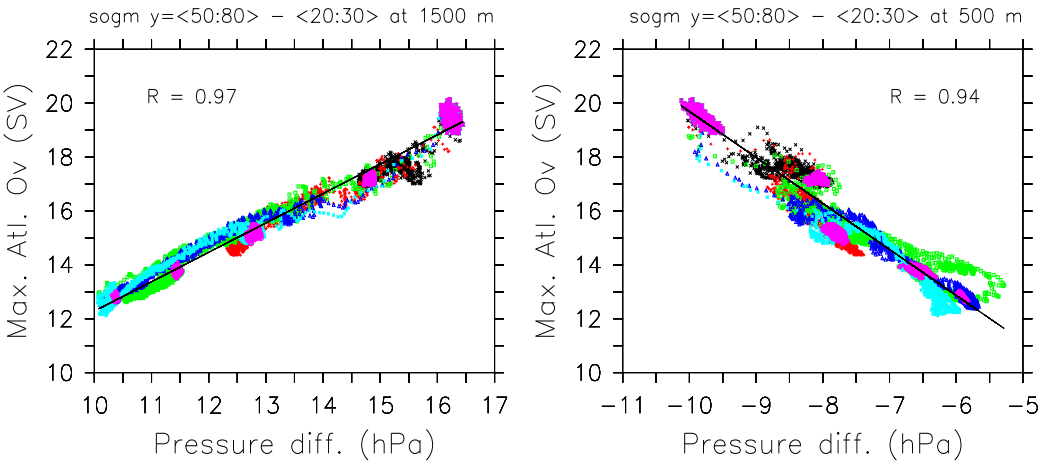

Figure 4.7: *Meridional pressure difference between latitude strip averages of 50 °N - 80 °N and 20 °N - 30 °N and zonally averaged over the Atlantic. Left: at 1500ṁ. Right: at 500 m. Different colours refer to the different experiments with different GM coefficients. Note that for the regression analysis, more weight is given to the equilibrium solutions with more datapoints (in purple). Other colours refer to the different GM coefficients as in figure 4.5*

The pressure in the MOM-3 framework is set up by the sum of the surface

pressure as essentially determined by the free surface elevation and by the baroclinic pressure defined as the vertical integral of the density from the given depth to the surface of the resting ocean at $z = 0$. Figure 4.8 displays the correlation for the surface pressure difference and the baroclinic pressure difference at depth 1500 m for the SOGM experiments. In this case, an *interhemispheric* difference is taken, since this gave a slightly better correlation coefficient than the hemispheric one. There still is a linear relation, however it is only for the equilibrium states of the experiments. Note the mirror like image for the two pressure gradients as expected, and the sum of both gives the relation with the total pressure difference as seen in figure 4.7 with *no preference* for an interhemispheric difference, meaning hemispheric and interhemispheric differences lead to the same result. The regression coefficient for the baroclinic pressure component is higher since the pressure range is larger than for the surface pressure. For the depth of 1500 m the baroclinic pressure gradient dominates over the surface pressure gradient and the larger the overturning, the more the baroclinic pressure gradient overcompensates the surface pressure gradient.

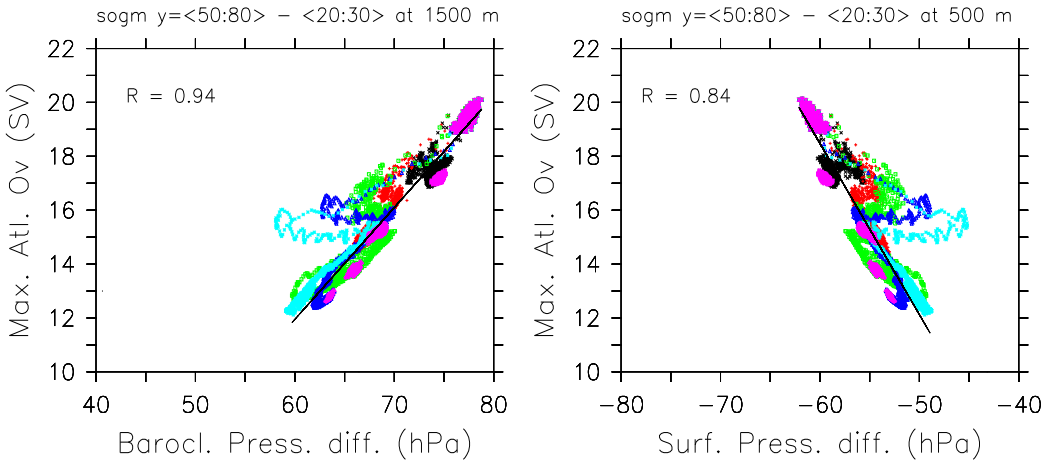

Figure 4.8: *SOGM. Left: Interhemispheric baroclinic pressure difference at 1500 m. Right: Interhemispheric surface pressure difference. Note again for the regression analysis more weight is given to the equilibrium solution (in purple).*

To obtain an idea, how the pressure components are distributed horizontally, 4.9 shows the two different pressure components for the depth of 1500 m. Since only the gradients count for the dynamics, pressures are normalized by a subtraction of the minimum value for this depth level. The total pressure in the lower panel of the figure is uniform throughout the Atlantic

south of 40°N *relative* to the high latitudes where the deep water formation occurs. Therefore, hemispheric and interhemispheric pressure differences are the same. In the baroclinic and surface pressure fields, the gyre circulations from the level above the level of no mean motion are apparent and they are neither zonally nor latitudinally uniform relative to the high latitudes.
Also included in the plots are the horizontal currents at that depth level. The linear relation of the maximum overturning with the meridional pressure difference arises because the zonal flow at 40°N turns into the western boundary current and is geostrophically balanced by the meridional pressure difference. For the baroclinic and surface pressures, since the gyre circulations from the upper level are apparent, the hemispheric pressure difference does not (only) capture the flow from the lower layer. The surface pressure gradient is directly related to the surface currents and the baroclinic pressure captures the whole density field from above 1500 m. The gradient with the zonally averaged pressures within the Southern part of the Atlantic seem to match better since it gives better correlation coefficients. The significance of the slightly better correlation can however be questioned since there is no direct explanation in terms of geostrophy why the zonal flow at 40°N should be better represented by an interhemispheric difference.

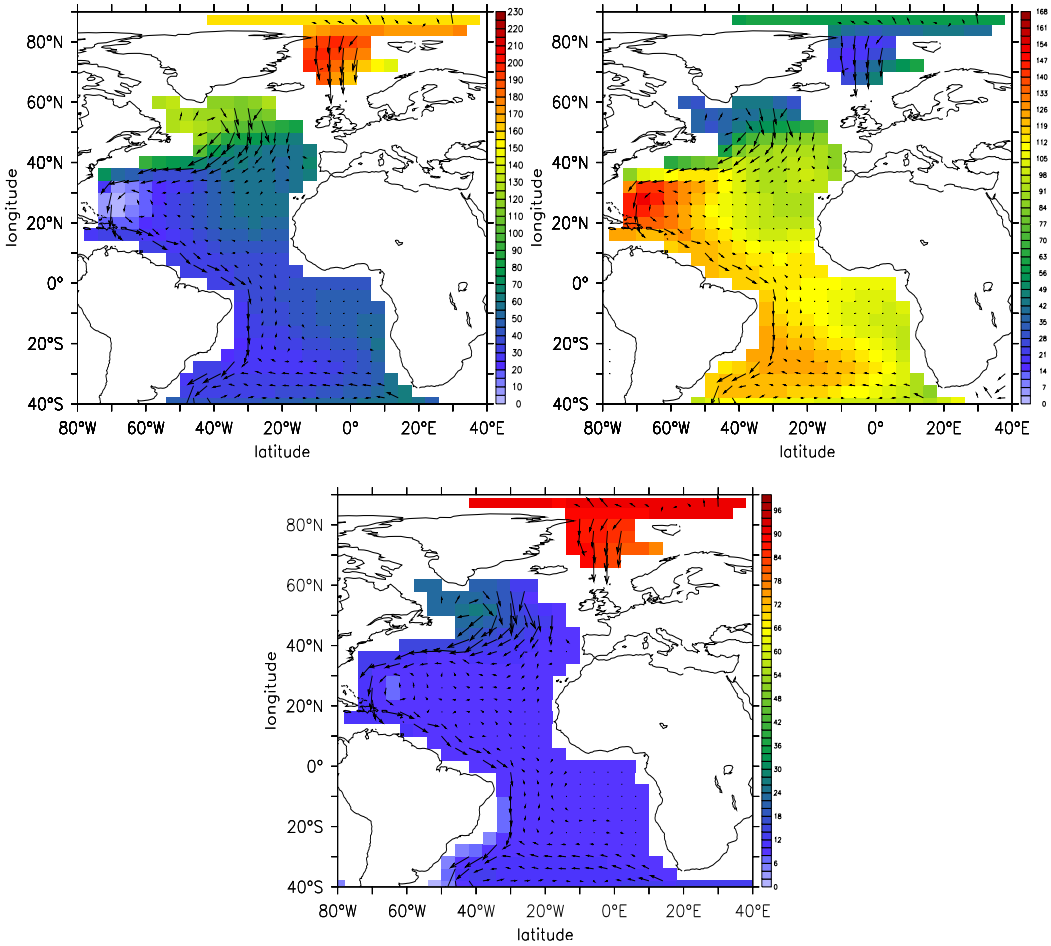

Figure 4.9: *Standard configuration with only background eddy mixing, pressures relative to minimum value at 1500m (hPa). Upper left: Baroclinic pressure. Upper right: Surface pressure. Lower panel: Total pressure.*

We turn to the experiments with changed GM coefficients in the northern North Atlantic only (NAGM). Figure 4.10 displays the same as the left panel of figure 4.7, except now for the NAGM experiments. The transient states now don't follow the same line any more and also specifically experiment NA1000 at 17 Sv is above the regression line for the SOGM experiments, meaning a higher maximum Atlantic overturning is achieved with the same pressure difference. At 1500 m, only the southward flowing NADW is captured, but not the water upwelling within the Atlantic at the boundaries as shown in figure 4.2. It is this upwelling which changes for the NAGM runs and determines the maximum overturning. For the SOGM runs, there is a linear relation of the SAO with the MAXA.

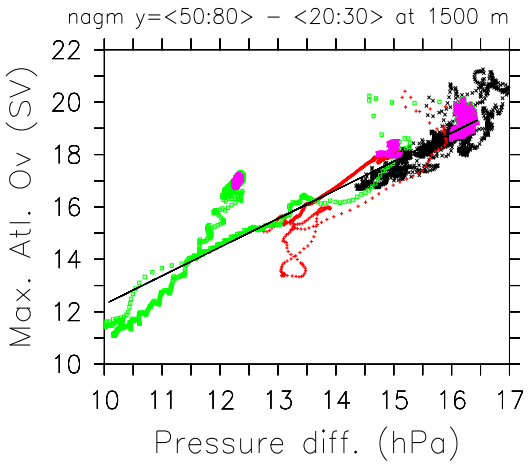

Figure 4.10: *Same as left panel of figure 4.7 except for NA experiments and correlation line from left panel of figure 4.7 included.*

To capture the whole meridional flow as given by the maximum of the Atlantic overturning or the South Atlantic outflow, the vertical integrals over the upper and lower layers above and below the level of no mean motion are needed. For all experiments, the level of no mean motion as given by the zonally integrated velocity field and as apparent from the Atlantic streamfunction, is the same and at a depth of 1000 m. The upper panels of figure 4.11 display the flow and pressure integrated over the upper and lower layer for the standard configuration. The gyre circulations are visible for the layer above the level of no mean motion, whereas the lower level refelects the uniformity of the pressure with respect to the high latitudes between 40°S and 40°N. The flow turns west zonally into the western boundary current from the deep water formation regions, then flows all the way down the equator until it turns zonally again to join the ACC. Interior circulations are negligible compared to the western boundary current. The pressure minimum is south of the ACC maximum for both layers, since the ACC is an eastward flow, extending all the way to the bottom. The flow of NADW in the lower layer is down the pressure gradient. The lower panels of figure 4.11 show the difference in integrated pressures for the SO1000 and NA1000 runs with respect to the standard configuration. It illustrates that also the differences are uniform over the Atlantic south of 40°N. For the run with changed GM coefficient in the Southern ocean, the decrease in meridional pressure gradient arises mainly from the uniform pressure in low latitudes increasing as compared to the standard experiment. For the NA1000 run this pressure decreases, however the most important change results from the pressure in

the high latitudes north of 40°N decreasing even more. Hence for both, the Atlantic overturning is decreased compared to the baseline experiment. As mentioned in section 4.2 an increase in the GM coefficient in the GIN-sea only decreases the density of the waters there and hence also the density of the overflowing water and the pressure.

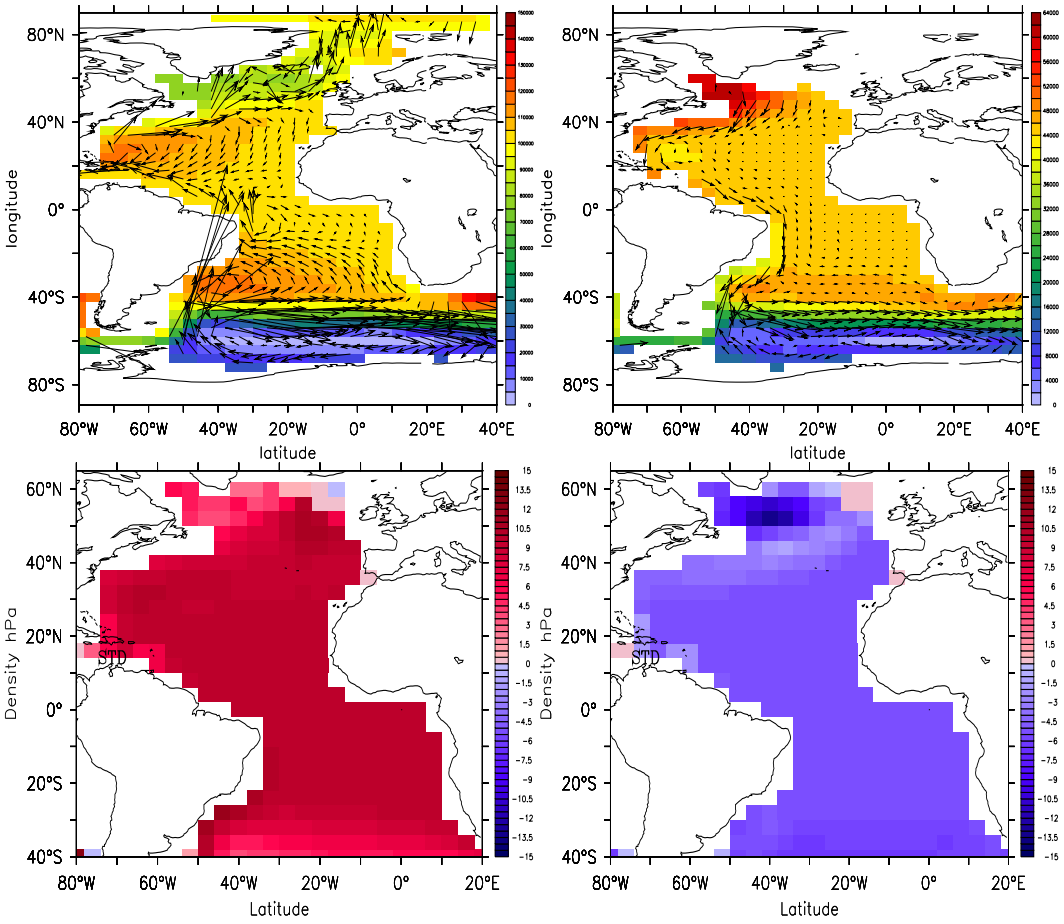

Figure 4.11: *Upper left: Pressure anomaly and flow integrated over the upper layer from 0-1000m. Upper right: Pressure anomaly and flow integrated over the lower layer from 1000-2500m. Pressures are normalized by subtraction of the minimum that occurs south of the ACC maximum. Lower panels: Zoom in into the Atlantic of pressure differences integrated over the lower layer. Left: STD - SO1000. Right: STD - NA1000.*

Figure 4.12 shows the zonally averaged pressures for all SO and NA experiments for the integral over the lower layer. The pressures are normalized by their values at the equator respectively. The pressure is uniform south of

30°N, relative to the high latitudes (as shown in the lower panels of figure 4.11 the pressure south of 30°N increases for the SO runs and decreases for the NA runs). The difference between the uniform low pressure over the low latitudes and the average over the higher pressure in the high latitudes reflects the one required to balance geostrophically the zonal flow that is collected into the western boundary current. Part of this flow then upwells at the boundaries or continues southwards until it upwells in the Southern Ocean. As a wrap up, figure 4.12 now shows the linear relation for the meridional pressure difference integrated over the lower layer for all NA, TROPNA and SO experiments. It is taken at a constant longitude of 44°W, the latitude where the flow that sunk is collected. The figure now shows the linear relation with the same line for all experiments.

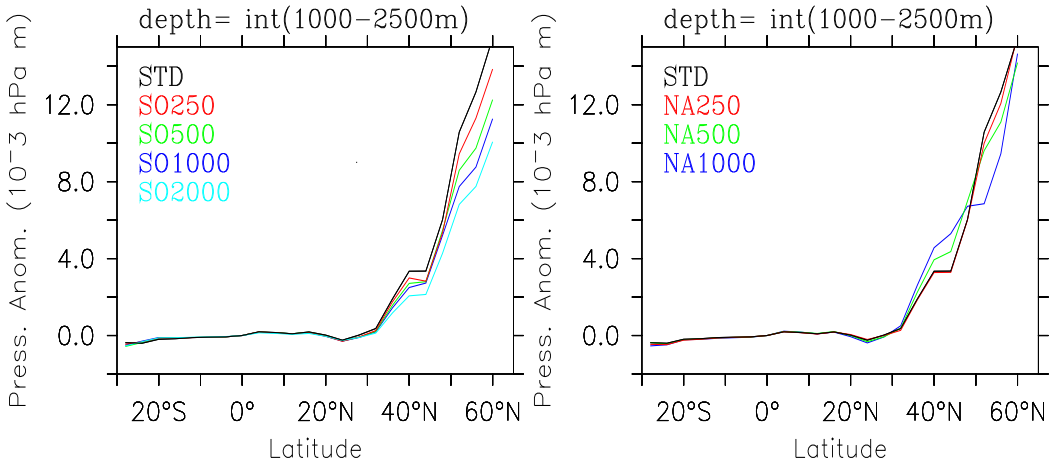

Figure 4.12: *Pressure anomaly integrated over the lower layer and zonally averaged over the Atlantic. Pressures are normalized by subtracting the zonally averaged pressure at the equator for every run. Left: SO. Right: NA.*

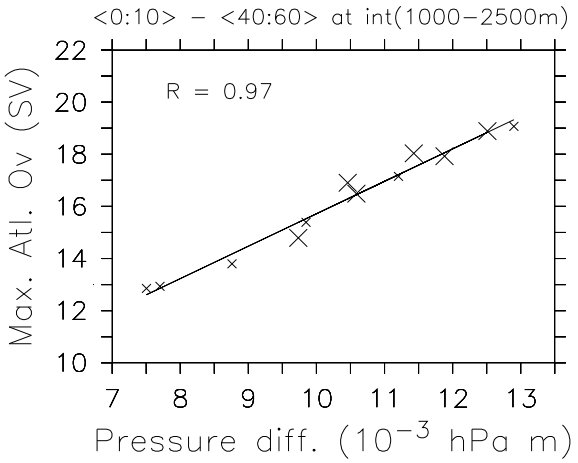

Figure 4.13: *Hemispheric pressure difference between averages 0-10°N and 40-60°N, integrated over the lower layer and taken at a constant longitude of 44°W for all NA, TROPNA (large crosses) and SO (small crosses) experiments (the linear regression coefficient with the zonal average is 0.85).*

In summary, we have shown in this section that the linear relation with the meridional pressure difference can be boiled down to the geostrophic balance of the zonal flow at around 30°N. For levels below the level of no motion, the pressure is uniform for the entire Atlantic south of 30°N *relative* to the pressure at high latitudes where deep water formation occurs. There is therefore no preference for hemispheric or interhemispheric pressure difference correlations with the maximum overturning. Including eddies south of 40°S mainly increases the uniform pressure in low latitudes whereas including eddies in the NA mainly reduces the pressure there, but the uniform low latitude pressure is less effected. Both effects lead to a decrease in meridional pressure gradient. For the SOGM runs, the linear relation holds even for the transient state of the switch-on experiments. Since the baroclinic or surface pressure is not the true dynamically relevant pressure the correlation at 1500m was not as good. Also, there is no correlation between any meridional pressure difference within the Southern ocean and the South Atlantic outflow, which we have not shown explicitly. This will be commented upon in the next section. Since we regard changing the eddy coefficients as influencing directly the density gradients in different regions under a constant wind forcing, we want to discuss in the next section how we can relate these changes in the 'thermodynamic components' of the system to the picture of a winddriven Atlantic overturning circulation as put forward by Toggweiler and Samuels (1993a) and supported by the conceptual picture in Nof (2003).

4.4 A conceptual picture

We refer here to the conceptual approach given by Nof (2003) who, similarly to Toggweiler and Samuels (1993a), related the vertically integrated net transport from the Southern Ocean to the North Atlantic solely to the windstress. This would mean that changes in pressure gradients under constant wind forcing would not alter both the maximum Atlantic overturning and the South Atlantic outflow. We will herein discuss to what extend this hypothesis is valid and from there develop how zonal pressure gradients are related to meridional ones in the Southern Ocean for the South Atlantic outflow and in the North Atlantic for the maximum overturning.
Refering to figure 4.14, the net northward transport at around 30°S is given by the northward interior transport minus the southwards western boundary current transport. As pointed out by Nof (2003), the net northward transport into both Indopacific and Atlantic across a contour passing the tips of the Americas and Africa, T_n, is given by an Ekman-like term, obtained through integrating the linearized and vertically integrated momentum equations with the net zonal pressure gradient being zero for an integral above silldepth:

$$f_0 T_n = \oint \frac{\tau_x}{\rho_0} dx \tag{4.1}$$

Nof (2003) came up with a net transport of roughly 10 Sv into the Atlantic by assuming this total net transport as determined from observed wind stress fields is partitioned between the Indopacific and Atlantic according to basin widths. The net northward transport in this picture is therefore solely detemined by the wind: It is in numbers given by the Ekman like term from equation (4.1), whereas the actual water mass that reaches the North Atlantic is not the water mass from the Ekman transport at the very surface but it is the fraction of the Sverdrup transport in the ocean interior that is not flushed back out of the Atlantic via the western boundary current (4.14). It needs to be stressed, that in the case of equation (4.1) being valid also for the net transport into the Atlantic basin and the interior northward flow being determined by the curl of the wind stress, the zonal pressure gradient within the western boundary current will adapt to accomodate the flow necessary to fulfill equation (4.1).

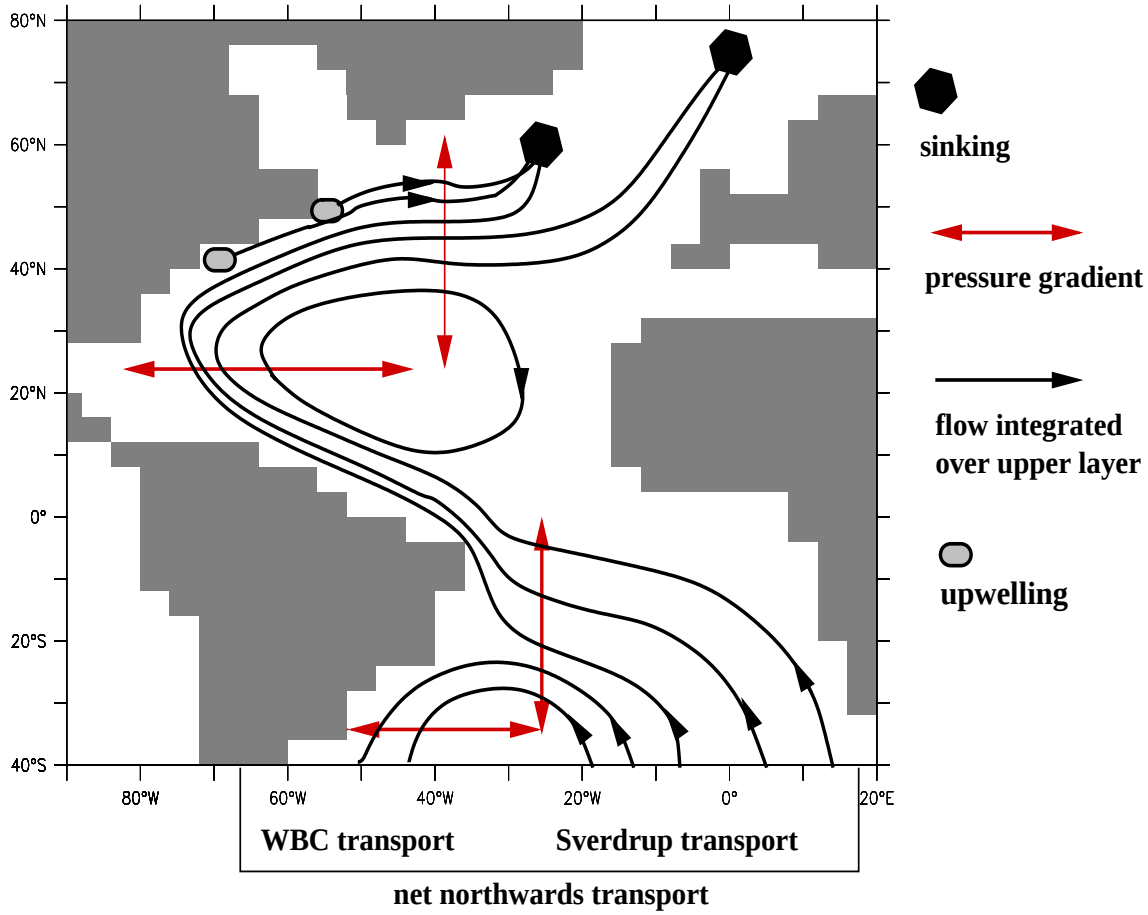

Figure 4.14: *Pattern of volume transport in the Atlantic, vertically integrated over the upper layer from the surface to the level of no mean motion as apparent from the Atlantic streamfunction. Drafted after figure 4.11 and consistent with Nof (2003). Red arrows represent relevant pressure gradients. Also sketched is the upwelling within the Atlantic which occurs along the western boundary.*

Refering to figure 4.14 and the above reasoning, the Southern Ocean inflow would be proportional to the zonal pressure gradient within the western boundary current, which, given the net northward flow is also predetermined by the wind stress, is also proportional to the meridional pressure gradient as indicated by the red arrows in figure 4.14.
A similar picture is obtained in the North Atlantic: the zonal pressure gradient as indicated in figure 4.14 partly accounts for the flow ultimately sinking in the IRM- and GIN-seas and partly for the recirculation in the

gyre. If this closed gyre circulation is constant and given solely by the windstress and there is no additional upwelling into the upper layer, there is immediately the proportionality of the zonal pressure gradient with the meridional one as indicated. We have seen however in the previous section for the NAGM experiments, that the boundary upwelling as indicated in figure 4.14 modifies the picture and the zonal and meridional gradients differ by the amount to balance the part of the flow that upwells along the western boundary.
We will now assess the magnitudes of the western boundary and interior transports. In particular, it will lead us to calculate the vorticity budget of the upper ocean in the model together with the zonal and meridional pressure gradients. We have the advantage here to asses the model's behaviour in the limit of no vertical mixing, i.e. there is no additional diffusivity driven upwelling within the Atlantic interior.

The general vorticity balance for any flow integrated between two levels z_1 and z_2 is (see e.g. Lu and Stammer (1998)):

$$\begin{aligned}\beta V = \nabla \times \left[-\partial_t U - \int_{z_1}^{z_2} \nabla p/\rho_0 \, dz + \tau(z_1) - \tau(z_2) \right] \\ + f\left[w - \mathbf{u}\cdot\nabla z_1\right](z_1) - f\left[w - \mathbf{u}\cdot\nabla z_2\right](z_2) + LFT + ADV \end{aligned} \tag{4.2}$$

Here, (U, V) is the horizontal flow integrated between z_1 and z_2, LFT and ADV are the curl of the lateral diffusion and advection respectively. When integrated between the surface η and the ocean bottom H, $\nabla \times \int_{-H}^{\eta} \nabla p/\rho_0 \, dz$ is the bottom pressure torque, which is nonzero when the bottom pressure gradient is not aligned with the contours of bottom topography.
The vorticity balance for the upper layer, away from topography gradients and when lateral advection and diffusion curls can be neglected reduces to:

$$\beta V = \nabla \times \tau(\eta) + f w_0 \tag{4.3}$$

with $\tau(\eta)$ being the surface wind stress and w_0 the upwelling at the base of the upper layer, which corresponds to the level of no mean motion. With the upwelling being zero, the equation reduces to the familiar Sverdrup relation.

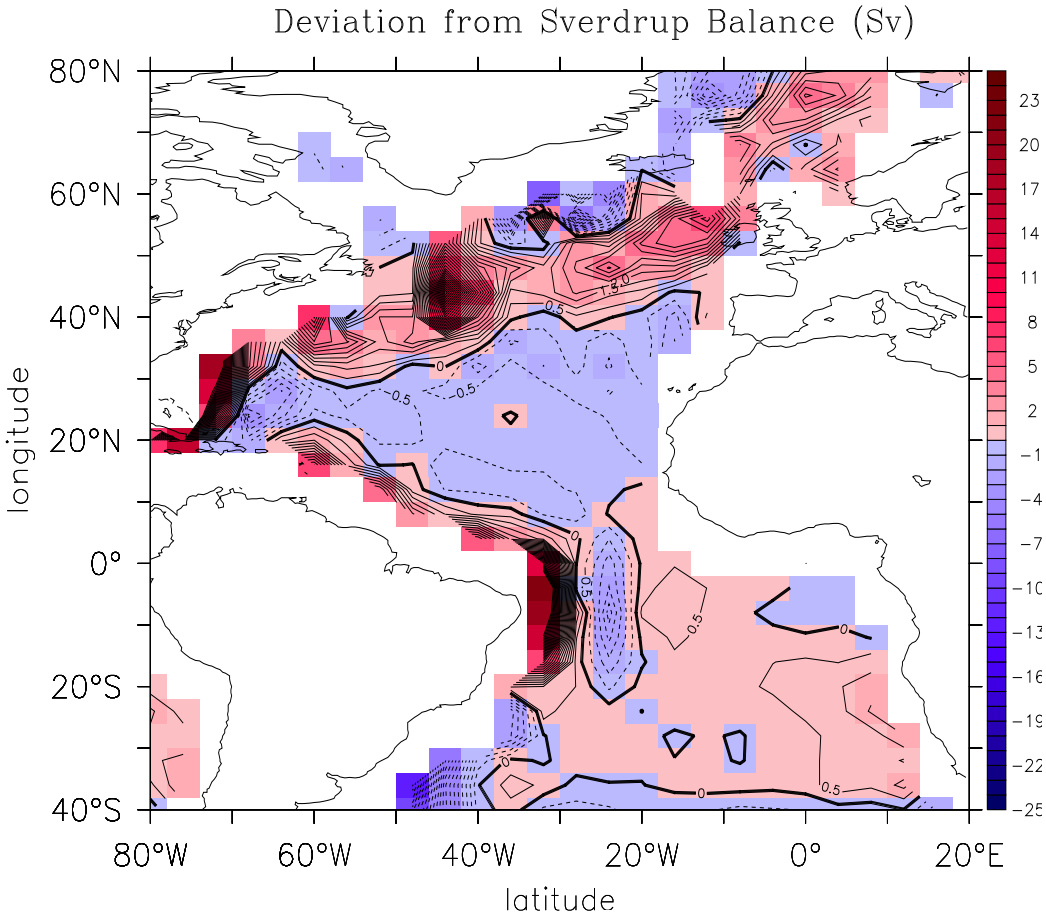

Figure 4.15: *Deviation from the Sverdrup balance* $-[\nabla \times \tau/(\rho_0\beta) - V]\Delta x$ *with* V *calculated as an integral over the upper layer from 0 - 1000 m and multiplied by the zonal grid size* Δx *such that the difference is given in Sv for every grid point. Contour interval is 0.5 Sv. Note that calculating the torque in coarse resolution models is very noisy. Positive deviation in the Southern Hemsiphere means the meridional northward flow is greater than predicted by the Sverdrup balance.*

Figure 4.15 shows the deviation from the Sverdrup balance for the standard model run for the upper layer integrated from 0 - 1000 m. As expected, the Sverdrup balance holds in low latitudes in the ocean interior away from the boundaries where deviations are smaller than 0.5 Sv. Vertical velocities across $z_0 = 1000\,m$ are large in the northern North Atlantic where the sinking occurs and along the western boundary currents where upwelling occurs and where friction is important. Since the vertical diffusivity in the runs is very small, there is no upwelling across 1000 m in the interior which would alter

the balance. Note also the deviation at the eastern boundary along Southern Africa.

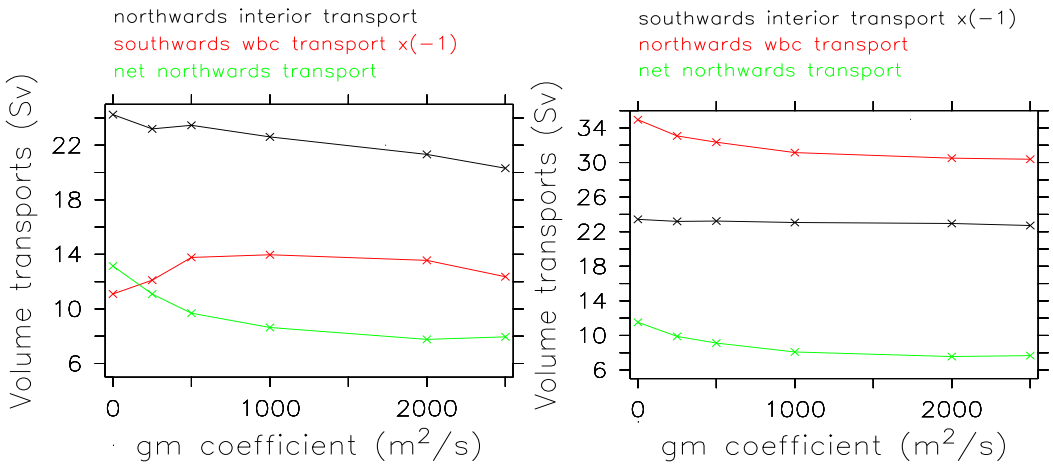

Figure 4.16: *Left: northward interior flow, southwards western boundary current transport and net northward flow at 30 °S for GMSO runs. Note that the Sverdrup interior flow as computed from the curl of the windstress is ca. 20 Sv (western boundary current excluded). Right: southward interior flow, northward western boundary current and net northward transport at 30° N*

We will now assess the balances for the GMSO runs for the Southern Ocean and North Atlantic and see what determines the Southern Ocean inflow and the maximum Atlantic overturning.
Figure 4.16 shows the partitioning of the net northward transport into the northward interior flow and the southwards western boundary current for the different GMSO configurations. There is a deviation for the interior transport from the Sverdrup transport of up to 5 Sv which is due to a decrease in eastern boundary current inflow with increasing GM coefficient (compare also figure 4.15 to see that Sverdrup balance is violated at the East coast of South Africa in the Benguelas current. In addition, the southward western boundary current increases with increasing GM coefficient ('Brazil current'). Since under fixed wind forcing the net northward transport is determined by both the zonal pressure gradient in the eastern and western boundary currents, there is no direct relation of the zonal and meridional pressure differences sketched in figure 4.14.

We now turn to the North Alantic (right panel of figure 4.16). There is upwelling across the 1000 m contour, but it does not occur in the ocean

interior but at the western boundary between 30°N and 44°N, when the flow detaches from the coast and turns eastward (figure 4.14). The interior flow is constant for all runs at 23 Sv. Hence, there is a direct relation between the zonal and meridional pressure gradient, except that the western boundary upwelling needs to be taken into account.
For the lower layer, there are no horizontal recirculations in the ocean interior as seen from figure 4.11 and as we have discussed in the previous section, there is the direct relation of the meridional pressure gradient in the North Atlantic and the meridional overturning.
We have seen in this section that the picture given by Nof (2003) can be altered by the transport in the southwards Western Boundary Current and the northward Estern Boundary Current. For the SOGM experiments, we can come up with an estimate for the South Atlantic outflow of $11 \pm 3\,Sv$. This is still very close to the estimate of around 10 Sv gicen by Nof (2003). In the next section we will extend the analysis to experiments which vary not only in the eddy coefficient but apply different surface forcings, increased vertical mixing and reduced wind stress.

4.5 Extension to a variety of experiments

In this section we repeat the previous analyses but extended to a variety of experiments in which the surfaces fluxes (freshwater and winds) or the vertical diffusivities were changed. We give an overview over the different kinds of experiments by putting them into classes for which different colours are used in the next figures:

- Experiments STD, SO, NA and TROPNA from the previous sections (black)
- Different surface freshwater forcing: restoring to sea surface salinity (SSS), restoring to SSS along the coastlines only (i.e. no fixed diagnosed river runoff), increased river runoff (red)
- Constant vertical background mixing increased to $0.3\,cm^2s^{-1}$, enhanced boundary mixing (see chapter 5) with diffusivities up to $10\,cm^2s^{-1}$ close to the ocean bottom and background diffusivity of 0.1 or $0.3\,cm^2s^{-1}$ (green)
- Reduced winds (compare chapter 3, section 3.3): $\times$ 0.01 everywhere and restoring to SSS, $\times$0.01 in the GIN-Sea region only, $\times$0.01 in the Southern Ocean only (dark blue).

- Miscellaneous experiments: GM coefficient increased to $250\,m^2s^{-1}$ everywhere, no background GM coefficient and very low vertical mixing, background GM coefficient at $100\,m^2s^{-1}$ and vertical mixing $0.1\,cm^2s^{-1}$ (light blue)

Some of the above experiments are also used as baseline experiments from which again GM-coefficients are increased in the Southern Ocean and North Atlantic. In the following figures, we denote the experiments with increased coefficient in the North Atlantic with large crosses ('+'), whereas all other runs, including baseline setups and increased GM coefficient in the Southern Ocean are denoted with small crosses ('×'). We don't discuss explicitly the outcome of those experiments but it should be noted that a restoring to SSS seems to reduce the effect of an increase of the GM coefficient in the North Atlantic GIN-sea region on the Atlantic overturning. This is because the caracteristics of the deep waters formed are then more predetermined through the salinity restoring and decreasing the density gradients will have less of an effect on the deep water formation. Increasing the vertical mixing to $0.3\,cm^2s^{-1}$ (but without salinity restoring) enhances the decrease in Atlantic overturning with increased eddy activity in the North Atlantic and it is not a robust feature any more that the South Atlantic outflow stays constant. The reaction of the Atlantic overturning to an increased GM coefficient in the Southern Ocean is relatively similar with all baseline setups.
Figure 4.17 relates meridional measures of the flow to the maximum Atlantic overturning. The upper left panel of figure 4.17 shows the linear correlation of all these runs with the meridional pressure difference integrated over the lower layer at a constant longitude where the flow is directed westward and collected into the western boundary current. It reveals a very good linear correlation with the same line for all the experiments. However, the regression coefficient drops down to 0.76 when the pressure is zonally averaged over the Atlantic. The upper right panel displays the correlation with the hemispheric density difference at the level of no mean motion for each run and the lower left panel the correlation with the surface elevation difference (which is through the surface density related to the surface pressure difference). The lower right panel shows the pycnocline depth at a latitude of 20°N and a longitude of 44°W. The weakest maximum Atlantic overturning with ca. 11 Sv is given by the run with a non-diagnosed restoring to SSS along the coastlines, a vertical mixing coefficient of $0.1\,cm^2s^{-1}$ and an increased GM eddy coefficient of $100\,m^2s^{-1}$ in the Southern Ocean. The strongest overturning with almost 26 Sv is achieved by the very low mixing experiment with no eddy activity and almost no vertical mixing.

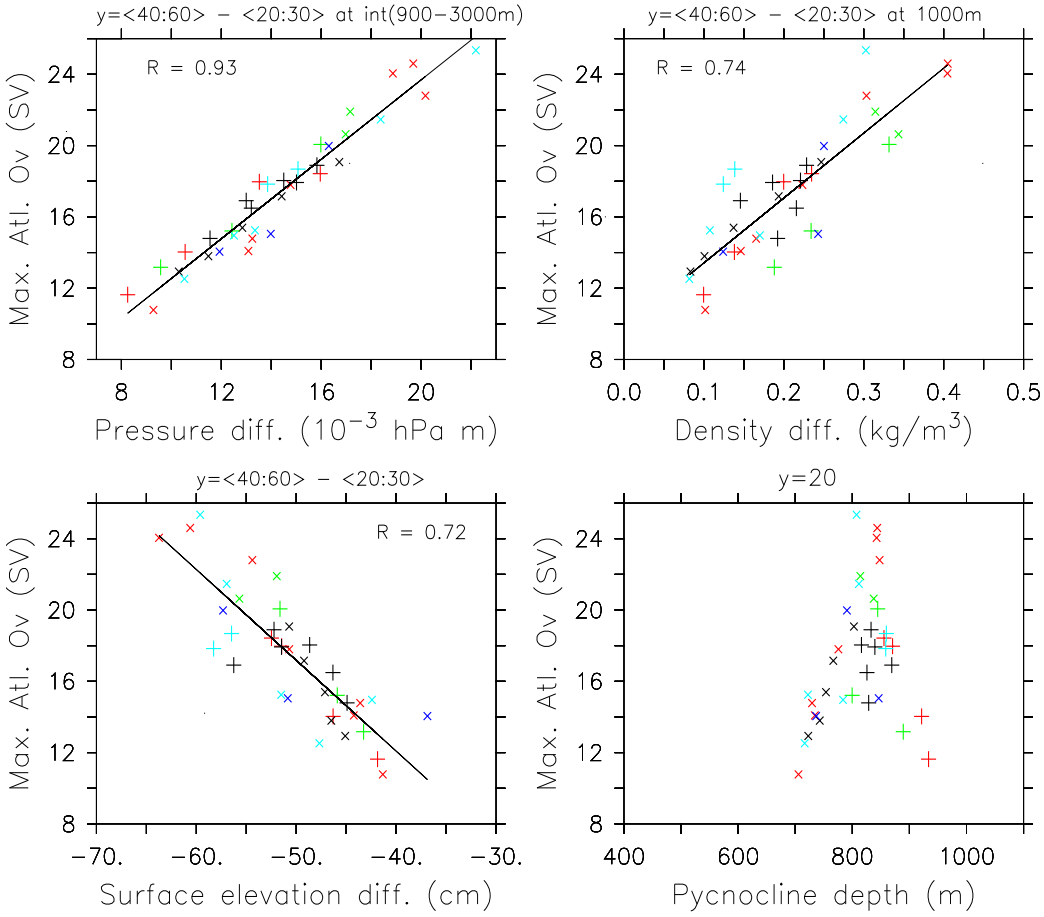

Figure 4.17: *Linear regressions between the maximum Atlantic overturning and hemispheric differences of several zonally and vertically averaged quantities at 44° W (averaging latitude and depth ranges are indicated on top of each panel). Different colours and symbols correspond to different classes of experiments as explained in the see text. SO and NA experiments from the previous sections are in black. Small crosses (×) refer to changed GM coefficients in the Southern Ocean, large crosses (+) in the North Atlantic. Upper left: meridional deep pressure difference from. Upper right: Density difference at the level of no mean motion (for Levitus (1982), the same density difference is 0.19 kg/m^3, yielding ca. 17 Sv). Lower left: Surface elevation difference. Lower right: pycnocline depth as diagnosed in Gnanadesikan (1999), except that it is taken at a constant latitude of 20° N and constant longitude 44° W.*

There principally is a linear correlation with the maximum Atlantic overturning for all the different meridional measures of the flow. The correlation coefficient for the density and surface elevation difference is

however much lower than for the integrated pressure difference, which is a more accurate measure of the maximum Atlantic MOC. Note that similar relations hold for the density difference at various depths and for the vertical average of the density from the level of no mean motion to the surface.
Perhaps the most revealing result displayed in 4.17 is that the depth of the pycnocline does not vary much from one experiment to another. The changes in the estimated depth of the pycnocline, which is calculated according to the formulation of Gnanadesikan (1999), are in the order of 100-200 m around a mean depth value of about 800 m. Since the model resolution at a depth of 800 m is above 200 m (compare table 3.1 from chapter 3), it does not resolve the possible changes in the pycnocline depth associated with the changes in diffusivities and surface forcing studied here. In other words, the model pycnocline is in practice "clampled" to a depth of around 800 m. We note that this comment is probably also valid for the original paper of Gnanadesikan (1999), who used a model with only 12 vertical levels (the vertical distribution of levels is unfortunately not provided in his paper). This is, we believe, a potentially important point, and so warrants further discussion.

Gnanadesikan (1999) related the strength of the Atlantic overturning to the pycnocline through taking into account three processes that influence its depth D: Southern Ocean winds, Southern Ocean eddies and diffusivity driven upwelling in low latitudes (chaper 1, section 1.3). In his framework, the meridional density difference is prescribed and the strength of the Atlantic overturning is solely determined by D. We can compare his approach to the model framework, where the free surface elevation, the level of no motion and density differences play together to set up the meridional pressure difference that determines the flow, the latter is given by $\Delta p = \Delta\rho\, D$. In Gnanadesikan (1999), the pycnocline depth acts like the level of no motion that changes its depth whereas the density difference and the surface elevation difference stay the same. An increase in Atlantic overturning would be associated with the downward shift of D. Note, that the Gnanadesikan model is not consistent with a linear scaling of the overturning with the pressure difference (Levermann and Griesel (2004)).
In contrast, our results suggest the following for a model with coarse vertical resolution: The mean depth of the level of no motion is constant but the density difference as given at the level of no motion decreases with decreasing overturning. Accordingly, the surface pressure gradient also decreases and $D\Delta\rho(z_0) = \Delta\eta\rho_s$ gives an estimate of the flow. D is the constant depth of the level of no motion to the surface of a resting ocean at $z = 0$, $\Delta\rho(z_0)$ is the density difference at the level of no motion and ρ_s is the imposed density at the surface. The left hand side of the equation can be identified with the

baroclinic pressure gradient at the level of no motion and the right hand side as the surface pressure gradient.
In the approach taken by Gnanadesikan (1999) the meridional density difference, $\Delta\rho$, is prescibed, and variations in the pycnocline depth D, leading to variations in meridional pressure gradients, control the strength of the Atlantic MOC. However, since the meridional density difference in the pycnocline does certainly change under varying ocean dynamics and surface forcing (even when restoring to surface temperatures and salinities, changes in the horizontal and vertical diffusivities, for example, will lead to variations in the density field), the meridional pressure difference (or the meridional density difference) should, in general, be treated as an independent variable in addition to the pycnocline depth. This is the path that has been followed in the present work, showing that, in the model, the maximum of the Atlantic MOC appears to scale linearly with meridional pressure differences (not only above the depth of the pycnocline, but as well below) and that the pycnocline depth does not change significantly under a variety of surface forcing and ocean parameter changes. Our results are consistent with the idealised box model of Stommel (1961) and with the results obtained in a recent investigation reported by Levermann and Griesel (2004) using the same ocean model that we have described here. Note however that neither our results nor those of Levermann and Griesel (2004) are necessarily in contradiction with those expected from the conceptual model of Gnanadesikan (1999) (which predicts a varying pycnocline depth and a complex dependence of the maximum of Atlantic MOC on meridional pressure gradients) since, we insist, the meridional density gradients are allowed to freely evolve in our simulations, while they are not in the model of Gnanadesikan (1999).

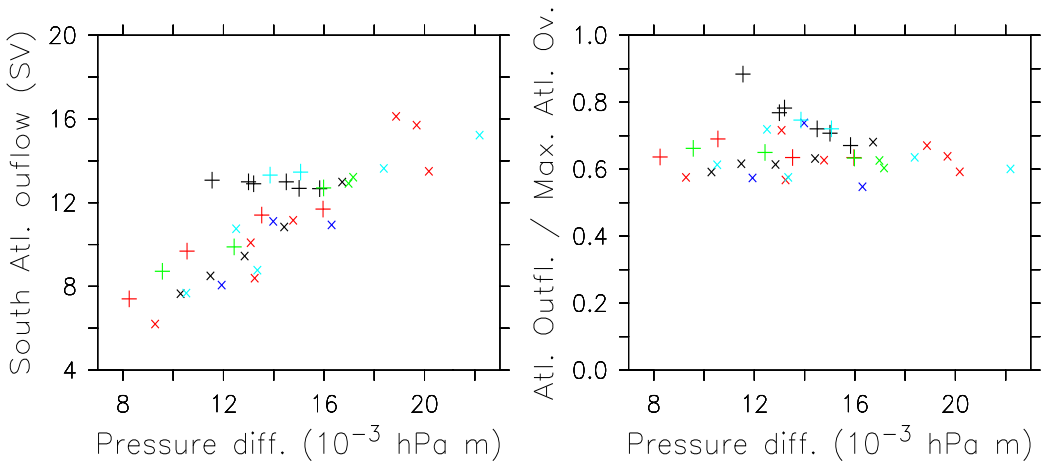

Figure 4.18: *Left: South Atlantic outflow as a function of interhemispheric pressure difference,integrated over lower layer (which is the same as the hemispheric one in figure 4.17). Right: Interhemispheric transport efficiency* $R = SAO/MAXA$. *The smallest ratio is obtained for the run with the winds in the Southern Ocean multiplied by 0.01 and a vertical mixing of* $0.3\,cm^2s^{-1}$ *(*$R = 0.55$*). The largest ratio is given for the run with the GM coefficient set to* $1000\,m^2s^{-1}$ *in the tropical Atlantic south of* $40°N$ *(*$R = 0.88$*)*

At last, we refer back to the discussion around the South Atlantic outflow. Figure 4.18 shows the correlation of the pressure difference integrated over the lower layer with the South Atlantic outflow. It is still linear for the experiments that show a linearity of the maximum overturning with the South Atlantic outflow. It also yields that the South Atlantic outflow varies in a range from 6-16 Sv, which, refering to the analysis in section 4.4 means the eastern and western boundary currents at around 30°S vary significantly with varying mixing and surface forcing. The right panel of the figure shows the ratio $R = SAO/MAXA$ which is between 0.6 and 0.8 for most experiments. The smallest ratio below 0.6 is given for the experiments where Southern Ocean winds are almost zero, meaning that relatively few waters are transported southwards. Note that 'small crosses' are located at around 0.6 whereas the experiments with changed GM-coefficients in the North Atlantic are above 0.6.

4.6 Discussion

In this chapter we have investigated the role of eddies in the Southern Ocean and North Atlantic and have interpreted it as a means by which density gra-

dients and hence 'thermohaline components' of the flow are changed under constant wind forcing and in the limit of very low vertical mixing.
We have emphasized that there is a residual upwelling within the Atlantic occuring along the western boundaries even with very low horizontal and vertical mixing which is decreased when higher GM coefficients are applied in the North Atlantic in either of the deep water formation regions, ultimately acting on the polar front. Also, we could identify some kind of independence between the maximum overturning and the South Atlantic outflow in the sense that applying eddies in the North Atlantic effects the maximum but not the outflow and applying eddies in the Southern Ocean only effects the South Atlantic outflow immediately and the maximum changes proportionally.
Principally, the maximum Atlantic overturning can be related to a difference between two main pressures: the one south of the sills where the dense sinking waters are collected and a relatively uniform smaller pressure south of 30°N. This pressure difference reflects the geostrophic balance of the zonal flow at 30-40°N. For experiments where the eddies are increased in the Southern Ocean, the decrease in Atlantic overturning can mainly be attributed to the increase in this uniform pressure in low latitudes, whereas for experiments with increased eddy activity in the North Atlantic the decrease in Atlantic overturning can mainly be related to the decrease in the density of the deep waters formed and the resulting decrease in the high latitude pressure. Also, due to the effect of the gyres in the upper layer above the level of no motion, the linear correlation for the lower layer below the level of no motion is stronger. Another important point is that there is no preference for taking an interhemispheric pressure difference instead of a hemispheric one as argued by some authors (Thorpe et al., 2001; Rahmstorf, 1996). It should be noted however, that the uniformity of the pressure is only relative to the high latitudes, there still are zonal pressure differences south of 30°S that balance the flow in the western boundary current.
With this we can explain the diagnostic findings of previous studies (chapter 1, section 1.3) of a linear relation of measures of the meridional pressure difference with the Atlantic overturning, which we have shown to hold for a variety of experiments, not only varying in surface freshwater forcing but also subgridscale parameterizations and wind forcing.
It seems that the Ansatz of Gnanadesikan (1999) cannot directly be associated with the ocean model behaviour concerning using a D for all the processes and not interpreting it as the level of no motion. It is crucial that in the model not the level of no motion changes but the density difference and hence the surface elevation and pressure difference. Our results hence suggest that the model behaviour is closer to the Stommel (1961) box model with

fixed boxes and meridional density differences determining the flow. We conclude that any change in Atlantic overturning, be it through increased eddy activity, changed wind stress, vertical mixing or surface fresh water fluxes can diagnostically be related to the change in meridional pressure difference. This illustrates once more the interaction of thermohaline with wind components since also in the experiments where only the windstress has changed, pressure gradients adapt as to fit the linear relation.

In section 4.4 we have related the picture of a wind driven Atlantic overturning to the changed density gradients in the North Atlantic and Southern Ocean. We have argued that for the South Atlantic outflow, the pressure gradients influencing the southwards western boundary current and northward eastern boundary current modify the wind driven picture. The analysis was extended to a variety of experiments. With the exception of two experiments in which the Southern ocean windstress hass been reduced, they all apply a constant wind forcing, however the South Atlantic outflow varies over a range of 10 Sv in our extended experiments. It is true that the net northward meridional volume transport into all ocean basins across a closed latitude circle at, say, 60°N is solely wind determined. However, how much of these waters then ultimately reach the North Atlantic depends on the distribution of pressure gradients along the paths of the northward travelling water masses, ultimately meaning how much southwards recirculation occurs between 60°S and 35°S. This is closely related to the discussion around the Deacon cell (chapter 1, section 1.2) and we have only approached this issue from a somewhat different angle.

For the North Atlantic, taking the upwelling along the western boundary into account is crucial. In all our experiments, including the ones with an increased vertical mixing coefficient of $0.3\,cm^2s^{-1}$ there is basically no significant upwelling within the Atlantic ocean interior and the dominant upwelling takes place along the boundaries. There are therefore no horizontal recirculations as in the original Stommel and Arons (1960) framework which could alter the picture in terms of meridional and zonal pressure gradient relations. We will discuss this further in chapter 5.

Chapter 5

The role of diapycnal mixing for the Atlantic Overturning dynamics

This chapter investigates the sensitivity of the Atlantic overturning to the vertical diffusivity and the role played by non-uniformely distributed vertical diffusivities for driving an AMOC. Since diapycnal mixing occurs vertically over most parts of the ocean, except in some regions of the high latitudes where isopycnals outcrop, changing the vertical diffusivity in the model is mostly equivalent to changing the diapycnal fluxes. In the first part of the chapter (section 5.2) we will concentrate on decomposing the Atlantic overturning circulation into different physical components and discuss their sensitivity and scaling with the background vertical diffusivity. The second part (section 5.3) is devoted to the role of vertical mixing location and tests some hypotheses discussed in the introduction concerning boundary enhanced mixing and mixing at depth. We will also discuss the amplifying mechanism of a diffusive tracer advection scheme. The experiments in this chapter are done with the coupled version of the ocean model, allowing, amongs others, the atmosphere-ocean temperature feedback to be taken into account. We will discuss some aspects comparing ocean only and the coupled model in section 5.1 and we will introduce a new parameterization for topographic roughness and stratification dependent vertical mixing in section 5.1.1 that is used throughout the whole chapter.

5.1 Ocean only and coupled model

Studies with the ocean model have shown, that inserting a vertical mixing with a coefficient larger than $0.4 - 0.5 \times 10^{-4} m^2 s^{-1}$ leads to a shutdown of the Atlantic overturning. As already discussed in chapter 4, the convection in the ocean model is GIN-sea dominant and a shutdown of GIN-sea convection leads to a shutdown of the whole Atlantic circulation. As shown in figure 3.5 of chapter 3, convection from the surface takes place only in the GIN-sea, whereas the surface waters are too fresh in the IRM-seas to induce convection from the surface downwards there. However, there still is sinking south of the sills.
We will discuss below the influence of vertical mixing in a version of the ocean model coupled to an interactive atmosphere. This coupled model CLIMBER-3α has been described in detail in Montoya et al. (2004). It consists of the same ocean model in however a slightly different horizontal resolution of 3.75°x 3.75°and it is coupled to the atmospheric component of the CLIMBER-2 model POTSDAM-2 (Potsdam Statistical Dynamical Model 2, Petoukhov et al. (2000)). It uses an isopycnal diffusivity of $1 \times 10^3 m^2/s$ and a Gent-McWilliams eddy coefficient of $2.5 \times 10^2 m^2/s$. It exhibits very similar features concerning tracer distributions and ocean dynamics as the uncoupled model described and used in chapters 2,3 and 4. However - it is not as GIN-sea convection dominant as the ocean-only model.

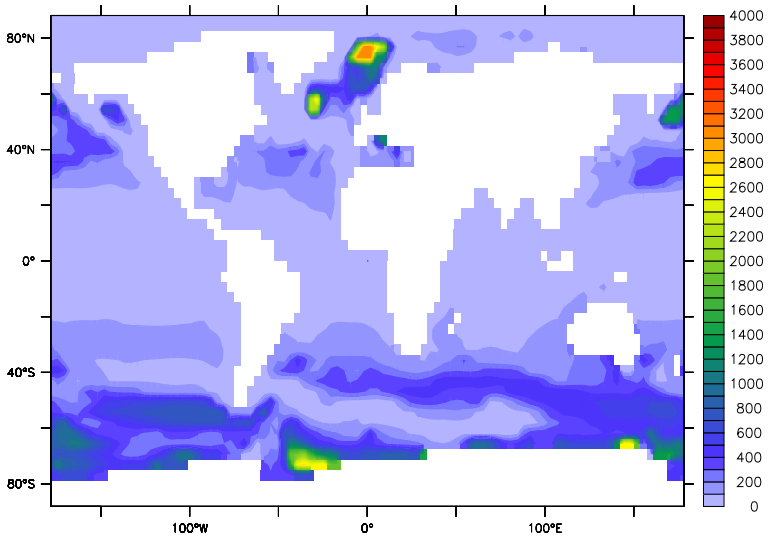

Figure 5.1: *maximum mixed layer depth for convection from the surface in CLIMBER-3α with a background vertical mixing coefficient of* $0.1 \times 10^{-4} m^2 s^{-1}$.

Figure 5.1 shows that convection from the surface takes place in both the GIN- and the IRM-sea and as will be discussed in the next sections, a shutdown of GIN-sea convection does not lead to a shutdown of the full circulation. The different behaviours of the coupled and uncoupled models can be explained partly by the fact that the freshwater input from river runoff into the Atlantic ocean is smaller than in the uncoupled model (figure 5.2). Specifically, the total Atlantic-arctic river runoff is about half as much as in the uncoupled version. Together with the fresh sea surface salinities in the region of the IRM-seas due to the insufficient representation of the surface currents, apparent in both versions of the model, the freshwater input in the ocean only version is such that it does prevent convection from the surface there, whereas in the coupled model it does not (in spite of the freshwater tongue).
Also, the sea surface temperatures in this region are colder in the coupled than in the uncoupled model. Presumably the most important atmosphere-ocean feedback that is neglected in the ocean-only model is the temperature feedback. An increase in heat transport through an increased overturning circulation leads to warmer sea surface temperatures in the northern North Atlantic that in turn tend to weaken the circulation again. Hence, on the other hand, a weakening of the circulation through a shutdown of the GIN-sea convection in the coupled model leads to colder sea surface temperatures

that tend to increase the convection (possibly elsewhere) again. Therefore, the different behaviour of the coupled and uncoupled model with respect to the dominance of the GIN-sea convection can probably be explained through these two factors, the different freshwater inputs into the Atlantic ocean as well as the neglect of the temperature feedback in the uncoupled model. The GIN-sea convection in the coupled model however is in a similar way sensitive to vertical mixing as in the ocean only model and this is one of the aspect is being discussed in the following sections.

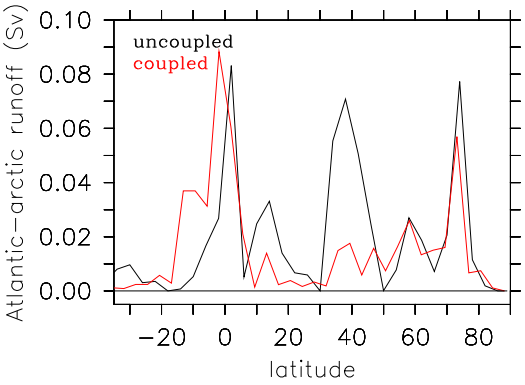

Figure 5.2: *Comparison of the Atlantic-Arctic runoff of the coupled and uncoupled model.*

5.1.1 Non-uniform vertical diffusivities

For the following analyses, we employ a parameterization of vertical mixing, mimicking enhanced mixing over rough topography. The parameterization is inspired by Hasumi and Suginohara (1999) who applied a stronger diffusivity for the deep ocean when the roughness of topography exceeded a certain threshold, decreasing exponentially with height above the bottom. Here, the diffusivity depends directly on the roughness and it decreases with height above the bottom depending on the stratification, following what Ledwell et al. (2000) found for the internal wave energy source strength in the deep ocean. The vertical diffusivity, away from the mixed layer, is given by:

$$\kappa_v(z) = \kappa_v^{bg} + \frac{A\, r}{\left[1 + \alpha(\rho(z_r) - \rho(z))\right]^2} \tag{5.1}$$

The roughness of bottom topography $r = (\sum(\overline{h} - h_i)^2)^{1/2}/\overline{h}$ for every model grid cell is determined by the standard deviation of the depths h_i of the 1/12°ETOPO topography dataset (National Geophysical Data Center,

1988) with respect to the model depths $\overline{h}$. In our setup, $A = 10 \times 10^{-4} m^2 s^{-1}$ and $\alpha = 12 m^3/kg$ and $\rho(z_r)$ is the density at the ocean bottom. This gives maximum diffusivities of $10\, cm^2 s^{-1}$ and minimum ones as given by the background coefficient κ_v^{bg}. On top, vertical diffusivity in the mixed layer is determined by the KPP (K-profile-parameterization) mixed layer scheme of Large et al. (1994).

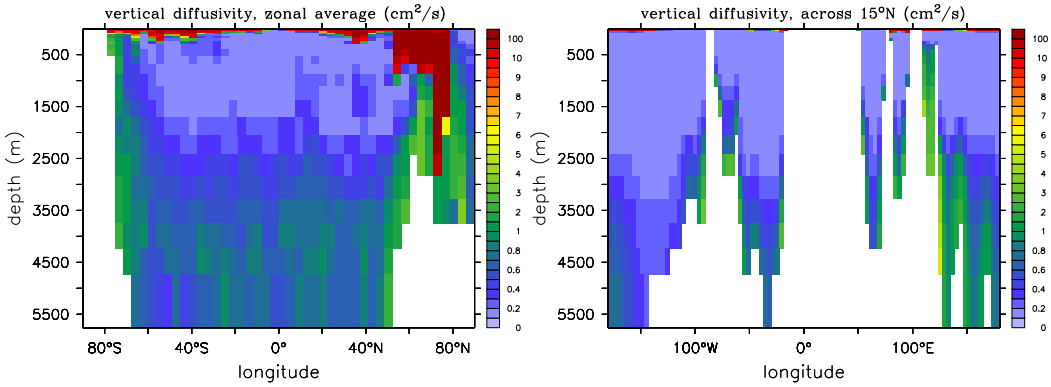

Figure 5.3: *Vertical diffusivities as computed in CLIMBER-3α from equation* (5.1) *with a background diffusivity of* $0.1 \times 10^{-4} m^2 s^{-1}$ *and from the KPP mixed layer scheme. Note the non-linear color scale. Left: Zonally averaged. Right: section across 15°N.*

Figure 5.3 shows the vertical diffusivities resulting from the topography enhanced mixing parameterization and the KPP-scheme for the diffusivities in the mixed layer. Note the very high mixing coefficients resulting from the mixed layer scheme where 'convection' takes place. In fact, the convective adjustment algorithm described in chapter 2 is not explicitly needed, since convection is already achieved through KPP.
These parameterizations are used throughout the chapter, in the next section, only the background diffusion coefficient κ_v^{bg} from equation (5.1) will be changed and the sensitivity to it will be discussed, whereas in the following section 5.3, we will specifically discuss the role of the enhanced mixing at the boundaries for driving the Atlantic MOC.

5.2 Decomposition of the AMOC into physical components and their scaling with vertical diffusivity

The Atlantic meridional overturning circulation includes a descending branch in the northern North Atlantic (deep water formation), an upwelling branch within the Atlantic under the influence of vertical mixing and the export of NADW to the Southern ocean. As described in the introduction (section 1.1), numerous studies exist that investigate the sensitivity and scaling of the Atlantic overturning to vertical mixing, however, most studies employ one hemisphere models without wind forcing, where all waters formed in the northern North Atlantic necessarily upwell within the Atlantic ocean. We here have the opportunity to reasses the scaling law from equation (1.7) in a global set up, where the Southern and the Indopacific ocean play crucial roles and with realistic topography and wind forcing. The wind stress is prescribed for all experiments from the NCEP/NCAR reanalysis (Kistler et al., 2001). As in the ocean only version, the application of the SOM-tracer advection scheme allows to eliminate spurious numerical diffusion and to attribute sensitivity to vertical mixing to the explicitly put one. The analysis is mainly based on 8 experiments that differ only in the background value of the vertical diffusivity, set to $\kappa_v^{bg} = 0.1, 0.2, 0.3, 0.4, 0.5, 0.6, 0.75$ and $1\,cm^2/s$.

5.2.1 Sensitivity of the AMOC to vertical diffusivity

Both, the magnitude as well as the shape of the AMOC are sensitive to the background diffusivity (figure 5.4). The upwelling in the Atlantic increases with κ_v^{bg}, the overflow over the Greenland-Scotland ridge as well as the depth of the NADW cell first increase with increasing κ_v^{bg}, for a diffusivity of $\kappa_v^{bg} = 1\,cm^2 s^{-1}$ however the overflow is lost and the NADW cell gets shallower again (figure 5.4, lower panel). Deep convection then takes place mainly in the Irminger Sea region, whereas it occured in both the Greenland-Iceland-Norwegian Seas and the Irminger Sea for lower diffusivites. Also, the amount of AABW coming into the Atlantic basin increased for $\kappa_v^{bg} = 1\,cm^2 s^{-1}$.

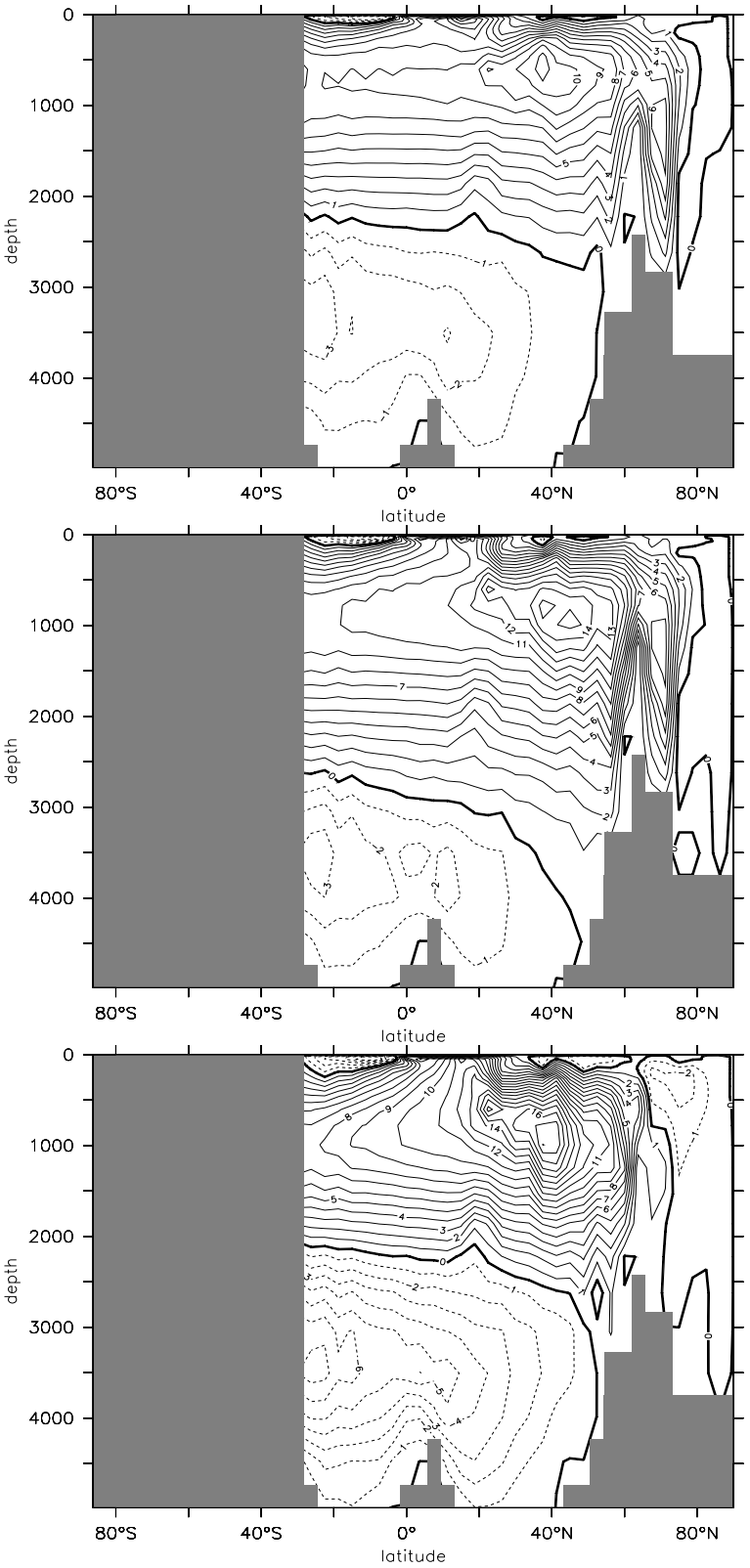

Figure 5.4: *Atlantic overturning streamfunctions for* $0.1\,cm^2s^{-1}$ *(upper panel),* $0.4\,cm^2s^{-1}$ *(middle panel) and* $1\,cm^2s^{-1}$ *(lower panel). Contour interval is* $1\,Sv$.

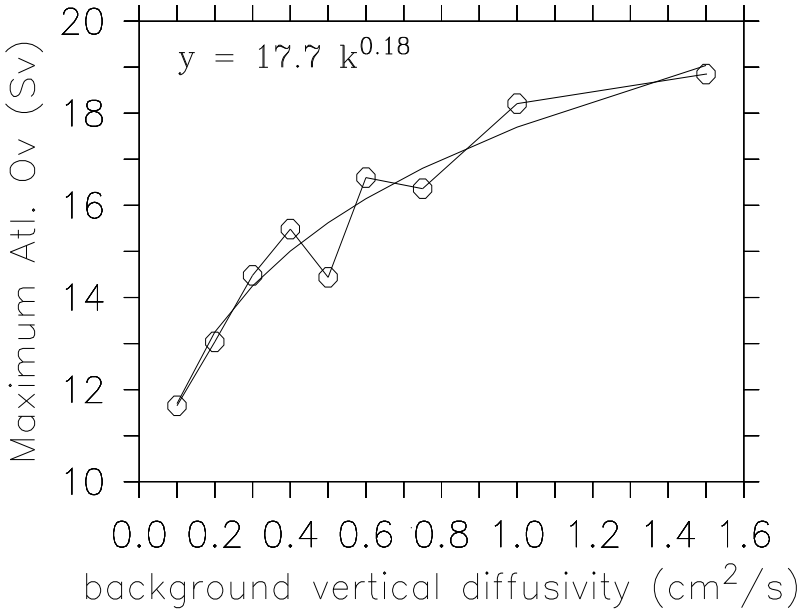

Figure 5.5: *maximum Atlantic overturning against background vertical diffusivity. Shown also a power law fit* $\kappa^{0.18}$.

In figure 5.5 we plot the maximum of the Atlantic streamfunction against the background diffusivity. The maximum occurs at depths between 600 and 900m and between latitudes 37°N - 45°N and it principally increases with increasing diffusivity consistent with numerous numerical studies, except for diffusivities of 0.5 and $0.75\,cm^2s^{-1}$. For diapycnal diffusivity less than $0.4\,cm^2s^{-1}$, the increase seems to be linear, whereas for diffusivities larger than that a change in regime seems to occur and the general increase is weaker. The maximum of the AMOC approximately follows a power law $(\kappa_v^{bg})^\alpha$ with $\alpha = 0.18$. This is much weaker than the 2/3 power law deduced from simple scaling arguments (chapter 1, equation (1.7)). The scaling law has mainly been tested in single hemisphere models without wind-forcing (section 1.3). Our global model includes wind forcing and part of the NADW is exported to the Southern Ocean. The scaling from equation (1.7) applies only if the maximum Atlantic overturning is determined solely by the vertical diffusivity that changes the pycnocline depth and by a prescibed density difference. Then, all North Atlantic downwelling is balanced by a diffusion driven upwelling in the Atlantic. We denote W_{Atl} the total upwelling (in Sv) taking place within the Atlantic basin between the latitude of the maximum overturning and 30°S:

$$W_{Atl} = MAXA - SAO \tag{5.2}$$

where SAO is the Atlantic outflow of NADW into the Southern Ocean at 30°S and MAXA the maximum Atlantic overturning. The ratio $R = SAO/MAXA$ gives a measure of the interhemispheric transport efficiency. If R is zero, there is no South Atlantic outflow and all upwelling takes place within the Atlantic, if it is equal to one, all of the waters that sink in the high latitudes of the North Atlantic are exported to the Southern Ocean.

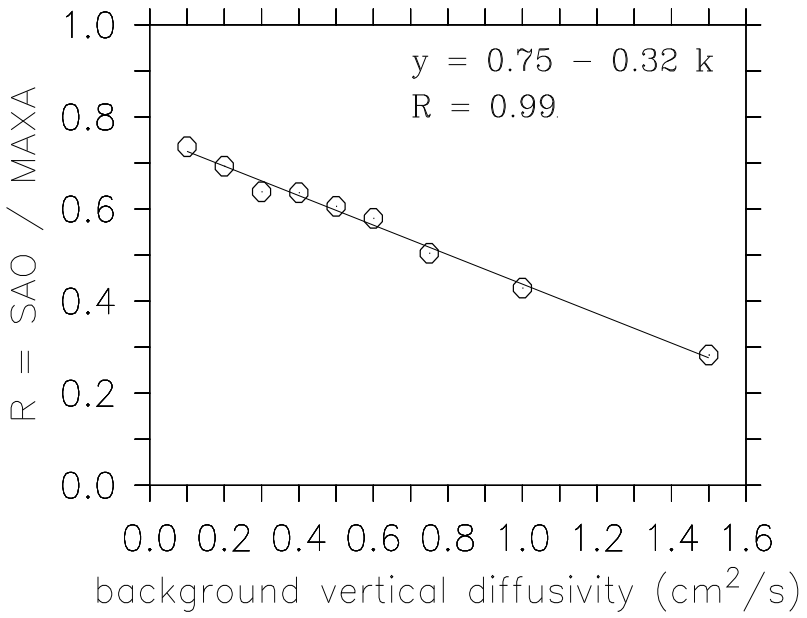

Figure 5.6: *Ratio of South Atlantic outflow and maximum Atlantic overturning against background vertical diffusivity.*

In a three-dimensional forced global ocean general circulation model with a horizontal resolution of 3.5°Prange et al. (2003) find that the efficiency R is constant at around 0.75 for vertical diffusivities at thermocline depths varying between 0.2 and 1.3 cm^2s^{-1}. R typically ranges between 0.65 and 0.75 for coupled GCMs with larger values obtained with finer resolutions (compare Mignot et al. (2004)). In general, R does not only depend on the vertical diffusivity but also on the amount of horizontal and isopycnal diffusion. In chapter 4 it was shown that R varies between 0.6 and 0.8 with the larger values obtained for increased eddy coefficients in the North Atlantic. It is difficult to deduce R from observations. Recent computations from Talley et al. (2003) indicate a value of R $\approx$ 0.8. For our model simulations, R

decreases linearly with vertical diffusivity (figure 5.6). For κ_v^{bg} greater than $0.75\,cm^2s^{-1}$ $R < 0.5$ meaning that more than half of the waters downwelling in the northern North Atlantic upwell within the Atlantic ocean.
A ratio constant with vertical diffusivity means that, assuming the wind-driven upwelling in the Southern ocean is rather independent of the background vertical diffusivity, both the upwelling within the Atlantic ocean as well as in the Indopacific increase in the same way with vertical diffusivity. In our case, the linear decrease of R pictures a situation in which the upwelling within the Atlantic is more dominant in determining the sensitivity of the maximum Atlantic overturning to κ_v^{bg}. Understanding what determines R and therefore both the maximum as well as the South Atlantic outflow and their sensitivity to vertical mixing is of primary importance for the full comprehension of the role of the ocean in climate and heat transport and also for the evaluation of oceanic models. In the following we will discuss the sensitivity of both the Atlantic upwelling and the South Atlantic outflow to the vertical diffusivity and the siginificance for the whole overturning dynamics. We will however restrict our analysis now to diffusivities $\leq 1\,cm^2s^{-1}$, since for a diffusivity as large as $1.5\,cm^2s^{-1}$ vertical mixing seems too dominant and circulations and tracer distribitions are too far away from observations.

5.2.2 Advection-diffusion balance and upwelling in the Atlantic

The total upwelling within the Atlantic as diagnosed from MAXA - SAO is plotted in figure 5.7 (circles). A fit of W_{Atl} by a power law $W = W_0\kappa^\alpha$ yielded a coefficient $\alpha = 0.5$, which is smaller than what the scaling from equation (1.7) suggests. However, it also implies that the Atlantic upwelling reaches zero for no vertical diffusion, which does not seem to be the case in figure 5.7. A linear fit of the form $W \propto \kappa$ as shown in figure 5.7 results in a much better agreement with the diagnosed upwelling yielding a residual upwelling of around 2.4 Sv for zero vertical mixing. A linear fit is consistent with Toggweiler and Samuels (1998)'s findings using an earlier version of MOM, although they obtained a much stronger slope. This strong slope might arise from their use of a more diffusive tracer advection scheme, which can amplify the upwelling (section 5.3.4).

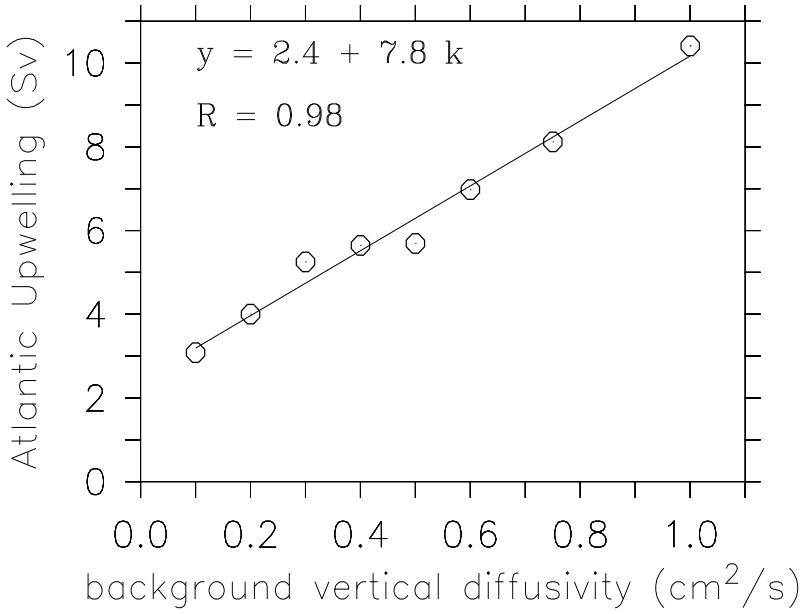

Figure 5.7: *Atlantic upwelling as a function of background diffusivity. Also shown is a linear fit* $w \propto \kappa_v^{bg}$.

Diapycnal upwelling is linked to vertical diffusivity through the thermodynamic advection-diffusion balance:

$$w_{AD}\,\partial_z \rho = \partial_z \left(\kappa_v\,\partial_z \rho\right) \tag{5.3}$$

Note that in our case with the topography and density dependent mixing parameterization, the vertical diffusivity in general depends on depth. With equation (5.3) we can estimate the amount of vertical diffusivity driven upwelling. We have to bear in mind that with equation (5.3) effects of the non-linearity of the equation of state (like thermobaricity and cabbeling) are neglected and that the balance holds mainly in the oceanic interior but not necessarily close to the ocean boundaries (cabbeling always causes a sinking or downwelling of fluid through neutral surfaces, whereas thermobaricity can lead to a vertical velocity, relative to neutral surfaces, of either sign, McDougall (1987)).
The upper panel of figure 5.8 shows the advection-diffusion driven upwelling as estimated from equation (5.3) (in red). It is diagnosed as the total upwelling occuring in the Atlantic between 30°S and the latitude of the maximum overturning for each run. The depth is chosen to be between the depth of the maximum MAXA and the depth of the maximum SAO, which differ by one grid cell for each run. For $\kappa_v \leq 0.3$, this depth lies at

682m and for $\kappa_v > 0.3$ at 876m. The total upwelling diagnosed in this way is equivalent to the upwelling as diagnosed from the streamfunction MAX - SAO (circles in figure 5.8 and figure 5.7). The advection diffusion driven upwelling is also linear in κ_v^{bg}. Also shown is the part of W_{AD} taking place in the ocean interior away from the boundaries (light blue) and at the oceanic boundaries (dark blue). Both of these parts are also linear in κ_v^{bg}. We have also distinguished the upwelling as computed with the total κ_v as in equation (5.1) from the one computed with the background coefficient κ_v^{bg} only (in green). It differs from the red line by up to 1 Sv, is however also linear in κ_v^{bg}. In fact, the W_{AD} computed from the total κ_v field is smaller than as computed from the background coefficient alone. The up to 1 Sv deviation can be boiled down to a few grid cells at the western boundary, where the effect of the increase of the diffusivity with depth dominates over the effect of the boundary enhanced mixing being higher than the background coefficient (see section 5.3.1). A more detailed discussion on the effect of boundary enhanced mixing as compared to interior mixing is deferred to section 5.3. For now, we want to concentrate on the robust result, that the linear scaling of the Atlantic upwelling with the vertical background diffusivity is due to the linear scaling of the diffusivity driven upwelling and that this is different from what the scaling law from equation (1.7) suggests.

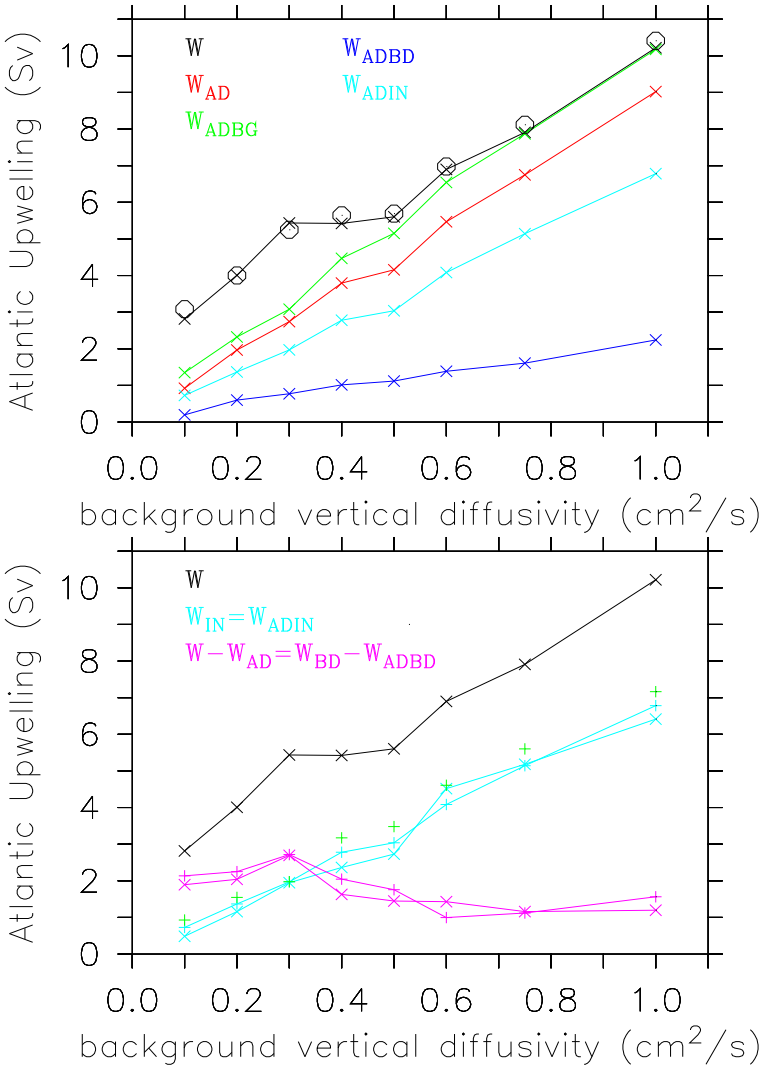

Figure 5.8: *Budget of the Atlantic upwelling:* *Upper panel:* *Upwelling as calculated from the advection-diffusion balance: Total Atlantic upwelling (black), Upwelling calculated from the total κ_v (red), upwelling calculated from the background κ_v^{bg} (green), upwelling calculated from the total κ_v in the ocean interior (light blue) and at the Atlantic boundaries (dark blue), $W_{AD} = W_{ADIN} + W_{ADBD}$.* *Lower panel:* *Comparison of the total upwelling (black) with the advection-diffusion driven upwelling: Upwelling in the interior (light blue) for advection-diffusion driven (×) and total (+) (also shown in green is the interior upwelling from the background coefficient κ_v^{bg} only). Residual upwelling as the difference of the total advection-diffusion balance and the total upwelling (purple) for the whole Atlantic (+) and at the boundaries (×).*

This scaling law of the Atlantic overturning with $\kappa^{2/3}$ only applies if the density difference $\Delta\rho$ between high and low latitudes is independent of κ_v and furthermore is derived by assuming that increased vertical diffusion will change the pycnocline depth.

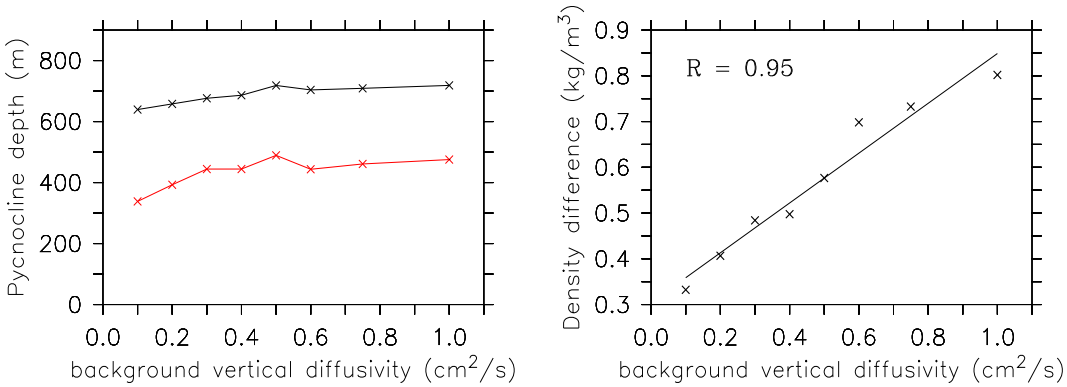

Figure 5.9: *Left: Measures of the variation in pycnocline depth as a function of κ_v^{bg}. Pycnocline depth diagnosed as in Gnanadesikan (1999) (black) and as computed from $\partial_{zz}\rho/\partial_z\rho$, zonally averaged over the Atlantic and meridionally from 30°S to the latitude of the maximum overturning (red) at the mean depth of the level of no motion. Right: Density difference as a function of κ_{vbg} at a depth of 680 m, zonally averaged over the Atlantic and between averages of latitude strips 50°N - 80°N and 20°N - 30°N.*

To first order, we can estimate the diffusion driven upwelling as coming from the background coefficient only :

$$W_{ADBG} = \kappa_{vbg} \frac{\partial_{zz}\rho}{\partial_z \rho} \tag{5.4}$$

The linear scaling suggests that the term $\frac{\partial_{zz}\rho}{\partial_z\rho}$ is constant with κ_v^{bg} in the model and it can be interpreted as a measure of one over the pycnocline depth. This term is plotted in figure 5.9 (red) together with the pycnocline depth diagnosed as in Gnanadesikan (1999) (black). The first is roughly constant at around 450 m and goes down to 350 m for diffusivities smaller than $0.3\,cm^2s^{-1}$. The latter is roughly constant between 650 and 700 m. Note that these depth ranges are not resolved in the model. The latter pycnocline depth would correspond to a constant level of 680 m in the model, i.e. the upper level of the ones from which advection-diffusion is diagnosed. The density difference at this depth does to a good approximation increase linearly with κ_v^{bg} (right panel of figure 5.9). In the model, enhanced vertical diffusion acts to decrease the density at low latitudes and hence increases the density

difference between low and high latitudes but does not influence the pycnocline depth. This would be consistent with the pycnocline depth being rather independent of the vertical diffusivity but determined by a balance between wind-induced Ekman pumping and eddy fluxes (compare section 1.3). The scaling from equation (1.7) therefore does not apply in our model. However, if the dependency of the density difference on the vertical diffusivity is incorporated in the scaling law from equation (1.7) then indeed a linear relation for W_{AD} is obtained: $\Psi \propto \kappa_v^{2/3}\kappa_v^{1/3} = \kappa_v$. Conceptually, if the strength of the Atlantic overturning is given by the pressure difference between low and high latitudes (compare chapter 4, Levermann and Griesel (2004)) then

$$\Psi \propto \Delta p = gD\Delta\rho \propto \kappa_v \tag{5.5}$$

However, since only the Atlantic upwelling and not the total Atlantic overturning is linear with κ_v, $\Psi = \Psi_{WAtl}$ and not the whole Atlantic overturning can be captured with equation (5.5). As shown in figure 5.10 there is no linear scaling of the Atlantic overturning with the meridional pressure difference as discussed in chapter 4 for all vertical diffusivities. A linear relation breaks down for integrated pressure differences greater than $90000\,hPa\,m$, corresponding to diffusivities greater than $0.4\,cm^2s^{-1}$. From the lower panel of figure 5.8 we deduce that for vertical background diffusivities larger than around $0.4\,cm^2s^{-1}$ the upwelling in the interior of the Atlantic ocean starts to dominate over the upwelling at the boundaries. When the interior upwelling is dominant, the conceptual picture of chapter 4 for explaining the linearity with the meridional pressure difference breaks down and the Stommel and Arons (1960) picture of the deep circulation is realized. When vertical mixing starts to control the circulation the linearity with the meridional pressure difference breaks down. In the model, tracer distributions for diffusivities larger than $0.4\,cm^2s^{-1}$ start to considerably worsened, underlining the fact that no significant amount of deep upwelling of NADW within the Atlantic is observed. It could be of importance for the interpretation with respect to a comparison to the scaling lawss, that the pycnocline depth or the level of no motion cannot be resolved in the model. Note that the surface pressure gradient is very important for the dynamics and it is determined by the gradient in sea surface elevation that is resolved in the free surface model within ranges of centimeters.

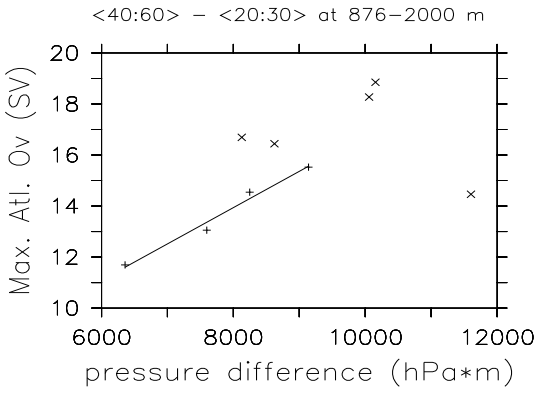

Figure 5.10: *Maximum Atlantic overturning as a function of the pressure difference between averages of 40 - 60°N and 20 - 30°N with the pressure integrated over the lower layer from 876 - 2000 m. The small crosses refer to experiments with background vertical diffusivity* $\leq 0.4\,cm^2s^{-1}$

We have explored the Atlantic upwelling and have explained the linear scaling with vertical diffusivity. However - not the whole Atlantic upwelling can be explained with it. The lower panel of figure 5.8 compares the total Atlantic upwelling with the advection-diffusion driven estimate: the total interior upwelling compares well with the advection-diffusion balance in the interior (light blue) and there is a residual upwelling as deduced from $W - W_{AD}$ which takes place at the ocean boundaries (in purple in lower panel of figure 5.8).
This connects to the upwelling at the western boundary described in chapter 4 in the limit of no vertical mixing, which depended on the eddy-mixing coefficient applied in the North Atlantic. Here, a constant eddy-coefficient is applied for all runs. Yang (2003) suggested that upwelling at the western boundary in coarse resolution models is directly linked to the effect of the wind stress curl on a poorly resolved western boundary layer. Mignot et al. (2004) indeed show that the residual upwelling at the boundaries increases with increasing wind-stress at low latitudes for low vertical mixing coefficients. From figure 5.8 it seems that the residual upwelling along the boundaries is smaller for diffusivities larger than $0.4cm^2s^{-1}$ and hence might also be linked to the cessation of GIN-sea convection. Since the decomposition into a diffusivity driven upwelling and the residual is not complete for the boundaries and we cannot say how much of the computed advection-diffusion driven upwelling is balanced by diapycnal upwelling and how much by lateral advection, interpretation of the magnitude of the boundary upwelling should be taken with care. For the ocean interior, the Sverdrup balance, linking the

meridional flow to the upwelling, holds, whereas for the boundaries, effects of lateral advection and diffusion are not negligible (compare also figure 4.15). That there is a residual upwelling however is out of question from the analyses in chapter c4 as well as from the extrapolation of W_{Atl} to around 2 Sv for zero vertical mixing.
In summary, the scaling of the maximum Atlantic overturning with $(\kappa_v^{bg})^{0.18}$ cannot be explained from the upwelling within the Atlantic but we need to look at another important component, the South Atlantic outflow.

5.2.3 South Atlantic outflow and North Atlantic sinking

The part of the NADW formed in the GIN- and IRM seas that does not upwell within the Atlantic is exported towards the Southern ocean. This component is plotted in figure 5.11 (black curve). It is only weakly dependent on the background vertical diffusivity and varies between 8 and 10 Sv for $0.1 \leq \kappa_v^{bg} \leq 1\, cm^2 s^{-1}\, cm^2 s^{-1}$. The increase in the Atlantic outflow is weak but linear for $\kappa \leq 0.4\, cm^2 s^{-1}$ and it is correlated with the increase and decrease in the GIN-sea sinking (dark blue curve in figure 5.11). For diffusivities larger than $0.4\, cm^2 s^{-1}$, the GIN-sea convection is shut down, it reverts back to 4 Sv for $\kappa_v^{bg} = 0.6\, cm^2 s^{-1}$ but then shuts down again for diffusivities larger than that. At the same time, there is an IRM-sea sinking increase that compensates for the GIN-sea sinking loss, but in a way that the increase of the total Atlantic overturning with vertical mixing is weaker than linear for $\kappa > 0.4\, cm^2 s^{-1}$ as shown in figure 5.5. The change in deep water formation regime is the result of the influence of vertical mixing on the high latitudes and we will further explore the reasons and implications in section 5.3.2.

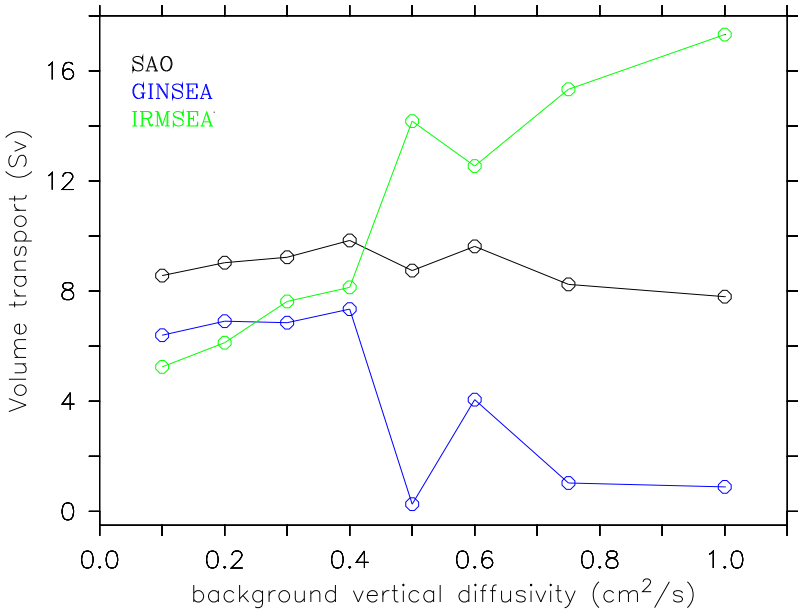

Figure 5.11: *South Atlantic outflow as diagnosed at 30°S, GIN sea sinking or overflow over Greenland-Scotland ridge (dark blue) and sinking in IRM-sea (green).*

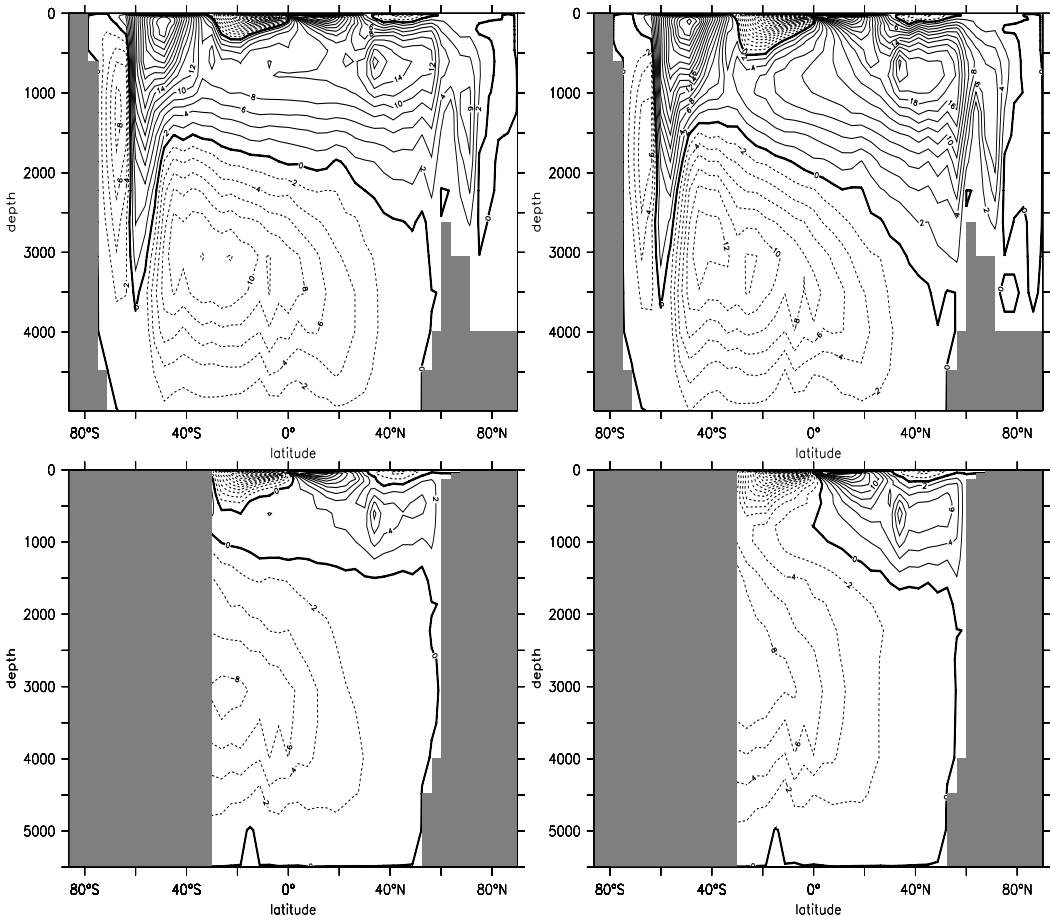

Figure 5.12: *Upper panels: Global overturning streamfunctions. Lower panels: Indopacific streamfunctions. Left:* $\kappa_v^{bg} = 0.1$ *Right:* $\kappa_v^{bg} = 0.4$. *Contour interval is 2 Sv. (Note there is a shallow overturning cell with sinking in the North Pacific of 5-6 Sv, which is not discussed here).*

Reverting back to figure 5.6, the linear decrease of the ratio R with increasing vertical diffusivity reflects the fact that the Atlantic upwelling increases linearly, whereas the South Atlantic outflow stays relatively constant. This is different from e.g. Prange et al. (2003) who find that the South Atlantic outflow scales in the same way with the vertical diffusivity as the maximum overturning, hence their ratio R is constant. However, although the South Atlantic outflow does not change that much with the vertical diffusivity, the deep upwelling in the Indian and Pacific oceans does increase with vertical diffusivity (figure 5.12. Hence, a varying amount of exported NADW upwells in the Indopacific. With κ_v^{bg}, all NADW upwells in the Southern Ocean.

5.2.4 Discussion

We have studied the sensitivity of the Atlantic overturning circulation to the background vertical diffusivity and used it to decompose the maximum of the Atlantic overturning into simple physical components. We can summarize the decomposition as follows:

$$MAXA = SAO + W_{AD} + W_{BD} \tag{5.6}$$

W_{AD} represents the upwelling in the Atlantic explainable with an advection-diffusion balance. It is linear in κ_v^{bg} and most of it can be explained as coming from the background coefficient in the ocean interior. The term W_{BD} represents a residual upwelling of 1-2 Sv that does not vary significantly with κ_v^{bg} and occurs mainly along the western boundary. Its exact magnitude is unclear, since it depends on the estimate of the diffusion driven upwelling part from the boundaries. This part decreases when the total κ_v field is considered, due to some points at the western boundary. Since the balance can be changed by 1-2 Sv from just a few points at the boundaries and since it is unclear, whether in these points, advection-diffusion balance does exactly hold, the error margin for the estimate of the boundary upwelling is also probably around 1-2 Sv. Likely, setting aside the effects of the non-linear equation of state, the upper limit of the total upwelling driven by advection-diffusion is W_{ADBG} and the lower limit is given by W_{ADBGIN}. However, the extrapolation of the Atlantic upwelling to zero vertical mixing suggests, that the residual boundary upwelling is indeed in the order of 2 Sv. This is also supported by the experiments in chapter 4, where with a very low vertical mixing of $0.05\,cm^2/s$ and a GM coefficient of $250\,m^2/s$ in the North Atlantic from 0°-90°N the boundary upwelling is also in the order of 2 Sv. Finally, the linear scaling of the advective-diffusive upwelling is a robust result.
The South Atlantic outflow at 30°varies only slightly with κ_v^{bg}. The interesting aspect is that its scaling with diffusivity depends mainly on the deep water formation site. The SAO is rather correlated with the change in convection sites in the northern North Atlantic. This suggests that vertical diffusion in the Indopacific does not drive an Atlantic overturning circulation as effectively as the vertical diffusion within the Atlantic in our model. It also connects to the discussion in chapter 4 that the SAO might mainly be determined by the Southern Ocean windstress. However, we have shown, that deep upwelling within the Indopacific does increase with κ_v^{bg}. Therefore, the partitioning of the fate of the SAO into a part that is upwelled winddriven in the Southern Ocean and one that upwells diffusively in the Indopacific decreases with vertical background diffusivity. The efficiency $R = SAO/MAXA$ de-

creases linearly with κ_v^{bg} and very weak values of $\kappa_v^{bg} \approx 0.1\, cm^2 s^{-1}$ are needed to obtain values similar to that inferred from observations. The Atlantic upwelling however depends on the Gent-McWilliams eddy diffusion coefficient (chapter 4). With stonger eddy mixing, probably higher vertical diffusivities are needed.
The variations of MAXA with κ_v^{bg} result from the combined variation of all the terms from the decomposition. Our analysis suggests that in general scalings of MAXA with κ_v should take a constant offset into account. The offset in our model is in the order of 10 Sv, with around 8 Sv coming from the South Atlantic outflow (figure 5.11), corresponding to the purely wind-driven part of the South Atlantic outflow in the limit of no vertical mixing, and around 2 Sv arising from the offset of W_{Atl} (figure 5.7). Again, the offset depends on the amount of eddy mixing in both the North Atlantic and Southern Ocean as shown in chapter 4.
We have shown, that vertical mixing in high latitudes affects the sensitivity of the Atlantic overturning to the mixing coefficient. In section 5.3.2 of the next part of this chapter we will discuss the scaling with diffusivity when this effect is eliminated.

5.3 The role of vertical mixing location for driving an Atlantic overturning

In the previous sections we have concentrated on the scaling of the Atlantic overturning with the background vertical mixing coefficient and emphasized the importance of decomposing the Atlantic overturning in a diffusivity driven part, a residual boundary upwelling and the export to the Southern Ocean. We now concentrate on exploring the importance of where the mixing takes place for driving the Atlantic overturning. We start with discussing what kind of spatial distribution of vertical mixing can potentially lead to upwelling.

5.3.1 Spatially nonuniform mixing coefficients and mixing energies

Consider again the balance equation for the vertical component of the cross isopycnal flow and the diffusion of buoyancy:

$$w_{AD}\partial_z\rho = \partial_z(\kappa_v\partial_z\rho) \tag{5.7}$$

The energy needed to sustain mixing with a rate κ_v and stratification $\partial_z \rho$ is given by (see section 1.1 in the introduction):

$$\epsilon = \gamma E = \kappa_v N^2 = -\frac{g}{\rho_0} \kappa_v \, \partial_z \, \rho \;\; (W/kg) \tag{5.8}$$

Here, γ is the mixing efficiency, that is the fraction of the turbulent kinetic energy coming from the winds and tides that goes into mixing and $N^2 = -\frac{g}{\rho_0} \partial_z \rho$ is the buoyancy frequency. Generally, assuming mixing in ocean models can potentially be represented either by a given mixing energy production and by a given mixing rate κ_v^0, the mixing coefficient κ_v can then be written as:

$$\kappa \, (x, y, z) = \kappa_v^0 (x, y, z) + \frac{\epsilon(x, y, z)}{N(x, y, z)^2} \tag{5.9}$$

Inserting equation (5.9) into equation (5.7) gives the diapycnal velocity as a function of the spatial variation of κ_v and ϵ (compare also Simmons et al. (2003)): (we have omitted the dependency on (x,y,z))

$$w_{AD} = 2 \frac{\kappa_v^0}{N} \partial_z N + \partial_z \kappa_v^0 + \frac{1}{N^2 g} \partial_z \epsilon \tag{5.10}$$

Now, the following statements about w_{AD} from equation (5.10) can be made (we assume stratification decreases with depth):

- the first term on the rhs is always positive (stratification decreases with depth and N is positive), hence this term leads to upwelling $w_{AD} > 0$.
- the sign of the second term on the rhs depends on the vertical profile of the mixing rate, a κ_v increasing with depth leads to downwelling from this term.
- the sign of the third term depends on the profile of the mixing energy conversion. It is negative if the mixing energy increases with depth and it is zero if a constant mixing energy rate is applied.

We can summarize that once only a mixing energy rate is supplied to the ocean model, diapycnal upwelling can be supported only in regions where ϵ decreases with depth. Prescribing the mixing rate, it will depend on the relative importance of term 1 and term 2 whether at a given depth upwelling or downwelling is given.
This has important consequences for the requirement to profiles if mixing was to drive an overturning circulation.

5.3.2 High latitude versus low latitude mixing

In section 5.2.3 we have seen that employing higher mixing coefficients leads to a shutdown of the GIN-sea convection and a partial compensation and increase of the IRM-sea convection and sinking. We will discuss here additional runs, where the background mixing coefficient is only changed in low latitudes between 40°S - 40°N and it is equal to $0.1\,cm^2s^{-1}$ for the high latitudes. The left panel of figure 5.13 shows that with increased low latitude mixing only, the maximum atlantic overturning increases continously for increasing background diffusivity. The right panel of figure 5.13 shows that both GIN- and IRM sea sinking continue to increase until for a vertical diffusivity of $1\,cm^2s^{-1}$ the mode change in sinking location occurs again. The South Atlantic outflow still varies only between 8 and 10 Sv and is still correlated with the GIN-sea deep water formation.

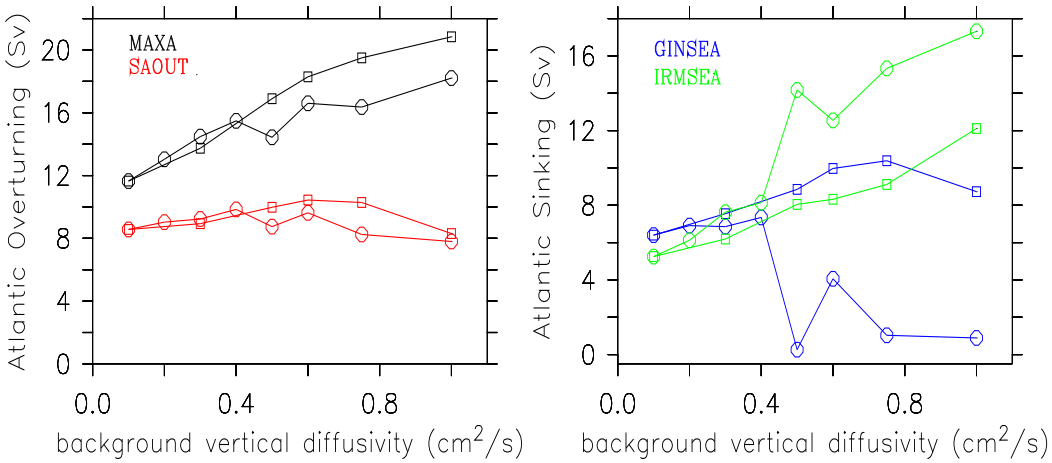

Figure 5.13: *Left: maximum Atlantic overturning (black) and Southern Ocean outflow (red). Right: Sinking in GIN-sea (dark blue) and in the region of the Irminger Sea (green). For background vertical mixing coefficient changed over the whole domain (circles) and in low latitudes only (squares)*

Figure 5.14 shows mixed layer depths for convection from the surface for a uniform background coefficient of $0.75\,cm^2s^{-1}$ (left) and for the run using $\kappa_v^{bg} = 0.75\,cm^2s^{-1}$ for the low latitudes only and $0.1\,cm^2s^{-1}$ in high latitudes (right). Consistent with figure 5.13, for higher mixing in high latitudes, convection in the GIN-seas is reduced and convection in the IRM-seas is both extended in depth and in space. The following mechanism can potentially

explain the shift in convection sites: With increasing background coefficient, the vertical mixing fluxes are increased especially where stratification is high.

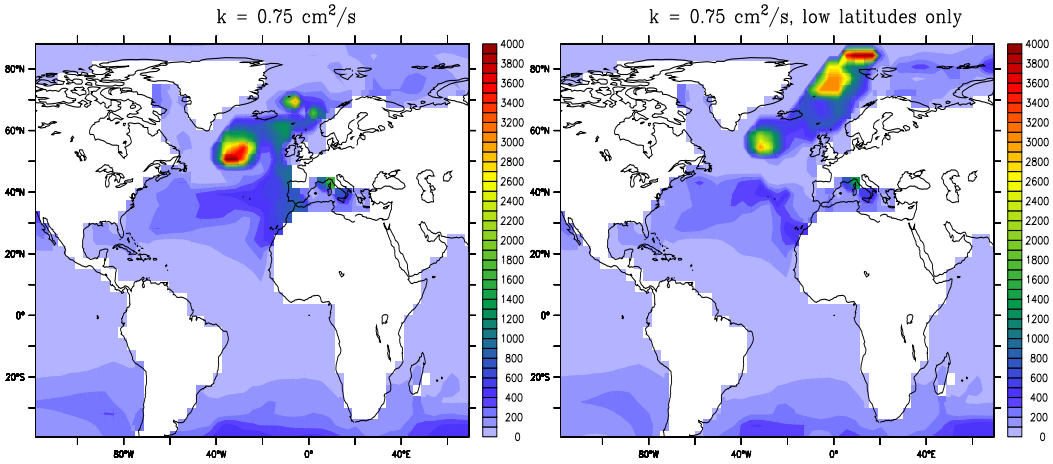

Figure 5.14: *Mixed layer depths (m). Left: for* $\kappa_v^{bg} = 0.75\,cm^2s^{-1}$. *Right: for* $\kappa_v^{bg} = 0.75\,cm^2s^{-1}$ *in low latitudes only and* $\kappa_v^{bg} = 0.1\,cm^2s^{-1}$ *in high latitudes.*

Figure 5.15 shows the zonally averaged salinity over the Atlantic ocean for the run with background mixing of $0.1\,cm^2s^{-1}$ and for comparison for the Levitus data. North of 40°N in the first few hundred meters there is a highly stratified freswhater tongue that extends further south into the Irminger Sea in the model as compared to the data. This is the region where the increased high latitude mixing operates on. High saline waters slide below these fresh surface waters and are partly transported towards the GIN-sea. Increased vertical mixing south of the sill will mix saline waters upwards leading to convection in before stratified grid cells. More waters therefore sink before they reache the GIN-sea. At the same time, the waters that still reach the GIN-sea are now fresher than before and decrease the convection in the GIN-sea further. The overall decrease in GIN-sea sinking with vertical background diffusivity is larger than the increase in IRM-sea sinking. Its is questionable whether these mechanisms can also be at play in the real ocean. The freshwater tongue does not extend as far southward. It is also limited to the zone of the East Greenland current and does not extend far into the interior of the GIN- and IRM-sea. Another mechanism could be at play as well, that involves some feedback of the deep water formation with the driving processes in low latitudes, since for a background diffusivity of $1\,cm^2/s$ in low latitudes only, the shift in convection occures nevertheless (figure 5.13).

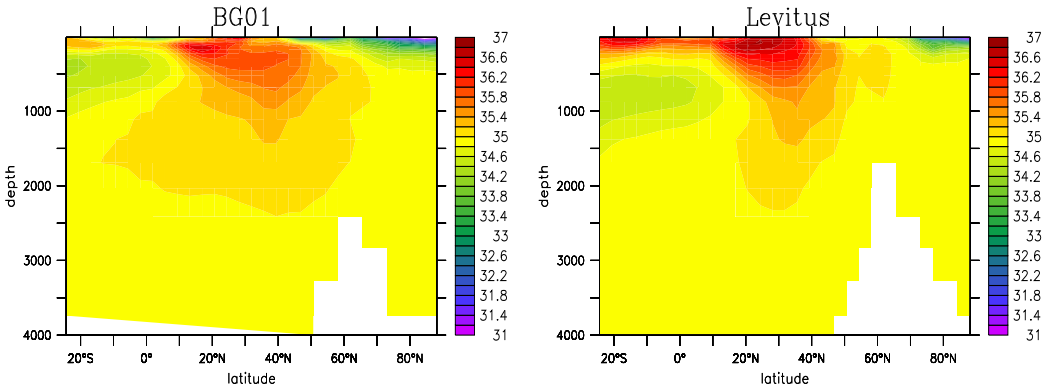

Figure 5.15: *Zonally averaged salinity (psu) in the Atlantic for the experiment with background vertical mixing of* $0.1\,cm^2s^{-1}$ *(left) and for Levitus, interpolated on the model grid (right).*

Usually, studies have shown, that an increased vertical mixing coefficient in the deep water formation regions would enhance convection and sinking (Schmittner and Weaver (2001),Oka et al. (2001)). In the model, increases in the background mixing coefficient in high latitudes have the largest effect in regions where stratification is high and rather decrease the overturning through the mechanisms described above.

We revise now the scaling laws with vertical diffusivity when the effect on the deep water formation is eliminated. The upwelling within the Atlantic still is linear with the background vertical mixing (not shown). Figure 5.16 shows the scaling for the maximum Atlantic overturning with low latitude vertical mixing only.

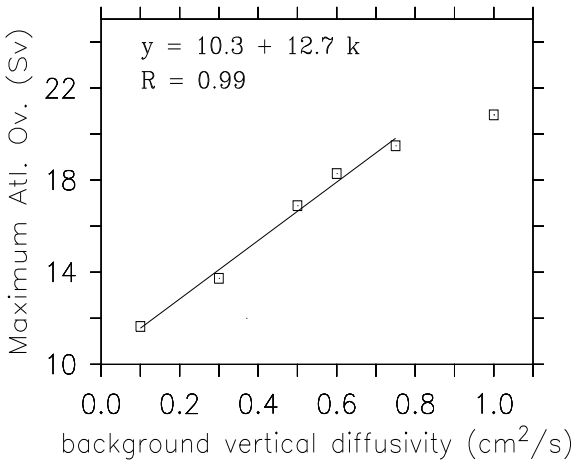

Figure 5.16: *maximum Atlantic overturning for the runs where vertical mixing is only increased in low latitudes and linear scaling for the runs* $\kappa_v^{bg} < 1\,cm^2 s^{-1}$ *where deep water formation characteristics are not changed.*

The scaling of the Atlantic overturning is linear in κ_v^{bg} when only the effect of vertical diffusion on the driving mechanisms (i.e. upwelling) is taken into account. This corresponds to values of vertical diffusivity smaller than $1\,cm^2 s^{-1}$ and it yields an offset for the limit of no vertical mixing of around 10 Sv.

5.3.3 The role of enhanced mixing at the boundaries

In this section we investigate to what extent enhanced mixing at the boundaries can drive the Atlantic overturning circulation. We first go back to the set of runs already discussed in the previous sections where only the background mixing coefficient is changed. In figure 5.8 it was shown that upwelling as calculated from the total vertical mixing coefficient is smaller than that from the background coefficient. As discussed in section 5.3.1, this can happen when the diffusivity increases with depth. Upwelling away from the boundaries in the ocean interior seems to be explainable through the upwelling as computed from the background coefficient. However, it is unclear whether the upwelling as calculated from advection-diffusion at the boundaries is the real diapycnal upwelling that is actually taking place at the boundaries (where the discrepancy of W_{AD} and W_{ADBG} stems from).

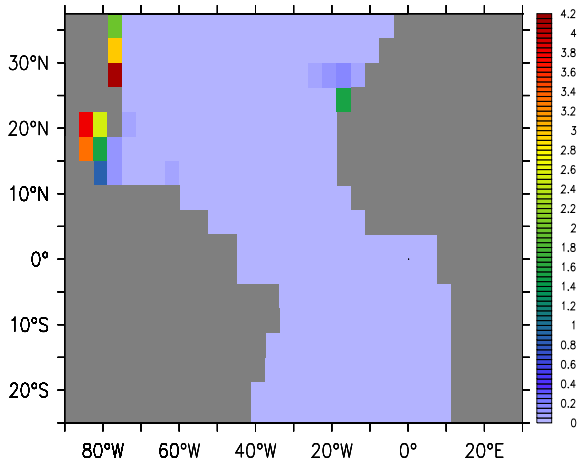

Figure 5.17: *Boundary enhanced mixing diffusivities (cm^2s^{-1}) for the experiment with background diffusivity of* $0.75\,cm^2s^{-1}$ *at a depth of ca. 900 m*

Figure 5.17 shows the difference between the non-uniform mixing coefficients with the background diffusivity of $0.75\,cm^2s^{-1}$ at a depth of ca. 900 m and reveals that the boundary enhanced mixing accounts for up to $4\,cm^2s^{-1}$ but only in a few points close to the boundaries. Two additional runs (not explicitly shown here) with a background mixing of $0.1\,cm^2s^{-1}$ and $0.75\,cm^2s^{-1}$ but no additional boundary enhanced mixing (meaning Ar from equation (5.1) is zero) indicate, that the Atlantic overturning is not affected by the deep boundary enhanced mixing. In these two runs, both the maximum overturning and the South Atlantic outflow are the same as when deep boundary enhanced mixing is included. This suggests that the difference in W_{AD} and W_{ADBG} is not a difference of real upwelling taking place.

We now move on to discuss further how enhanced boundary mixing could drive an Atlantic overturning and study three additional runs, where the mixing coefficient is further enhanced at the boundaries but now up to the ocean surface. Based on the outcome of section 5.3.2, to eliminate any effect on the deep water formation directly, we compare here only runs where the vertical mixing is modified in low latitudes.

EXP	κ_v^{bg} $(10^{-4}m^2/s)$	$\kappa_{tot}^{z=lonm}$ $(10^{-4}m^2/s)$	$\kappa_{tot}^{z=1000-4000}$ $(10^{-4}m^2/s)$	$E_{mix}^{200-5500m}$ (TW)
BG01	0.1	0.13	0.40	
BG03	0.3	0.33	0.61	1.65
BG05	0.5	0.55	0.80	2.34
BG06	0.6	0.65	0.89	2.73
BG075	0.75	0.79	1.00	3.31
BG1	1	1.03	1.22	4.40
BG01BD1	0.1	0.30	0.55	1.54
BG01BD2	0.1	0.50	0.70	2.21
BG01BD3	0.1	0.69	0.89	2.91

Table 5.1: *First column describes the experiment, second column is the background vertical mixing coefficient away from the boundaries, third column is the total mixing coefficient averaged over the low latitudes and at the depth of the level of no motion and zonally averaged over the whole ocean, fourth column is the same as the third column except that a vertical average is taken between 1000 and 4000m. The fifth column is the associated energy mixing rate $E = \epsilon/\gamma$ and γ set to 0.2 being the mixing efficiency.*

Table 5.1 summarizes the experiments under consideration: runs "BG01 - BG1" are the runs from section 5.3.2, with the background mixing increased in low latitudes only. The three last rows of table 5.1 are runs where the background coefficient at the boundaries only is set to 1,2 and 3 cm^2s^{-1} respectively, but the background mixing in the ocean interior is constant at $0.1cm^2s^{-1}$ (BG01BD1,BG01BD2,BG01BD3).

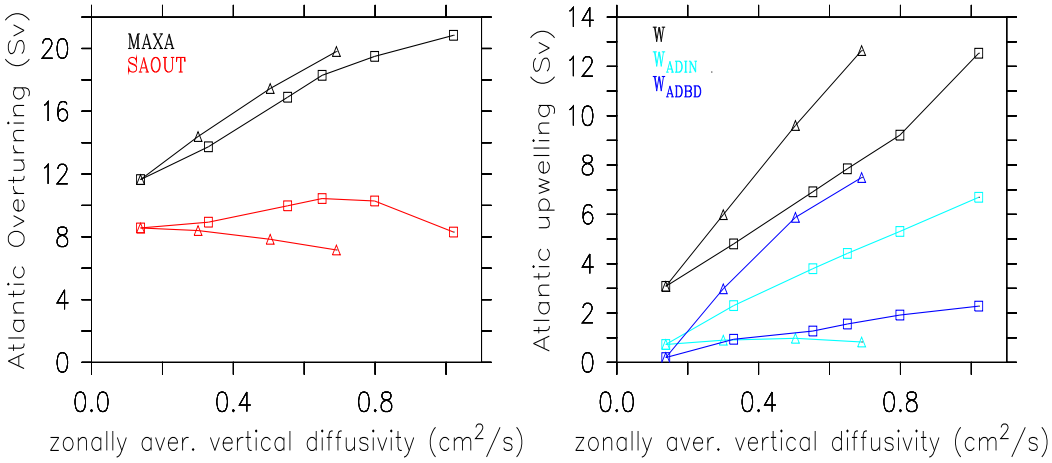

Figure 5.18: *Comparison of the runs with changed background coefficient only (BG01 - BG1, squares) and the runs where mixing is increased at the boundaries only (BG01BD1 - BG01BD3, traingles) as a function of the zonally averaged diffusivity for each experiment. Left: maximum overturning and South Atlantic outflow. Right: Total upwelling and advection-diffusion driven upwelling for the boundaries and the ocean interior.*

We plot the maximum overturning and South Atlantic outflow as a function of the zonally averaged vertical diffusivity in the left panel of figure 5.18. As shown in table 5.1, the zonally averaged diffusivity for the "BG01 - BG1" experiments is not very much different from the background diffusivities used. The maximum overturning for both sets of experiments have similar values for the same zonally averaged diffusivity, meaning that for the maximum, the circulation "feels" the same driving from a mixing that is concentrated at the boundaries as compared to one distributed equally over the low latitude ocean. However, the South Atlantic outflow is decreased as compared to the uniformely distributed mixing, meaning that the upwelling within the Atlantic is increased (right panel of figure 5.18).

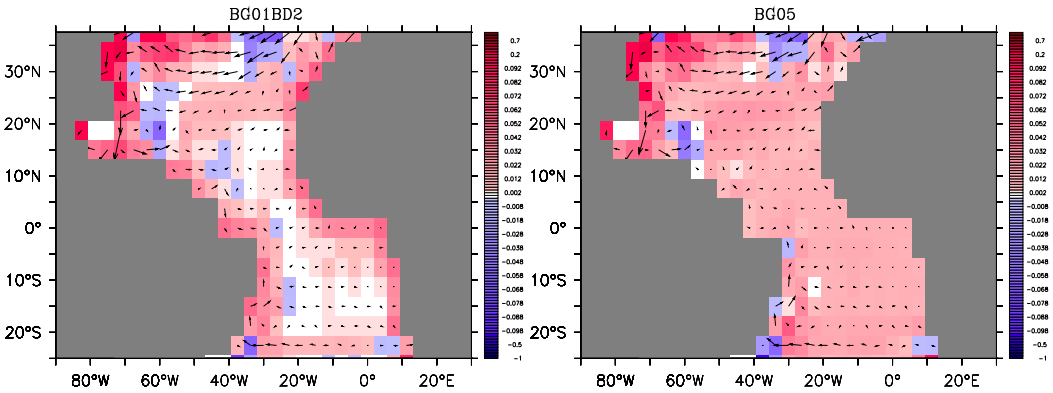

Figure 5.19: *Upwelling in Sv (red) and horizontal currents at 876 m corresponding to the mean level of no motion. Left: for experiment with* $\kappa_v^{bg} = 2\,cm^2s^{-1}$ *at the boundaries and* $0.1cm^2s^{-1}$ *elsewhere (BG01BD2). Right: for experiment with* $\kappa_v^{bg} = 0.5\,cm^2s^{-1}$ *(BG05). Upwelling* $< 0.02Sv$ *is white.*

The advection-diffusion driven upwelling is relatively constant at around 1 Sv for the ocean interior for the boundary enhanced mixing runs and it is much increased at the boundaries. Figure 5.19 compares the 'true' upwelling taking place of the run with $2cm^2s^{-1}$ at the boundaries and $0.1cm^2s^{-1}$ in the ocean interior with the one having approximately the same zonally averaged value of diffusivity of $\kappa_v^{bg} = 0.5cm^2s^{-1}$. Although patchy and with cancellations of upwelling and downwelling of neighbouring points, it shows that indeed most upwelling for the boundary enhanced mixing run takes place at or close to the boundaries, whereas in the run with mixing distributed over the whole low latitude ocean, more upwelling occurs in the ocean interior, however small for each cell, but given the large interior ocean area, it adds up to several Sv. However, still a significant amount of upwelling takes place close to the boundaries and the upwelling pattern at the western boundary between 25°N and 40°N are very similar. In the figure are also shown the horizontal currents at the level of no mean motion and the upwelling along the western boundary takes place where the flow hits the coast.
With imposing mixing rates, we have taken for granted the energy supply that must ultimately come from the winds and tides in order to sustain that kind of mixing. Generally, it depends on the stratification, whether a supply of energy to the ocean can lead to a substantial amount of bouyancy diffused into the ocean interior.

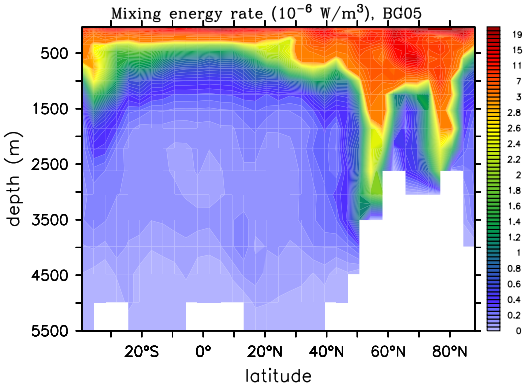

Figure 5.20: *Associated mixing energy rates for BG05, zonally averaged over the whole ocean ($10^{-6}\,W/m^3$).*

Figure 5.20 shows the associated mixing energy rates as computed from equation (1.2) for the experiment BG05. It reveals the high mixing energy rates associated with the KPP mixed layer scheme within the first 500 m and in the regions where convection takes place. The mixing energy rates generally decrease with depth. The last column of table 5.1 lists the energy rates that need to be supplied to the ocean to lead to the vertical diffusivities as imposed by the model. Here, the rate is already divided by the efficiency γ set to 0.2 (section 1.1), hence assuming that 20% of the supplied energy rate are directly converted to mixing. As we have discussed in the introduction, a very crude estimate is that around 2 TW are available from winds and tides. The experiments with background vertical mixing $< 0.75\,cm^2s^{-1}$ and with boundary mixing $< 2\,cm^2s^{-1}$ lead to energy rates below that value for depths between 200 m and the ocean bottom.
Studies with the ocean-only model and imposing a constant energy rate for the mixing or an energy profile decreasing with depth have shown, that the Atlantic overturning is weakened as compared to the experiment with very low vertical mixing of $0.05\,cm^2s^{-1}$ from chapter 4. It confirms the conclusions drawn in section 5.3.1 that in general, energy profiles decreasing with depth are needed if they should lead to a driving of the Atlantic overturning (compare also Griesel and Montoya (2005)).

5.3.4 The role of the tracer advection scheme

We want to briefly discuss the role of the tracer advection scheme for driving the AMOC. We employ three runs, that are the same as in section 5.2 except that the diffusive tracer advection scheme FCT is used. For an explicitly

prescribed diffusivity of $0.1 cm^2 s^{-1}$, there is only a very shallow and weak overturning cell (left panel of figure 5.21). Increasing the background coefficient to $0.4\, cm^2 s^{-1}$ switches a deep overturning circulation on again (right panel of figure 5.21). For the same explicitly put parameters, the vertical diffusivity 'needed' for driving an Atlantic overturning now is between 0.1 and $0.4\, cm^2 s^{-1}$ as compared to the extremely low amount of vertical mixing needed with the SOM tracer advection scheme (practically zero as shown from the interpolation to zero mixing from the first part of this chapter). This could lead to the erroneous conclusion that a diffusivity of $0.4\, cm^2 s^{-1}$ is needed in general for driving a deep circulation if one disregards the numerical diffusion. The relative 'difficulty' with the FCT scheme in achieving a realistic Atlantic overturning in terms of its volume transport can probably be explained with the spurious amount of horizontal diffusion in high latitudes making deep water formation more difficult (chapter 3). Note, that for all runs employing the fct tracer advection scheme, the convection and deep water formation in the Southern ocean is significantly increased (not shown). Also, fct kills the GIN sea deep water formation (compare chapter 3).

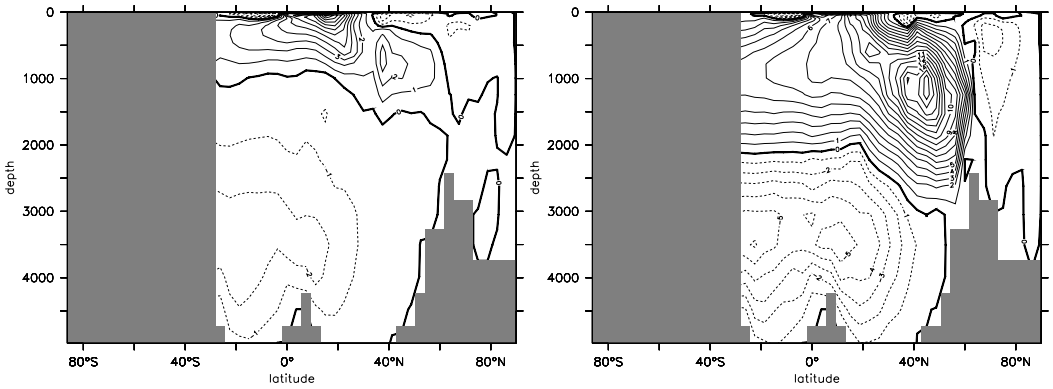

Figure 5.21: *Atlantic overturning streamfunction for two of the experiments employing the fct tracer advection scheme. Left: explicit vertical diffusivity of* $0.1 cm^2 s^{-1}$. *Right: explicit vertical diffusivity of* $0.4 cm2/s$. *Contour interval is 1 Sv.*

Note that the numerical diffusion in itself cannot drive any overturning, but once a driving mechanism in the form of Southern Ocean westerlies or explicit diapycnal diffusion exists, the role of numerical diffusion is to amplify the circulation. Vertical numerical diffusion will be large where the vertical velocities are large (section 2.5.2). Table 5.2 summarizes the associated numerical diffusivities for salinity and temperature at the depth of the mean level of no motion and zonally averaged over the whole ocean. They are in

the order of $0.1-0.2\,cm^2s^{-1}$ for temperature and $0.2-0.3\,cm^2s^{-1}$ for salinity. However, as revealed in the left panel of figure 5.22 the numerical diffusivity for temperature locally reaches values up to $3\,cm^2s^{-1}$ close to the oceanic boundaries. The right panel of figure 5.22 shows the dependence of the maximum Atlantic overturning, the South Atlantic outflow and the upwelling within the Atlantic on the explicitly put vertical background diffusivity.

EXP	κ_v^{bg} $(10^{-4}m^2/s)$	κ_{num}^{T} $(10^{-4}m^2/s)$	κ_{num}^{S} $(10^{-4}m^2/s)$	$E_{mix}^{200-5500m}$ (TW)
FCT01	0.1	0.13	0.22	
FCT04	0.3	0.15	0.25	1.65
FCT075	0.75	0.18	0.31	3.31

Table 5.2: *Experiments with the fct tracer advection scheme. First column: explicit background vertical mixing applied. Second column: associated numerical diffusivity for temperature at the depth of the maximum overturning and zonally averaged. Third column: same but for salinity. Fourth column: Mixing energy rate associated with the numerical diffusion.*

With the FCT tracer advection scheme, the sensitivity of the maximum atlantic overturning to explicit vertical background diffusivity is larger than for the same runs but employing the SOM tracer advection scheme, illustrating the amplifying mechanism of the more diffusive scheme. With an explicitly put diffusivity of $0.75\,cm^2s^{-1}$ a very large Atlantic overturning of 28 Sv is achieved, whereas with the SOM scheme, it drops down to 16 Sv. On the other hand, with the FCT scheme, no deep Atlantic overturning can be achieved with a background coefficient of $0.1\,cm^2s^{-1}$ whereas with the SOM tracer advection scheme a robust deep circulation with ca. 11Sv is obtained (figure 5.5). Figure 5.22 also reveals that it is the upwelling within the Atlantic that determines the increase in the maximum and not the South Atlantic outflow.

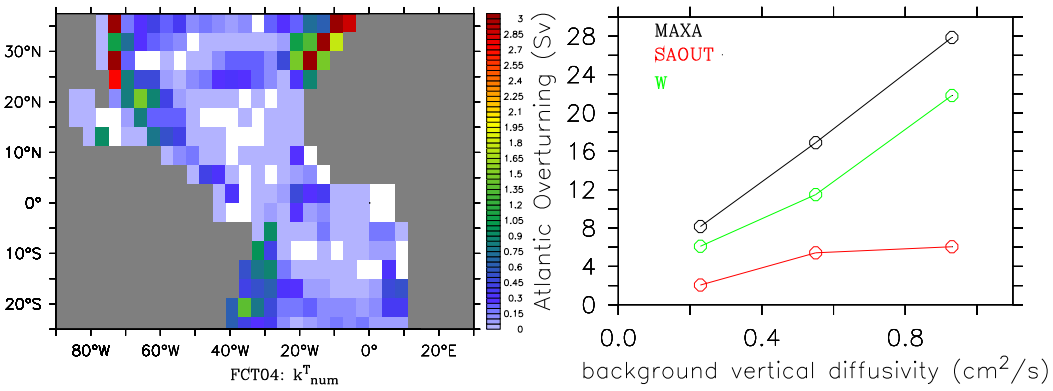

Figure 5.22: *Left: Experiment FCT04: Associated numerical diffusivity (cm^2s^{-1}) for temperature at a depth of ca. 900 m. Right: maximum Atlantic overturning, South Atlantic outflow and Atlantic upwelling f or the tree experiments employing the fct tracer advection scheme.*

5.3.5 Discussion

In the second part of this chapter we have analyzed the role of vertical mixing in different regions for determining the strength of the AMOC. We can distinguish between the effect on the driving mechanisms in low latitudes and the effect on the deep water formation in high latitudes. In our model, as opposed to other studies, increased vertical mixing in high latitudes leads to a decrease rather than increase in circulation.
We have shown, that enhanced mixing at the boundaries at depth does not drive any overturning. This is consistent with the findings of Scott and Marotzke (2002) for a single hemisphere model without wind forcing and it falsifies the hypothesis put forward that the missing mixing for driving an overturning can be found in the deep ocean (Kerr, 2000). In fact, a mixing increasing with depth can potentially lead to a decrease in upwelling. If however the enhanced boundary mixing is extended upwards to the surface, the Atlantic overturning is increased and the maximum is the same as if the enhanced boundary mixing is distributed over the whole ocean.

If it turns out to be a robust observation, that interior mixing rates are very low, then for driving a circulation indeed enhanced mixing at the boundaries but at the appropriate depths needs to be identified.

Theoretically hence, if vertical mixing was to drive an Atlantic overturning considerably, vertical mixing at the boundaries but at thermocline depths up to the surface has to be identified within the Atlantic in obervations. However, it is unclear whether large amounts of NADW indeed upwell within the Atlantic. In terms of mixing energy production, the energy has to be con-

verted to mixing where stratification is high and a profile of energy increasing with depth generally cannot drive any deep overturning circulation. It seems to count whether one can get a fair amount of energy being dissipated in regions with strong stratification at thermocline depths which decreases again for depths below that.
In the last part of this chapter we have shown that it depends crucially on the tracer advection scheme employed how much vertical mixing is needed for driving a deep Atlantic overturning circulation. With the FCT tracer advection scheme, possibly also the scaling behaviour could be modified as compared to the one with the SOM scheme discussed in the first part of this chapter.

Chapter 6

Conclusions

6.1 Summary

This work focused on the representation of the Atlantic meridional overturning circulation in a global ocean general circulation model with particular emphasis on the role of spatially inhomogeneous mixing and the meridional pressure gradient.
A model with a non-linear free surface formulation was used, allowing the ocean volume to change through explicit freshwater fluxes. A conservation problem was identified with this formulation when the time integration is done asynchronously with a stretched tracer timestep as compared to the momentum one as is common practice in ocean models. A new time stepping scheme was introduced that leads to volume and tracer conservation and at the same time still allows for stretched time steps. It was shown that the introduced distortion is negligible for a seasonal steady state equilibrium.

Due to the application of a very low diffusive tracer advection scheme it was possible to investigate the model's behaviour in the limit of very low vertical mixing. A realistic state of the Atlantic overturning circulation was obtained being purely wind driven by Southern ocean westerlies. Tracer distributions in this simulation were reasonable but with no net meridional circulations in the Indopacific and with an overly-stratified deep and bottom ocean, that arose from the spreading of relatively cold water masses formed around Antarctica. However, the upper ocean salinity and temperature distributions were well represented and especially the Southern ocean water masses were much more realistic than with the more diffusive FCT tracer advection scheme.
The role of numerical diffusion was assessed. It was shown that for the

ocean model in a low vertical mixing configuration no Atlantic overturning circulation could be achieved with the more diffusive FCT tracer advection scheme without restoring to sea surface salinities. Along the same lines, for the coupled version of the model and the FCT scheme, with a background vertical mixing coefficient of only $0.1\,cm^2s^{-1}$, there was no Atlantic overturning, whereas for a background coefficient of $0.4\,cm^2s^{-1}$ a vigorous overturning existed that was much stronger than for the equivalent experiment with the SOM tracer advection scheme. It was the horizontal numerical diffusion that tended to destabilize the Atlantic overturning, whereas the vertical numerical diffusion denoted an amplifying mechanism. Interpretations in models on how much vertical mixing is required for driving an overturning circulation should hence be taken with care. It strongly depends on the amount of spurious numerical diffusion. This might explain the relatively large range of present day Atlantic overturning strengths found in different climate models although similar explixit mixing parameters are employed (compare e.g. Boer et al. (2001)).

The implication of a localized enhanced mixing *in the deep to bottom ocean* for driving an Atlantic overturning circulation was analyzed. It was shown that this kind of mixing does not effect the Atlantic overturning. But a vertical mixing concentrated at the boundaries at thermocline depths extending up to the surface did have a driving effect. In terms of the maximum Atlantic overturning, these experiments had the same maximum Atlantic overturning as experiments with the same zonally averaged value but uniformly distributed at that depth.

An important point to be stressed is that in all experiments with changed vertical mixing, the South Atlantic outflow was hardly affected, even when the effects of vertical mixing on high latitudes were eliminated and any driving mechanism for the Atlantic overturning arised mainly from within the Atlantic ocean (however, the fate of the NADW was increasingly mixing driven upwelling within the Indopacfific ocean). This would be consistent with a South Atlantic outflow predominantly determined by the Southern Ocean windstress. On the other hand, the experiments in chapter 4 illustrated how changes in the pressure gradients within the Southern Ocean outflow region can modify the wind-driven picture presented by Nof (2003). The experiments with changed Gent-McWilliams coefficients effected the South Atlantic outflow by only a few Sv, but the extension to runs employing a variety of surface forcings and mixing parameters revealed a range of 6-16 Sv for the South Atlantic outflow. This is consistent with several studies having shown the sensitivity of the Atlantic overturning and South Atlantic outflow to the freshwater forcing within the Southern ocean (Weijer et al., 2001; Knorr and Lohmann, 2003). Also, the experiments with

decreased winds from chapter 3 have demonstrated that an interhemispheric Atlantic overurning can still exist in the limit of no winds in the Southern ocean once the driving in the form of diapycnal mixing is devised. Overall, the hypothesis put forward by Nof (2003) was not supported.

Applying different magnitudes of the Gent-McWilliams eddy coefficients in the Southern Ocean and North Atlantic was interpreted as changing the thermohaline component of the system through changing the density gradients in the different regions. The linear relation found in previous studies between measures of the meridional pressure gradient and the maximum Atlantic overturning was confirmed. This relation was shown to be due to one significant pressure gradient between the pressure at high latitude deep water formation regions and a relatively uniform pressure in low latitudes between 30°N and 30°S and it could directly be related to a zonal flow through geostrophy. In the framework of the coarse resolution model with large vertical grid extends, the pycnocline depth was found to be constant. Hence, the linear dependence on the meridional pressure difference and the fixed vertical scale for the volume transport is more consistent with the Stommel box model.

. It is important to note that the upwelling along the boundaries within the Atlantic was identified to be dominant for vertical mixing coefficients smaller or equal to $0.4\,cm^2s^{-1}$. For diffusivities larger than that the upwelling within the interior of the Atlantic ocean started to dominate and the linear relation with the pressure difference seemed to break down. The model then moves more to the Stommel and Arons (1960) realization of the deep circulation with horizontal recirculations and interior upwelling.

The scaling of the Atlantic overturning with $\kappa^{2/3}$ could not be confirmed in the global model. Instead, a linear scaling of the Atlantic upwelling was found with the background vertical diffusivity, consistent with a constant pycnocline depth. The linear dependence on the background vertical diffusivity held also for the other Atlantic overturning components when the effect of vertical mixing on the deep water formation in the North Atlantic was eliminated.

Overall, the following new view on the Atlantic meridional overturning circulation has emerged from this work:

1. A realistic purely wind-driven circulation can be realized in which Southern Ocean wind stress and not diapycnal mixing provides the main energy source for the upwelling of North Atlantic Deep Water.
   However, the actual strength of the maximum Atlantic MOC is not uniquely determined by the Southern Ocean wind stress but also by the density/pressure gradients in the deep-water formation regions as well as in the Southern Ocean.
   The role of the Southern Ocean windstress is therefore to provide the ability for North Atlantic Deep Water to upwell, but not to determine the rate at which it is formed and exported out of the Atlantic ocean.

2. The meridional pressure gradient between low and high latitudes is the key quantity, that determines the strength of the circulation. The importance of this result might be connected to a recent discussion about wether a circulation whose ultimate potential driving mechanisms (in the sense of providing the ability for deep waters to upwell) are winds and tides should still be called "Thermohaline Circulation"(Wunsch, 2002; Rahmstorf, 2003). If the term Thermohaline Circulation strictly refers to its driving mechanism, the term is not applicable since surface heat and freshwater fluxes are not the drivers. However - if the definition is disconnected from the driving issue, one can still speak of a Thermohaline Circulation. Surface heat and freshwater fluxes do provide the ocean with the ability to form density and pressure gradients. Although the ultimate meridional pressure gradient in the ocean interior is determined by the winds, mixing and the circulation itself, it determines the strength of the circulation in a diagnostic sense, one of the main results of this work.

6.2 Outlook

This work has suggested that diapycnal mixing is not as essential for driving an Atlantic overturning as previously thought, since already a realistic Atlantic overturning could be achieved with virtually no diapycnal mixing. However, the amount of vertical mixing needed for achieving an Atlantic overturning circulation might depend crucially on the amount of eddy mixing and the scaling with vertical diffusivity should be reassesed with

different eddy mixing coefficients. In terms of the relative contribution of winds and mixing as the drivers for the meridional overturning circulations, the argument of Webb and Suginohara (2001a,b) should be considered. They note that not all of the 30 Sv of deep waters formed need to upwell through mixing to the surface. In this work, the Atlantic overturning was the focus, leaving out the role of Antarctic Bottom Water (AABW) formation. Webb and Suginohara (2001a,b) consider separately the two MOC cells, the AABW cell and the NADW cell. They argue AABW is brought up to NADW levels by diapycnal mixing. Beyond that, it reaches the surface by wind-driven upwelling. They suggest that in the NADW cell, 9-12 Sv of deep water upwell in the Southern Ocean to the surface via Ekman suction. The rest, about 5-7 Sv, is upwelled by mixing. It seems that this is the way to reconcile the two paradigms on the driving mechanisms for the MOC. It is also in accordance with the inverse analysis of hydrographic sections in the Southern Ocean (Sloyan and Rintoul, 2001b).

It seems important to move away from using spatially uniform mixing coefficients for both eddy and small scale mixing in ocean models. Several authors have suggested to use a parameterization of eddy mixing coefficients depending on the growth rate of baroclinic eady waves. This parameterization requires the use of a length scale for which different formulations have been introduced (Stone, 1972; Visbeck et al., 1997; Bryan et al., 1999) Preliminary model simulations employing the different length scales (width of the baroclinic zone, Rossby radius of deformation or a constant length scale) have shown that the associated eddy coefficients are very different for the different formulations, leading to opposite distributions of eddy coefficients.

The origin of the residual boundary upwelling within the North Atlantic should be further explored. To test the hypothesis put forward by Yang (2003), experiments with increased horizontal viscosity at the western boundary only, leading to a better resolution of the western boundary current with more grid points or increasing the horizontal resolution could better clarify wether his mechanisms holds. Also, the effect of an increase in vertical resolution could be crucial. This can also clarify the implications of the fact that the horizontal gradients in pycnocline depth cannot be resolved with a coarse vertical resolution.

The experiments in chapter 4 could be reassessed by taking into account the temperature feedback with the atmosphere which has been neglected in the ocean only experiments. Especially, experiments where Southern ocean winds are modified are needed for the coupled version of the ocean model, in which temperature feedback is taken into account.

In terms of the implications of non-uniform distribution of mixing and

numerical diffusion for the stability of the Atlantic overturning circulation, hysteresis experiments should be undertaken. Preliminary results with the coupled model have indicated that the model with the low diffusive tracer advection scheme is much more stable than found in previous studies with respect to a shutdown of the THC with increased freshwater forcing in the North Atlantic. The amplifying mechanism of vertical numerical diffusion on the one hand and the destabilizing factor of horizontal numerical diffusion on the other could provide positive or negative feedback mechanisms explaining different behaviours of low- and high diffusive tracer advection schemes with respect to the hysterees. Not only should the dependence of the hysteresis behaviour on vertical mixing be assessed, but also the dependence on the eddy and horizontal diffusion. On top, the apparent inconsistency between hysteresis behaviour in 3-d and zonally averaged ocean models with respect to vertical mixing, as noted by Prange et al. (2003), needs to be clarified. They found a decreased width of their hysteresis curves with decreasing vertical mixing for an ocean general circulation model as opposed to an increase in width found in zonally averaged models (Schmittner and Weaver, 2001).

Bibliography

Arakawa, A., Computational design of long-term numerical integration of the equations of fluid motions., *J. Comp. Phys.*, *1*, 119 – 143, 1966.

Bacon, S., Gould, W., and Jia, Y., Open-ocean convection in the Irminger sea., *Geophys. Res. Lett.*, *30*, 2003.

Berliand, M. and Berliand, T., Measurements of the effective radiation of the earth with vvarign cloud amounts., *Izv. Akad. Nauk SSR, Ser. Geofiz.*, *1*, 1952.

Boer, G., Stouffer, R., Dix, M., Noda, A., Senior, C., Raper, S., and Yap, K., Projections of Future Climate Change., in *Climate Change 2001: The Scientific basis.*, Intergovernmental Panel of Climate Change, Cambridge University press, 2001.

Böning, C., Holland, W., Bryan, F., Danabasoglu, G., and McWilliams, J., An overlooked problem in model simulations of the thermohaline circulation and heat transport in the Atlantic ocean., *J. Clim.*, *8*, 515 – 523, 1995.

Boris, J. and Book, D., Flux-corrected transport, i. shasta: A fluid transport algorithm that works., *Journal of Comp. Phys.*, *11*, 38 – 69, 1973.

Bryan, F., On the parameter sensitivity of primitive equation ocean general circulation models, *J. Phys. Oceanogr.*, *17*, 970 – 985, 1987.

Bryan, K., A numerical method for the study of the circulation of the world ocean, *J. of Comp. Phys.*, *4*, 347 – 376, 1969.

Bryan, K., Accelerating the convergence to equilibrium of ocean-climate models, *J. Phys. Oceanogr.*, *14*, 666 – 673, 1984.

Bryan, K. and Cox, M., A numerical investigation of the oceanic general circulation, *Tellus*, *19*, 54 – 80, 1967.

Bryan, K. and Lewis, L., A water mass model of the world ocean, *J. Geophys. Res.*, *20*, 817 – 830, 1979.

Bryan, K., Dukowicz, J., and Smith, R., On the mixing coefficient in the parameterization of bolus velocity, *J. Phys. Oceanogr.*, *29*, 2442 – 2456, 1999.

Cummins, P., Holloway, G., and Gargett, A., Sensitivity of the GFDL ocean general circulation model to a parameterization of vertical diffusion., *J. Phys. Oceanogr.*, *20*, 817 – 830, 1990.

Danabasoglu, G. and McWilliams, J., Sensitivity of the global ocean circulation to paramterizations of mesoscale tracer transports., *J. Clim.*, *8*, 2967 – 2987, 1995.

de Verdiere, A. C., Buoyancy driven planetary flows., *J. Mar. Res.*, *46*, 215 – 265, 1988.

Dickson, R. and Brown, J., The production of North Atlantic Deep Water: sources, rates and pathways., *J. Geophys. Res.*, *99*, 12 319 – 12 341, 1994.

Döös, K. and Coward, A., The Southern ocean as the major upwelling zone of north Atlantic deep water, *International Woce Newsletter*, *27*, 3–4, 1997.

Döös, K. and Webb, D., The Deacon cell and other meridional cells of the southern ocean., *J. Phys. Oceanogr.*, *24*, 429 – 442, 1994.

Fichefet, T. and Maqueda, M. M., Sensitivity of a global sea ice model to the treatment of ice thermodynamics and dynamics, *J. Geophys. Res.*, *102*, 12,609–12,646., 1997.

Ganachaud, A. and Wunsch, C., Improved estimates of global ocean circulation, heat transport and mixing from hydrographic data, *Nature*, *408*, 453 – 457, 2000.

Gent, P. and McWilliams, J., Isopycnal mixing in ocean circulation models, *J. Phys. Oceanogr.*, *20*, 150 – 155, 1990.

Gent, P., Willebrand, J., McDougall, T., and McWilliams, J., Parameterizing eddy-induced tracer transports in ocean general circulation models, *J. Phys. Oceanogr.*, *25*, 463 – 474, 1995.

Gerdes, R., Köberle, C., and Willebrand, J., The influence of numerical advection schemes on the results of ocean general circulation models., *Clim. Dyn.*, *5*, 211 – 226, 1991.

Gill, A., *Atmosphere-Ocean Dynamics.*, Academic Press Inc., 1982.

Gnanadesikan, A., A simple predictive model for the structure of the oceanic pycnocline, *Science*, *283*, 2077 – 2079, 1999.

Gnanadesikan, A. and Toggweiler, J., Constraints placed by silicon cycling on vertical exchange in general circulation models, *Geophys. Res. Lett.*, *26*, 1865 – 1868, 1999.

Greatbatch, R., A note on the representation of steric sea level in models that conserve volume rather than mass, *J. Geophys. Res.*, *99*, 12 767 – 12 771, 1994.

Gregg, M., Sanford, T., and Winkel, D., Reduced mixing from the breaking of internal waves in equatorial waters, *Nature*, *422*, 513 – 515, 2003.

Griesel, A. and Maqueda, M. M., The relation of meridional pressure gradients to North Atlantic Deep Water volume transport in an Ocean General Circulation Model, *submitted to Clim. Dyn.*, 2005.

Griesel, A. and Montoya, M., The role of diapycnal mixing location and numerical diffusion for Atlantic overturning dynamics in a coupled climate model, *to be submitted*, 2005.

Griffies, S., The Gent-McWilliams skew flux, *J. Phys. Oceanogr.*, *28*, 831 – 841, 1997.

Hasumi, H. and Suginohara, N., Effects of locally enhanced vertical diffusivity over rough bathymetry on the world ocean circulation, *J. Geophys. Res.*, *104*, 23,367–23,374, 1999.

Hibler, W., A dynamic-thermodynamic sea-ice model., *J. Phys. Oceanogr.*, *9*, 815 – 846, 1979.

Hofmann, M. and Morales-Maqueda, M., Performance of a second-order moments advection scheme in an Ocean General Circulation Model, *in preparation for ..*, 2004.

Huang, R., Mixing and energetics of the oceanic thermohaline circulation, *J. Phys. Oceanogr.*, *29*, 727 – 746, 1999.

Huck, T., de Verdiere, A. C., and Weaver, A., Interdecadal variability of the thermohaline circulation in box-ocean models forced by fixed surface fluxes, *J. Phys. Oceanogr.*, *29*, 865 – 892, 1998.

Hughes, T. and Weaver, A., Multiple equilibria of an asymmetric two-basin model, *J. Phys. Oceanogr.*, *24*, 619 – 637, 1994.

Hunke, E. and Dukowicz, J., An elastic-viscous-plastic model for sea ice dynamics., *J. Phys. Oceanogr.*, *27*, 1849 – 1867, 1997.

Kalnay, E., Kanamitsu, M., Kistler, R., Collings, W., Deaven, D., Gandin, L., Iredell, M., Saha, S., White, G., Woollen, J., Zhu, Y., Chelliah, M., Ebisuzaki, W., Higgins, W., Janowiak, J., Mo, K., Ropelewski, C., Wang, J., Leetmaa, W., Reynolds, R., Jenne, R., and Joseph, D., The NCEP/NCAR 40-year Reanalysis Project, *Bull. Amer. Meteor. Soc.*, *77*, 437 – 471, 1996.

Kamenkovich, I. and Sarachik, E., Mechanisms controlling the sensitivity of the Atlantic thermohaline circulation to the parameterization of eddy transports in ocean GCMs, *J. Phys. Oceanogr.*, *34*, 1628, 2004.

Kerr, R., Missing mixing found in the deep sea, *Science*, *288*, 1947 – 1949, 2000.

Killworth, P. and Nanneh, M., Isopycnic momentum budget of the Antarctic Circumpolar Current in the Fine Resolution Antarctic Model., *J. Phys. Oceanogr.*, *24*, 1201 – 1223, 1994.

Killworth, P., Smeed, A., and Nurser, A., The effects on ocean models of relaxation towards observations at the surface., *J. Phys. Oceanogr.*, *30*, 160 – 174, 2000.

Kistler, R., Kalnay, E., Saha, S., White, G., Woollen, J., Chelliah, M., Ebisuzaki, W., Kanamitsu, M., Kousky, V., van den Dool, H., Jenne, R., and Fiorino, M., The NCEP/NCAR 50-year reanalysis, *Bull. Amer. Meteor. Soc.*, *82*, 247 – 267, 2001.

Klinger, B., Drijhout, S., Marotzke, J., and Scott, J., Sensitivity of basin-wide meridional overturning to diapycnal diffusion and remote wind forcing in an idealized Atlantic-Southern ocean gemopetry, *J. Phys. Oceanogr.*, *33*, 2003.

Knorr, G. and Lohmann, G., Southern ocean origin for the resumption of atlantic thermohaline circulation during deglaciation, *letters to nature*, *424*, 532 – 536, 2003.

Kuhlbrodt, T., Griesel, A., Montoya, M., Levermann, A., Hofmann, M., and Rahmstorf, S., On the driving processes of the oceanic meridional overturning circulation., *submitted to Reviews of Geophysics*, 2005.

Large, W. and Pond, S., Open ocean momentum flux measurements in moderate to strong winds., *J. Phys. Oceanogr.*, *11*, 324 – 336, 1981.

Large, W. and Pond, S., Sensible and latent heat flux measurements over the ocean., *J. Phys. Oceanogr.*, *12*, 464 – 482, 1982.

Large, W., McWilliams, J., and Doney, S., Oceanic vertical mixing: A review and a model with a nonlocal boundary layer parameterization., *Rev. Geophys.*, *32*, 363 – 403, 1994.

Lazar, A., Madec, G., and Delecluse, P., The deep interior downwelling, the Veronis effect, and mesoscale tracer transport parameterizations in an OGCM., *J. Phys. Oceanogr.*, *29*, 2945 – 2961, 1999.

Ledwell, J., Watson, A., and Law, C., Evidence for slow mixing across the pycnocline from an open-ocean tracer release experiment, *Nature*, *364*, 701 – 703, 1993.

Ledwell, J., Montgomery, E., Polzin, K., Laurent, L., Schmitt, R., and Toole, J., Evidence for enhanced mixing over rough topography in the abyssal ocean, *Nature*, *403*, 179 – 182, 2000.

Levermann, A. and Griesel, A., Solution of a model for the oceanic pycnocline depth: Scaling of overturning strength and meridional pressure difference, *Geophys. Res. Lett.*, *31*, 2004.

Levermann, A., Griesel, A., Hofmann, M., Montoya, M., and Rahmstorf, S., Dynamic sea level changes following changes in the thermohaline circulation., *Clym. Dyn.*, *accepted*, 2004.

Levitus, S., Climatological atlas of the world ocean., *NOAA Prof. Pap.*, *13*, 173 pp., 1982.

Levitus, S., Burgett, R., and Boyer, T., World ocean atlas 1994, volume 3: Salinity, *NOAA ATLAS NESDIS 3*, *4*, 99 pp., 1994.

Losch, M., Adcroft, A., and Campin, J.-M., How sensitive are coarse General Circulation Models to fundamental approximations in the equations of motion?, *J. Phys. Oceanogr.*, *34*, 306 – 319, 2003.

Lu, Y. and Stammer, D., Vorticity balance in coarse-resolution global ocean simulations, *The ECCO Report Series*, *15*, 1998.

Manabe, S. and Stouffer, R., Multiple-century response of a coupled ocean-atmosphere model to an increase of atmospheric carbon dioxide., *J. Clim.*, *7*, 5 – 23, 1994.

Marotzke, J., Boundary mixing and the dynamics of the three-dimensional thermohaline circulation, *J. Phys. Oceanogr.*, *27*, 1713 – 1728, 1997.

Marshall, J. and Schott, F., Open-ocean convection: observations, theory, and models, *Rev. of Geophys.*, *37*, 1 – 64, 1999.

Marshall, J., Jones, H., Karsten, R., and Wardle, R., Can eddies set ocean stratification?, *J. Phys. Oceanogr.*, *32*, 26 – 38, 2002.

McDougall, T., Thermobaricity, cabbeling and water-mass conversion, *J. Geophys. Res.*, *92*, 5448 – 5464, 1987.

Mignot, J., Levermann, A., and Griesel, A., A decomposition of the Atlantic meridional overturning circulation into simple physical processes using its sensitivity to vertical mixing, *J. Phys. Oceanogr.*, *accepted*, 2004.

Montoya, M., Griesel, A., Levermann, A., Mignot, J., Hofmann, M., Ganopolski, A., and Rahmstorf, S., The earth system model of intermediate complexity climber-3α: Part 1: description and performance for present day conditions, *submitted to Clim. Dyn.*, 2004.

Moum, J. and Osborn, T., Mixing in the main thermocline., *J. Phys. Oceanogr.*, *16*, 1250 – 1259, 1986.

Moum, J., Caldwell, D., Nash, J., and Gunderson, G., Observations of boundary mixing over the continental slope., *J. Phys. Oceanogr.*, *32*, 2113 – 2130, 2002.

Munk, W., On the wind-driven ocean circulation, *J. Meteorol.*, *7*, 79 – 93, 1950.

Munk, W., Abyssal recipes I, *Deep Sea Res.*, *13*, 707 – 730, 1966.

Munk, W. and Wunsch, C., Abyssal recipes II: energetics of tidal and wind mixing, *Deep Sea Res.*, *45*, 1977 – 2010, 1998.

National Geophysical Data Center, 1988, *Data Announcement 88-MGG-02, Digital relief of the surface of the Earth*, National Oceanic and Atmospheric administration (NOAA), Boulder, Colorado, 1988.

Nof, D., The Southern Ocean's grip on the northward meridional flow., *Prog. Oceanogr.*, *56*, 223 – 247, 2003.

Oakey, N., Ruddick, B., Walsh, D., and Burke, J., Turbulence and microstructure measurements during NATRE., *Eos*, *75*, 130, 1994.

Oka, A., Hasumi, H., and Suginohara, N., Stabilization of thermohaline circulation by wind-driven and vertical diffusive salt transport, *Clim. Dyn.*, *18*, 71 – 83, 2001.

Oke, P., England, M., and Reason, C., On the sensitivity of a coarse resolution world ocean model to different wind stress climatologies, *J. Phys. Oceanogr.*, *submitted*, 2004.

Pacanowski, R. and Griffies, S., *The MOM-3 manual.*, GFDL Ocean Group, NOAA/Geophysical Fluid Dynamics Laboratory, Princeton, NJ, 1999.

Paluszkiewicz, T. and Romea, R., A one-dimensional model for the parameterization of deep convection in the ocean, *Dyn. Atmos. and Oceans*, *26*, 95 – 130, 1997.

Park, Y.-G., The stability of thermohaline circulation in a two-box model., *J. Phys. Oceanogr.*, *29*, 1999.

Park, Y.-G. and Bryan, K., Comparison of thermally driven circulations from a depth-coordinate model and an isopycnal-layer model. part I: Scaling-law sensitivity to vertical diffusivity., *J. Phys. Oceanogr.*, *30*, 590 – 605, 2000.

Parkinson, C. and Washington, W., A large-scale numerical model of sea ice., *J. Geophys. Res.*, *84*, 311 – 337, 1979.

Petoukhov, V., Ganopolski, A., Brovkin, V., Claussen, M., Eliseev, A., Kubatzki, C., and Rahmstorf, S., Climber-2: A climate system model of intermediate complexity, *Clim. Dyn.*, *16*, 1 – 17, 2000.

Polzin, K., Toole, J., Ledwell, J., and Schmitt, R., Spatial variability of turbulent mixing in the abyssal ocean, *Science*, *276*, 93 – 96, 1997.

Prange, M., Lohmann, G., and Paul, A., Influence of vertical mixing on the hysteresis: analysis of an OGCM, *J. Phys. Oceanogr.*, *33*, 1707 – 1721, 2003.

Prather, M., Numerical advection by conservation of second-order moments, *J. Geophys. Res.*, *91*, 6671 – 6681, 1986.

Radko, T. and Marshall, J., Eddy-induced diapycnal fluxes and their role in the maintenance of the thermocline, *J. Phys. Oceanogr.*, *34*, 372 – 383, 2004.

Rahmstorf, S., On the freshwater forcing and transport of the Atlantic thermohaline circulation, *Clim. Dyn.*, *12*, 799 – 811, 1996.

Rahmstorf, S., Ocean circulation and climate during the past 120,000 years., *Nature*, *419*, 207 – 214, 2002.

Rahmstorf, S., The current climate, *Nature*, *421*, 699, 2003.

Rahmstorf, S. and England, M., Influence of southern hemisphere winds on north Atlantic deep water formation, *J. Phys. Oceanogr.*, *27*, 2040 – 2054, 1997.

Rahmstorf, S. and Ganopolski, A., Long-term global warming scenarios computed with an efficient coupled climate model, *Climatic Change*, *43*, 353 – 367, 1999.

Redi, M., Oceanix isopycnal mixing by coordinate rotation, *J. Phys. Oceanogr.*, *12*, 1154 – 1158, 1982.

Rintoul, S., Hughes, C., and Olbers, D., The Antarctic circumpolar current system, in *Ocean Circulation and Climate*, edited by Siedler, pp. 271–301, Academic, 2001.

Robbins, P. and Toole, J., The dissolved silica budget as a constraint on the meridional overturning circulation of the Indian ocean., *Deep Sea Res.*, *44*, 879 – 906, 1997.

Robinson, A. and Stommel, H., The oceanic thermocline and the associated thermohaline circulation, *Tellus*, *3*, 295 – 308, 1959.

Saenko, O. and Weaver, A., Southern ocean upwelling and eddies: sensitivity of the global overturning to the surface density range., *Tellus*, *55A*, 2003.

Sandström, J., Dynamische Versuche mit Meerwasser, *Annalen der Hydrographie und Maritimen Meteorologie*, pp. 6 – 23, 1908.

Schaeffer, M., Selten, F., Opsteegh, J., and Goosse, H., Intrinsic limits to predictability of abrupt regional climate change in IPCC SRES scenarios, *Geophys. Res. Lett.*, *29*, 2002.

Schmittner, A. and Weaver, A., Dependence of multiple climate states on ocean mixing parameters, *Geophys. Res. Lett.*, *28*, 1027 – 1030, 2001.

Schmitz, W., On the interbasin-scale thermohaline circulation., *Rev. of Geophys.*, *33*, 151 – 173, 1995.

Schmitz, W., On the world ocean circulation., *Woods Hole Technical Report*, *WHOI-96-08*, 141 pp, 1996.

Scott, J. and Marotzke, J., The location of diapycnal mixing and the meridional overturning circulation, *J. Phys. Oceanogr.*, *32*, 3578 – 3595, 2002.

Semtner, A., A model for the thermodynamic growth of sea ice in numerical investigations of climate, *J. Phys. Oceanogr.*, *6*, 379 – 389, 1976.

Shine, K., Parameterization of shortwave flux over high albedo surfaces as a function of cloud thickness and surface albedo., *Q.J.R. Meteorol. Soc.*, *110*, 747 – 764, 1984.

Simmons, H., Jayne, S., Laurent, L. S., and Weaver, A., Tidally driven mixing in a numerical model of the ocean general circulation, *Ocean Modelling*, *82*, 2003.

Sloyan, B. and Rintoul, S., Circulation, renewal and modification of Antarctic mode and intermediate water., *J. Phys. Oceanogr.*, *32*, 1005 – 1030, 2001a.

Sloyan, B. and Rintoul, S., The Southern Ocean limb of the global deep overturning circulation., *J. Phys. Oceanogr.*, *31*, 143 – 173, 2001b.

Speer, K., Rintoul, S., and Sloyan, B., The diabatic deacon cell., *J. Phys. Oceanogr.*, *30*, 3212 – 3222, 2000.

Stommel, H., Thermohaline convection with two stable regimes of flow., *Tellus*, *13*, 224 – 230, 1961.

Stommel, H. and Arons, A., On the abyssal ciruclation of the world ocean - I. Stationary planetary flow patterns on a sphere, *Deep Sea Res.*, *6*, 151 – 173, 1960.

Stone, P., A simplified radiative-dynamical model for the static stability of rotating atmospheres., *J. Atmos. Sci.*, *29*, 405 – 418, 1972.

Talley, L., Reid, J., and Robbins, P., Data-based meridional overturning streamfunctions for the global ocean, *J. Clim.*, *16*, 3213–3224, 2003.

Thorpe, R., Gregory, J., Johns, T., Wood, R., and Mitchell, J., Mechanisms determining the Atlantic thermohaline circulation response to greenhouse gas forcing in a non-flux-adjusted coupled climate model, *J. Climate*, *14*, 3102 – 3116, 2001.

Timmermann, A. and Goosse, H., Is the wind-stress forcing essential for the meridional overturning circulation?, *Geophys. Res. Lett.*, *31*, 2004.

Toggweiler, J. and Samuels, B., Is the magnitude of the deep outflow from the Atlantic ocean actually governed by southern hemisphere winds?, in *The Global Carbon Cycle*, edited by M. Heimann, NATO ASI Series, pp. 333–366, Springer-Verlag, 1993a.

Toggweiler, J. and Samuels, B., New radiocarbon constraints on the upwelling of abyssal water to the ocean's surface, in *The Global Carbon Cycle*, edited by M. Heimann, NATO ASI Series, pp. 303–331, Springer-Verlag, 1993b.

Toggweiler, J. and Samuels, B., Effect of Drake passage on the global thermohaline circulation, *Deep Sea Research*, *42*, 477–500, 1995.

Toggweiler, J. and Samuels, B., On the ocean's large-scale circulation near the limit of no vertical mixing, *J. Phys. Oceanogr.*, *28*, 1832 – 1852, 1998.

Veronis, G., The role of models in tracer studies., *Numerical Models of Ocean Circulation*, *Natl. Acad. Sci.*, 133 – 146, 1975.

Visbeck, M., Marshall, J., and Haine, T., Specification of eddy transfer coefficients in coarse-resolution ocean circulation models, *J. Phys. Oceanogr.*, *27*, 381 – 402, 1997.

Webb, D. and Suginohara, N., Vertical mixing in the ocean, *Nature*, *409*, 37, 2001a.

Webb, D. and Suginohara, N., The interior circulation of the ocean, in *Ocean Circulation and Climate*, edited by Siedler, pp. 205–214, Academic, 2001b.

Weijer, W., DeRuijter, W., Sterl, A., and Drijfhout, S., Response of the atlantic overturning circulation to south atlantic source of buoyancy., *Global and Planetary Change*, *34*, 293 – 311, 2001.

Wood, R., Keen, A., Mitchell, J., and Gregory, J., Changing spatial structure of the thermohaline circulation in response to atmospheric CO_2 forcing in a climate model., *Nature*, *399*, 572 – 575, 1999.

Wright, D., Vreugdenhil, C., and Hughes, T., Vorticity dynamics and zonally averaged ocean circulation models, *J. Phys. Oceanogr.*, *25*, 2141 – 2154, 1995.

Wunsch, C., What is the thermohaline circulation, *Science*, *298*, 1180–1181, 2002.

Wunsch, C. and Ferrari, R., Vertical mixing, energy and the general circulation of the oceans, *Annual Reviews of Fluid Mechanics*, *36*, 281 – 314, 2004.

Wunsch, C., Hu, D., and Grant, B., Mass, heat, salt and nutrient fluxes in the south Pacific ocean., *J. Phys. Oceanogr.*, *13*, 725 – 753, 1983.

Yang, J., On the importance of resolving the western boundary layer in wind-driven ocean general circulation models, *Ocean Modelling*, *5*, 357 – 379, 2003.

Zalesak, S., Fully multidimensional flux-corrected transport algorithms for fluids., *J. of Comp. Phys.*, *31*, 335 – 362, 1979.

Zhang, J., Schmitt, R., and Huang, R., The relative influence of diapycnal mixing and hydrologic forcing on the stability of the thermohaline circulation., *J. Phys. Oceanogr.*, *29*, 1096 – 1108, 1999.

Zillmann, J., A study of some aspects of the radiation and the heat budgets of the southern hemisphere oceans., *Meteor. Stud.*, *26*, 562 pp., bur. of Meteorology, Dep. of the Interior, Canberra, Australia, 1972.

Danksagung

Ich danke sehr herzlich Stefan Rahmstorf, der es mir ermöglichte, am PIK promovieren zu können, für seine Unterstützung.

Ich danke herzlich der restlichen 'ocean group' fuer die zahlreichen Diskussionen, das gemeinsame Problemlösen, die emotionale Unterstützung, die Kaffeerunden in der Kantine, die Aufmunterungen und vieles mehr:
Miguel Angel Morales Maqueda, Marisa Montoya, Till Kuhlbrodt, Anders Levermann, Susanne Nawrath, Juliette Mignot, Matthias Hofmann, Brigitta Krukenberg, Eva Bauer und Heiko Goelzer. Miguel sei insbesondere für die enthusiastische Wissensvermittlung und die Betreuung der Arbeit gedankt.

Andrey Ganopolski danke ich für mehrere wichtige Diskussionen.

Weiterhin sei der gesamten CLIMBER-Gruppe für die offene und freundliche Arbeits-Atmosphäre gedankt.

Ohne den IBM Supercomputer des PIK und die Unterstützung des "Data und Computation Teams"unter Karsten Kramer wären die vielen verschiedenen Sensitivitätsstudien unmöglich gewesen. Danke!

Ich danke Anke Bauer, Milena Jokisch, Florian Kronast, Sandra Leinen, Kerstin Müller und Thomas Schneider für die Freundschaft und Unterstützung in den Tiefphasen der Doktorandenzeit.

Meiner Familie gilt ein ganz besonderer, tiefer, lieber Dank:
Ursula und Heinz Griesel, Olaf Griesel und William Blackledge.